

Copyright
by
Eric Robert Brooks
2014

The Dissertation Committee for Eric Robert Brooks Certifies that this is the approved version of the following dissertation:

Control of intraflagellar transport: studies of the planar cell polarity effector Fuz, the small GTPase Rsg1, and the novel protein TTC29

Committee:

John B. Wallingford, Supervisor

Jeffrey M. Gross

Steven A. Vokes

Edward M. Marcotte

Arturo De Lozanne

Control of intraflagellar transport: studies of the planar cell polarity effector Fuz, the small GTPase Rsg1, and the novel protein TTC29

by

Eric Robert Brooks, B.S.

Dissertation

Presented to the Faculty of the Graduate School of

The University of Texas at Austin

in Partial Fulfillment

of the Requirements

for the Degree of

Doctor of Philosophy

The University of Texas at Austin

May 2014

Dedication

This work is dedicated to my parents, James and Elizabeth--for instilling in me a sense of curiosity and determination, and for their unwavering support.

Acknowledgements

A doctoral campaign is a long and taxing process, and one that would have been impossible for me to undertake alone. As such I have many people to thank. First, Ryan Gray, Tae Joo Park, Jacqui Tabler, Mitch Butler, Airon Wills, Kuba Sedzinski, Katherine Smith, Esther Keiserman, Asako Shindo, and Mei-I Chung all provided significant help, both material and philosophical. In addition, I would like to thank all of the other members of the Wallingford Lab, past and present, for their insights and camaraderie. In a similar vein, the developmental biology community at UT Austin has been a wonderful resource and sounding board, and I would like to thank everyone involved. It is impossible to thank Tawisy Lamech enough for her understanding and composure in the face of stress-induced grouchiness, nor for her constant warmth and support. All the members of my dissertation committee have been of immeasurable assistance in ways too numerous to list individually, and therefore I would simply like to thank Jeff, Steve, Edward and Arturo for making this process both successful and worthwhile. Finally, as any doctoral candidate knows, it all comes down to your mentor. I have had the great privilege to study with John Wallingford and I cannot in any way adequately express the depth of my gratitude for the experience, so I will simply say: thanks for everything.

Control of intraflagellar transport: studies of the planar cell polarity effector Fuz, the small GTPase Rsg1, and the novel protein TTC29

Eric Robert Brooks, Ph.D.

The University of Texas at Austin, 2014

Supervisor: John B. Wallingford

Cilia are small microtubule based protrusions found on most cells of the vertebrate body. In humans, defects in the structure or function of cilia results in a large class of developmental and homeostatic diseases known collectively as the ciliopathies. Ciliogenesis is accomplished by the concerted action of a number of molecular pathways including the intraflagellar transport (IFT) system. IFT is a group of ~20 highly conserved proteins that assemble into large macromolecular complexes known as trains. These trains act to carry cargo bi-directionally between the cell body and ciliary tip, via interaction with the microtubule motors kinesin and dynein. IFT train dynamics are required for both cilia structure and function, however the controls on these dynamics are still incompletely understood. Here, I present the first platform for study of IFT dynamics within vertebrate multiciliated cells, an understudied population with critical functions in development and homeostasis. Using this platform, I demonstrate that the planar cell polarity effector protein Fuz is required for IFT dynamics via its control of the cytoplasmic localization of a subset of IFT proteins. Subsequently, I find that a Fuz binding partner, the putative small GTPase Rsg1, is also required for IFT protein localization and dynamics. Additionally, I describe a role for Rsg1 in basal body docking, one of the earliest events of ciliogenesis. Finally, I show that the poorly studied protein

TTC29 is required for a specific subset of IFT dynamic behaviors. These data reveal novel regulatory motifs for ciliogenesis and demonstrate, specifically, the complexities of IFT regulation in the cytoplasm and within the cilium itself. Finally, they suggest that multiciliated cells provide a tractable platform for generating robust datasets for the investigation ciliary dynamics. Such studies are critical for informing our understanding of the molecular etiology of human ciliopathic diseases.

Table of Contents

List of Figures	xi
Chapter 1: Cilia, ciliogenesis, intraflagellar transport and multiciliated cells	1
1.1: Cilia and human disease	1
1.2: Ciliary genomics and proteomics	4
1.3: Ciliary anatomy.....	6
1.3.1: The basal body	6
1.3.2: The transition zone.....	8
1.3.3: The ciliary necklace	11
1.3.4: The doublet zone.....	13
1.3.5: The ciliary tip.....	14
1.4: Ciliogenesis and intraflagellar transport	15
1.4.1: The mother centriole to basal body transition	15
1.4.2: Cytoplasmic trafficking during ciliogenesis	18
1.4.3: The actin cytoskeleton and ciliogenesis.....	20
1.4.4: Intraflagellar transport and axoneme extension.....	26
1.5: Cilia, IFT, and Hedgehog signaling	34
1.6: Multiciliated cells	36
1.6.1: Transcriptional controls on multiciliogenesis.....	37
1.6.2: Cell biology of multiciliogenesis	40
1.7: Planar Cell Polarity and ciliogenesis	46
1.8: Concluding remarks	47
Chapter 2: Control of vertebrate intraflagellar transport by the planar cell polarity effector Fuz	49
2.1: The planar cell polarity effector Fuz is required for vertebrate ciliogenesis	49
2.2: Fuz is required for appropriate proximo-distal patterning of axonemes	50
2.3: Development of an <i>in vivo</i> system for analysis of IFT dynamics in multiciliated cells	59

2.4: Fuz is required for appropriate anterograde IFT dynamics	63
2.5: Fuz is required for the localization of the retrograde IFT protein IFT43 to axonemes.....	66
2.6: Fuz is required for the localization of IFT43 but not IFT20 to peri-basal body pools.....	69
2.7: Model for Fuz function during ciliogenesis.....	70
2.8: Discussion.....	76
Chapter 3: The small GTPase Rsg1 is important for the cytoplasmic localization and axonemal dynamics of intraflagellar transport proteins.....	79
3.1: The putative small GTPase Rsg1 physically interacts with Fuz and is required for ciliogenesis.....	79
3.2: Rsg1 function is required for the correct organization of the axonemal proximo-distal axis	80
3.3: Rsg1 is required for normal intraflagellar transport dynamics within axonemes.....	83
3.4: Rsg1 function is required for the localization of IFT43 but not IFT20 to peri-basal body pools of IFT in <i>Xenopus</i> multiciliated cells	90
3.5: Rsg1 loss of function leads to defects in basal body apical migration ..	95
3.6: Discussion.....	97
Chapter 4: Control of intraflagellar transport by the novel Rfx2 target TTC29 ..	100
4.1: Introduction.....	100
4.2: TTC29 is required for normal anterograde, but not retrograde IFT dynamics	101
4.3: Can the defects in anterograde cycling explain the shortened axonemes of TTC29 impaired MCCs?.....	106
4.4: Conclusions.....	110
Chapter 5: Conclusions and future directions	111
5.1: General functions of Fuz.....	111
5.2: Cytoplasmic controls of intraflagellar transport	115
5.3: Do the planar cell polarity effectors and Rsg1 function together during ciliogenesis?	118
5.4: Understanding the mechanisms of IFT	119

5.5: Concluding remarks	123
Appendix: Materials and Methods	124
A.1: <i>Xenopus</i> embryo manipulations	124
A.2: Plasmids and cloning	124
A.3: Morpholino and mRNA injections.....	125
A.4: IFT imaging and quantification	126
A.5: Axoneme compartment imaging	127
A.6: Axoneme compartment analysis and quantification	127
A.7: Basal body IFT enrichment analysis.....	128
List of commonly used abbreviations	130
References.....	131
Vita	158

List of Figures

Figure 1: An illustration of common cilia morphologies and their associated functions.....	3
Figure 2: Schematic illustration of ciliary anatomy.....	10
Figure 3: Schematic illustration of ciliogenesis.....	17
Figure 4: Schematic representation of IFT localization.....	29
Figure 5: Fuz is required for ciliogenesis in multiple tissue types	51
Figure 6: Axonemes in <i>Xenopus</i> MCCs display a highly stereotyped proximal-distal organization, and this organization is disrupted upon Fuz KD.....	54
Figure 7: Intensity profiles of CLAMP-RFP along the length of axonemes reveal a role for Fuz in the distal enrichment of CLAMP.....	55
Figure 8: Quantification of ciliary compartments in control and Fuz KD axonemes	56
Figure 9: Quantification of compartment occupancy of axonemes	57
Figure 10: Analysis of intraflagellar transport dynamics in the multiciliated cells of the <i>Xenopus</i> epidermis	61
Figure 11: GFP-IFT20 behavior at the base and tips of axonemes.....	62
Figure 12: Loss of Fuz leads to disrupted anterograde IFT	64
Figure 13: Fuz is required for IFT80 cycling dynamics	65
Figure 14: Reduced IFT43 localization in the axonemes of Fuz KD MCCs.....	67
Figure 15: Loss of dynamic retrograde machinery from cycling axonemal IFT trains	68

Figure 16: Fuz is required for the localization of GFP-IFT43 but not GFP-IFT20 to peri-basal body IFT pools	71
Figure 17: Schematic explanation of quantification methodology used for assessing IFT enrichment at apically localized basal bodies	72
Figure 18: Quantification of GFP-IFT localization to basal bodies	73
Figure 19: Model for Fuz function during ciliogenesis	75
Figure 20: The putative small GTPase Rsg1 is required for correct proximal-distal axonemal patterning in <i>Xenopus</i> MCCs	81
Figure 21: Rsg1 is required for appropriate IFT dynamics within the axonemes of MCCs	84
Figure 22: IFT20 accumulates in the axonemes of Rsg1 KD MCCs	85
Figure 23: Axonemes from Rsg1 KD MCCs have reduced dynamic IFT43 signal	88
Figure 24: Loss of GFP-IFT43 from axonemes of Rsg1 KD MCCs	89
Figure 25: Rsg1 controls the localization of GFP-IFT43, but not GFP-IFT20 to basal bodies	92
Figure 26: Quantification of GFP-IFT localization in control and Rsg1 KD MCCs	93
Figure 27: Quantification of GFP-IFT localization in control and Rsg1 KD2 MCCs	94
Figure 28: Rsg1 controls apical trafficking of basal bodies	96
Figure 29: Loss of TTC29 does not lead to gross defects in IFT cycling dynamics	102
Figure 30: TTC29 KD leads to a reduction in the average anterograde, but not retrograde velocity of IFT trains	103

Figure 31: TTC29 KD does not lead to an increase in deviation between individual IFT velocity observations105

Figure 32: Correlation analysis between observed IFT velocity and axoneme length in control and TTC29 KD cells.....108

Chapter 1: Cilia, ciliogenesis, intraflagellar transport, and multiciliated cells

1.1: CILIA AND HUMAN DISEASE

Cilia, also termed eukaryotic flagella in some unicellular organisms, are microtubule-based cellular protrusions nucleated from modified centrioles known as basal bodies. These structures are found throughout the eukaryotes--from single celled organism such as the green alga *Chlamydomonas reinhardtii* to vertebrates, including humans. Cilia can be broadly categorized into two types: motile and primary (Fig. 1). Motile cilia generally contain nine outer doublet microtubule-pairs and a central pair of non-doublet microtubules (also known as a 9+2 arrangement). These cilia undergo a whip-like motion known as ciliary beating, which is driven by the regulated sliding of adjacent doublets. A second class of motile cilia lack the central pair and instead demonstrate a rotational motility (9+0 motile cilia). Primary cilia are non-motile, and generally lack the central pair of non-doublet microtubules (9+0 non-motile cilia) (Ishikawa and Marshall, 2011). Motile cilia serve a variety of functions which require the generation of local fluid flow, from locomotor activity in unicellular eukaryotes (Kozminski et al., 1993) to mucous clearance in the human airway (Wanner et al., 1996). Primary cilia were long ignored because their function was nonobvious--see (Satir et al., 2010), for a brief

historical discussion. Recently these cilia have become the subject of intense interest given that they are critical for the transduction of developmental signals in vertebrates--most notably the Hedgehog family of morphogens ((Huangfu et al., 2003; Huangfu and Anderson, 2005; Qin et al., 2011; Ocbina et al., 2011) and see (Eggenchwiler and Anderson, 2007) for a recent review).

Cilia function is a key requirement for early human development and later homeostasis. Given that primary cilia are critical mediators of developmental signaling, it is unsurprising that their dysfunction results in an array of human pathologies. Strong defects in the basic machinery of ciliogenesis lead to early, pre-natal lethality in mouse models and are likely to do so in humans (Huangfu et al., 2003; Pazour and Rosenbaum, 2002). Additionally, a large clade of multi-symptomatic diseases have been etiologically linked to milder defects in cilia structure and function. These diseases—known collectively as the ciliopathies—result in a broad spectrum of debilitating conditions including retinal degeneration and blindness, gross malformations (such as polydactyly), obesity, and mental retardation (Hildebrandt et al., 2011).

Motile cilia also have important roles during human development and homeostasis. For example, the motile monocilia of nodal cells are important to establish appropriate left-right patterning (Gray et al., 2011; Komatsu and Mishina, 2013), and defects in this process can lead to a spectrum of left-right mis-patterning issues and, in severe cases, the complete reversal of the left-right axis (situs inversus

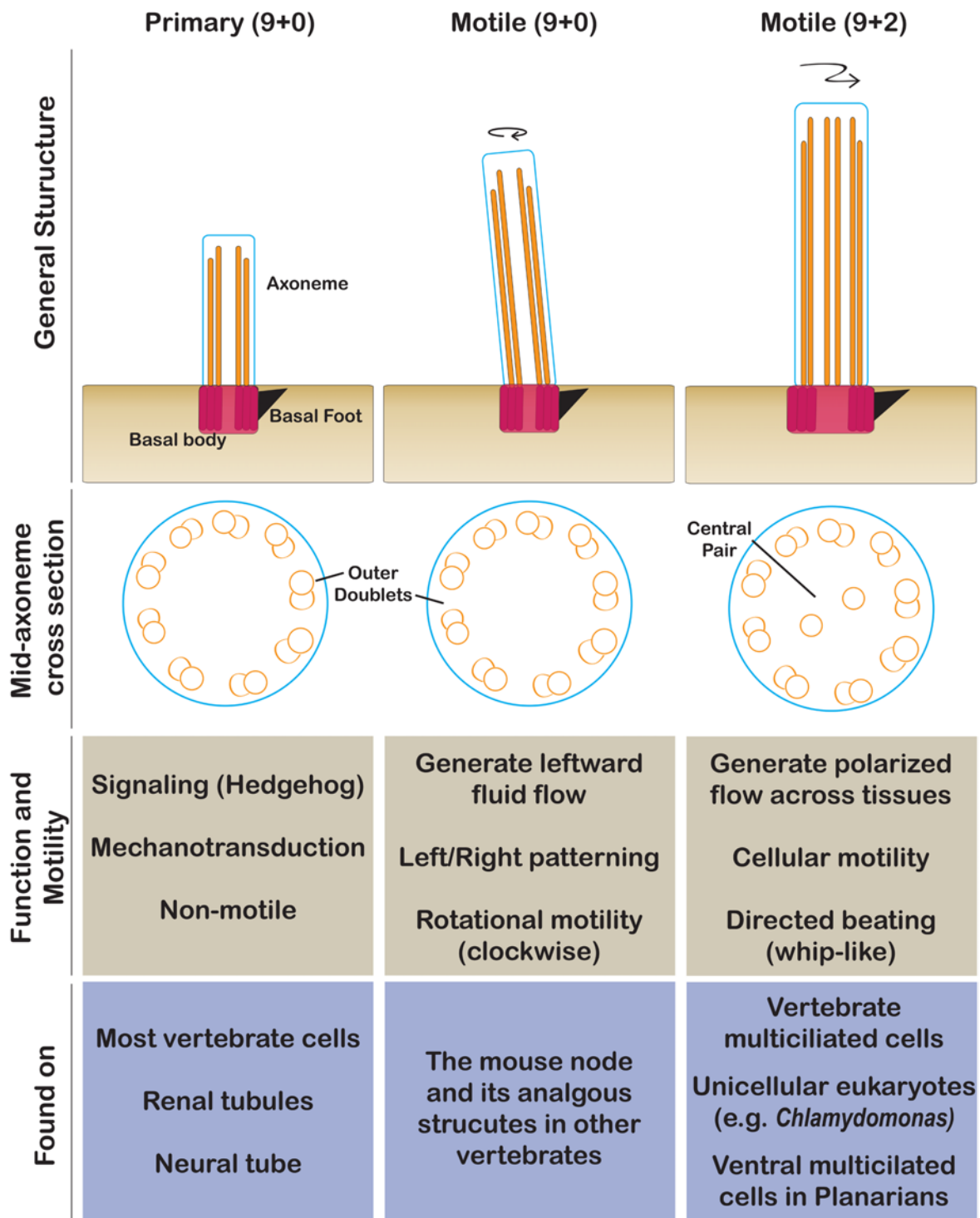


Figure 1: An illustration of common cilia morphologies and their associated functions.

totalis) (Afzelius, 1976; Guichard et al., 2001). Motile cilia are also found on specialized multiciliated cells (MCCs) where many dozens of cilia beat in a coordinated, polarized fashion to drive fluid flow across the epithelium. MCCs are found, for example: in the airway, where they are important in protective mucous clearance; in the ventricles of the brain, where they generate polarized fluid flow that is critical for neuronal morphogenesis; and in the oviduct/fallopian tubes, where they are important for ovum transport. Therefore, defects in MCC function can lead to respiratory, neural, and reproductive diseases (Lyons et al., 2006; Sawamoto et al., 2006; Tissir et al., 2010; Wanner et al., 1996).

The strong links between cilia dysfunction and human disease have spurred intensive research into the basic machinery and signaling functions of these organelles. The following sections provide brief summaries of key aspects of cilia biology, including: the protein composition and underlying anatomy of these organelles, a review of the molecular processes underlying their construction (the process of ciliogenesis), and an examination of the specialized events underlying the multiciliation of a single cell.

1.2: CILIARY GENOMICS AND PROTEOMICS

The anatomy of a cilium can be subdivided into at least three structures: the basal body, which anchors the organelle in the plasma membrane and serves as a nucleator for microtubule doublets; the axoneme, a set of nine microtubule

doublets arrayed in a ring (and in some cilia, two non-doublet central microtubules) and a host of structural and accessory proteins; and the ciliary membrane, a specialized patch of membrane enclosing the axoneme distinct from, but contiguous with the cellular plasma membrane.

Genomically and proteomically, cilia are fairly complex. Early estimates of the proteome of purified *Chlamydomonas reinhardtii* flagella (essentially cilia) suggested that these structures contain ~250 proteins (Luck, 1984; Piperno et al., 1977). Early studies of the human cilia proteome (the ciliome), found a similar number of ciliary proteins, ~200 (Ostrowski et al., 2002). However, these studies were limited, in that they identified predominately axonemal proteins. More recent studies, which have attempted a fuller picture by including basal body proteins and ciliary membrane proteins, have estimated that there are anywhere from ~450 to ~1,200 proteins depending on how a ciliary gene/protein is defined (i.e. ciliary resident versus transient localization, ciliary structure versus ciliary function, etc.) (Pazour, 2004; Ishikawa et al., 2012; Gherman et al., 2006; Li et al., 2004).

Filtering these data sets can be difficult, especially as many cilia resident proteins have not yet been functionally defined. Nonetheless, some interesting findings have come out of this work. One example is *BBS5*--one of the genes whose function is compromised in human patients with Bardet-Biedl Syndrome (BBS) one of the best-studied ciliopathies. The identification of *BBS5* in a

comparative genomics study looking for novel ciliary genes (Li et al., 2004) was one of the early links between BBS and cilia. This finding inspired later studies and a greater understanding of the molecular defects in the cilia of BBS patients (Nachury et al., 2007; Loktev et al., 2008; Jin et al., 2010).

Given the high proteomic complexity of cilia, it is unsurprising that they also exhibit a great deal of structural complexity, as detailed in the following section.

1.3: CILIARY ANATOMY

Cilia can best be described along a proximal-distal axis, with proximal indicating the cell body and distal indicating the ciliary tip in the extracellular space (Fig. 2). The microtubules of the organelle are oriented along this axis with the minus end proximal and the plus-end distal. Cilia can be subdivided into a number of compartments along this axis, as delineated by specific structural features. Each of these regions is briefly described below, starting proximally.

1.3.1: The basal body

Proximally, cilia are nucleated and anchored in the cytoplasm/cell membrane by the basal body, which in most eukaryotic cells is a modified

centriole. In the case of specialized multi-ciliated cells, a large number of basal bodies are generated *de novo* (see below). Structurally, the centriole/basal body consists of a radial array of nine microtubule triplets, each angled inward like a blade. Each triplet is composed of an A-, B-, and C- tubule. The A-tubule is complete, containing 13 microtubule protofilaments and shares 4 protofilaments with the B-tubule, which is incomplete containing only 10 unique protofilaments. The B-tubule is, in turn, connected to the C-tubule which is also incomplete, again containing 10 protofilaments (Li et al., 2012). These triplet structures are the template from which the microtubule doublets of the protruding axoneme will be nucleated (Li et al., 2012; Mizuno et al., 2012).

Recent studies have shown that the nine-fold triplet structure of centrioles and basal bodies depends on the function of the protein SAS-6. Nine monomers of SAS-6 homo-oligomerize to form a ring structure with 9-fold symmetry reminiscent of the basal body macro structure (Nakazawa et al., 2007; Kitagawa et al., 2011). This suggests that this SAS-6 macrostructure acts as a scaffold for patterning the microtubule triplet; consistent with this idea, loss of SAS-6 function leads to centrioles and basal bodies with an inappropriate number of microtubules (Nakazawa et al., 2007; Kitagawa et al., 2011; Jerka Dziadosz et al., 2010). Additionally, *Chlamydomonas* null for SAS-6 have structurally impaired basal bodies, with ~90% of cells lacking flagella (Nakazawa et al., 2007; Jerka Dziadosz et al., 2010). The presence of centrioles

and basal bodies, even impaired ones, in SAS-6 null cells suggests that there are more proteins involved in giving shape to these structures. Indeed, a recent study found that centrioles in *Chlamydomonas* contain on the order of 50 proteins, not including tubulins (Keller et al., 2005), suggesting a complex structural organization.

One very interesting problem is that of the maturation of a centriole into a basal body. During this process centrioles must acquire specialized accessory structures including: ciliary vesicles, which cap the distal end of the centriole (Sorokin, 1962); basal feet, which anchor the basal body within the perimembrane cytoplasm (Anderson, 1972); and striated rootlets, which are thought to be both a structural support and a docking region for ciliary cargos (Tachi et al., 1974; Yang and Li, 2005). The molecular events leading centrioles to elaborate these structures are discussed later in this chapter.

1.3.2: The transition zone

Just distal to the basal body is the transition zone (Fig. 2), which encompasses a region where the triplet microtubules of the basal body begin to nucleate the outer doublet microtubules of the axonemal body (Gilula and Satir, 1972; Fisch and Dupuis-Williams, 2011). The transition zone region contains a number of specialized structures, the best understood of which are the

transition fibers. These fibers are specialized radial protrusions connecting the B-tubule of basal body triplets to the plasma membrane (Fisch and Dupuis-Williams, 2011; Anderson, 1972; Gibbons and Grimstone, 1960). Outer dense fiber 2 (Odf2) and Cep164 both localize to these fibers and loss of either leads to severe defects in ciliogenesis (Ishikawa et al., 2005; Graser et al., 2007). The core Intraflagellar transport proteins required for building the axoneme (see below) also localize to these fibers by immuno-gold EM (Deane et al., 2001), indicating that these fibers serve as a docking site for the machinery of ciliogenesis. Further, these fibers have been proposed to be components of the so-called ciliary pore complex, which functions to regulate entry of proteins into the axoneme (Kee and Verhey, 2013; Rosenbaum and Witman, 2002). Although the exact molecular nature of this pore is still in question, recent work has suggested a subset of ciliary import requires importins and a Ran-GTP cycle similar to the mechanisms underlying nuclear import (Dishinger et al., 2010; Kee et al., 2012; Kee and Verhey, 2013).

At the distal-most end of the transition zone in 9+2 motile cilia there is a structure known as the terminal plate that serves as a nucleator for the central pair of non-doublet microtubules. The terminal plate also serves as the fracture point in the process of autotomy, where cilia undergo self-severing in cases of physiological stress (see (Fisch and Dupuis-Williams, 2011) for an excellent recent review of this process). The distal transition zone region also contains

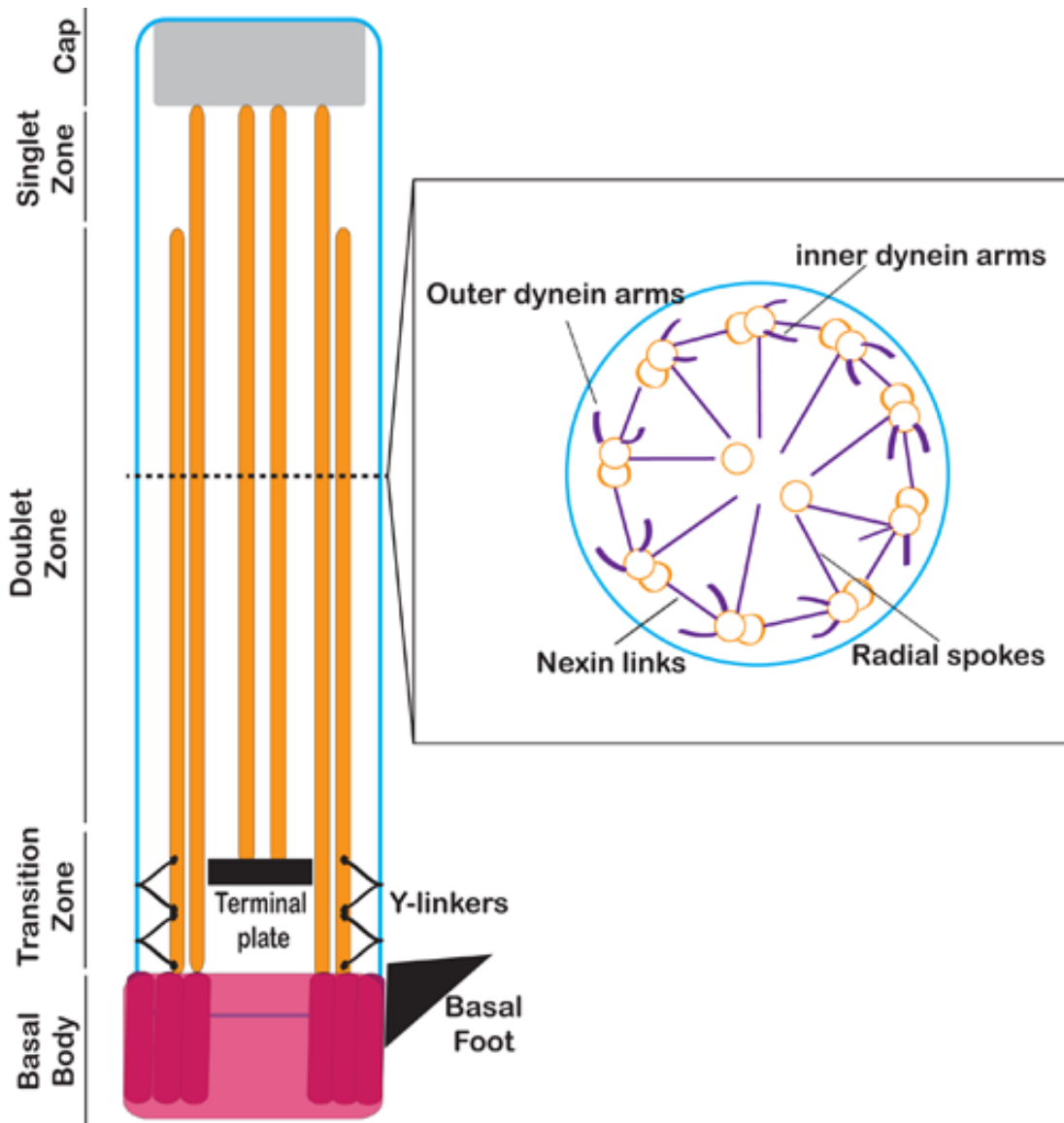


Figure 2: A schematic representation of a motile 9+2 axoneme along the proximal-distal axis, with a cross section through the doublet zone. The various proximal-distal axoneme compartments are indicated in the long axis. The cross section shows the radial organization of the doublets and their accessory structures.

champagne-glass shaped radial linkers, sometimes termed Y-linkers (Gilula and Satir, 1972; Anderson, 1972; Fisch and Dupuis-Williams, 2011), which have recently been determined to link the outer microtubule doublets of the proximal axoneme to the membrane (Craigie et al., 2010). Cep290 has recently been identified as a key structural component of these linkers, as *Chlamydomonas* mutants lacking this protein show a complete loss of these structures. In addition, Cep290 deficient cells have increased microtubule doublet-membrane spacing, supporting a functional role for these structures in linking the doublets to the membrane (Craigie et al., 2010). This data is especially interesting given that Cep290 is mutated in some human ciliopathy patients (Baala et al., 2007; Gordon et al., 2008). In fact, the products of many genes associated with ciliopathies localize to this region of the transition zone, and dysfunction of the region is linked to broad defects in ciliogenesis and ciliary protein localization ((Singla et al., 2010; Garcia-Gonzalo et al., 2011) and see (Czarnecki and Shah, 2012) for an excellent review). Taken together, these studies suggest that the transition zone has key roles in ciliogenesis, including as a structural support, as a docking site for ciliary cargoes delivered from the cell body, and as a selective barrier or pore, which regulates protein entry and exit from the cilium.

1.3.3: The ciliary necklace

The ciliary necklace is the region of the axoneme where the ciliary membrane meets the plasma membrane of the cell, and at least partially overlaps the transition zone. It is identified by a series of bumps arranged in parallel strands around the circumference of the axoneme. These bumps are known as intramembrane particles, or IMPs, and their composition is currently unknown (see (Fisch and Dupuis-Williams, 2011) for review). The precise function of this region of the axoneme is unclear. In *Paramecium*, the necklace contains high-affinity calcium binding sites with a geometric localization pattern resembling that observed for IMPs (Plattner, 1975). This has led to the hypothesis that the necklace contains stretch activated calcium channels that help regulate ciliary beat frequency (Gilula and Satir, 1972). However, given that the necklace also appears on primary cilia--which do not beat--it seems unlikely that this is the only role for IMPs. Another proposed function for this region is that it acts as a diffusion barrier, selectively limiting the translocation of integral membrane proteins into the axonemal sheath (see (Fisch and Dupuis-Williams, 2011) and (Pedersen et al., 2012) for discussion). In support of this idea, recent work has demonstrated the presence of a septin ring in the necklace region, and disruption of this ring leads to a loss of restriction on diffusion, and defects in ciliogenesis (Hu et al., 2010; Kim et al., 2010b).

1.3.4: The doublet zone

The doublet zone of the axoneme begins distal to the transition zone and is the longest proximal-distal segment of the cilium. In both 9+0 and 9+2 cilia this zone contains nine outer doublet microtubules (Fig. 2). Each doublet contains a complete A-tubule, and an incomplete or B-tubule that shares protofilaments with the A-tubule. (Fisch and Dupuis-Williams, 2011; Satir and Christensen, 2007). In motile 9+2 cilia, there is an additional pair of non-doublet microtubules in the center of the radial array of doublets. These axonemes exhibit a repeating macromolecular architecture with a periodicity of $\sim 96\text{nm}$ (Porter and Sale, 2000). Within a 96nm repeat, each outer doublet is connected to the adjacent doublets by a nexin protein bridge (Warner, 1976) and to the central pair of microtubules by a multi-protein complex known as a radial spoke (Pigino and Ishikawa, 2012). Additionally, each repeat contains four outer dynein arms (ODAs) attached to the outer circumference of the A-tubule, as well as a variable number of inner dynein arms (IDAs) attached to the inner circumference of the A-tubule (Porter and Sale, 2000; Mizuno et al., 2012). Primary 9+0 cilia, which are non-motile, lack radial spokes, ODAs, and IDAs.

Ciliary motility is accomplished by the concerted action of both ODAs and IDAs, which cause regulated sliding between adjacent doublets. Given that adjacent doublets are connected by nexin links, and all the doublets are connected to the central pair, this sliding action is under constraints which cause

it to result in axonemal bending rather than helical sliding (Fisch and Dupuis-Williams, 2011; Satir and Christensen, 2007; Mizuno et al., 2012).

1.3.5: The ciliary tip

The distal tip of the axoneme is a critical site of ciliary dynamics, given that axonemal microtubule polymerization and depolymerization appear to be restricted to this region (Marshall and Rosenbaum, 2001; Rosenbaum and Child, 1967). At the distal end of the doublet zone, the B-tubules of the outer doublets terminate but the A-tubules continue to extend, as do the central pair microtubules in 9+2 cilia (Fig. 2). There is a good deal of interspecies variation in this transition, as different organisms have differing singlet extents, and even different organizations. However, the biological importance of this variation is not apparent in most cases (see (Fisch and Dupuis-Williams, 2011) for a detailed discussion of variation in this region).

At the very distal tip of the cilium, the singlet tubules within the ciliary tip terminate in an electron dense structure known as a ciliary cap. The precise molecular components of this cap are still under active study. Candidate molecules include the microtubule-end binding protein EB1 (Pedersen et al., 2003; Schröder et al., 2011; Pedersen et al., 2005) and FAP256/Cep104 (Satish Tammana et al., 2013), both of which localize to the distal tips of cilia and are required for appropriate ciliogenesis.

Broadly, the ultra-structural and molecular observations catalogued above demonstrate that the cilium is a complex and highly ordered organelle. It should not be surprising, then, that the process of building this structure reflects this ordered complexity, as discussed in the following section.

1.4: CILIOGENESIS AND INTRAFLAGELLAR TRANSPORT

Ciliogenesis is an umbrella term for the complex series of events underlying the biogenesis of the organelle. The generation of a single cilium is discussed in a stepwise manner in the following sections. Several caveats apply when considering the generation of multiple cilia within a single cell, and these are discussed in the later section of this chapter dedicated to multiciliated cells.

1.4.1: The mother centriole to basal body transition

The first apparent morphological indication of the ciliogenic program in fibroblast cells is the association of one centriole with a post-golgi cytoplasmic vesicle known as the primary ciliary vesicle (Sorokin, 1962; Sotelo and Trujillo-Cenóz, 1958a). However, the process actually begins before this, with a series of molecular events that make a centriole competent to nucleate a cilium (Kim and Dynlacht, 2013). Recent work has shown that it is always and specifically the

mother centriole (*i.e.* the oldest centriole in a cell) that serves as the template for primary ciliogenesis. This seems to be a result of the mother centriole having already acquired all of the appendages required for ciliogenesis, whereas the daughter centriole will not gain these appendages until the succeeding cell cycle (see (Hoyer-Fender, 2010) for a review).

In order for the mother centriole to become a basal body, it must migrate to the cell surface and elaborate anchoring structures known as distal appendages (Fig. 3), which become the transition fibers of mature basal bodies (Tateishi et al., 2013; Fisch and Dupuis-Williams, 2011). This process requires the function of several centrosome associated proteins (Ceps), including: FOR20, a protein in the FOP family of centrosome proteins, Cep83 and Cep164, which are required to elaborate the distal appendages (see below) and Odf2, a key structural component of transition fibers (Aubusson-Fleury et al., 2012; Ishikawa et al., 2005; Tanos et al., 2013).

The elaboration of distal appendage/transition fiber structures is initiated by a molecular cascade that begins when Cep83 (Centrosomal protein of 83 kD), which itself is required for centriole-membrane docking, initiates a cascade of protein recruitment, culminating with the localization of Cep164, which is required for ciliogenesis (Tanos et al., 2013; Graser et al., 2007). Interestingly, loss of Cep83 function leads to defects in basal body docking,

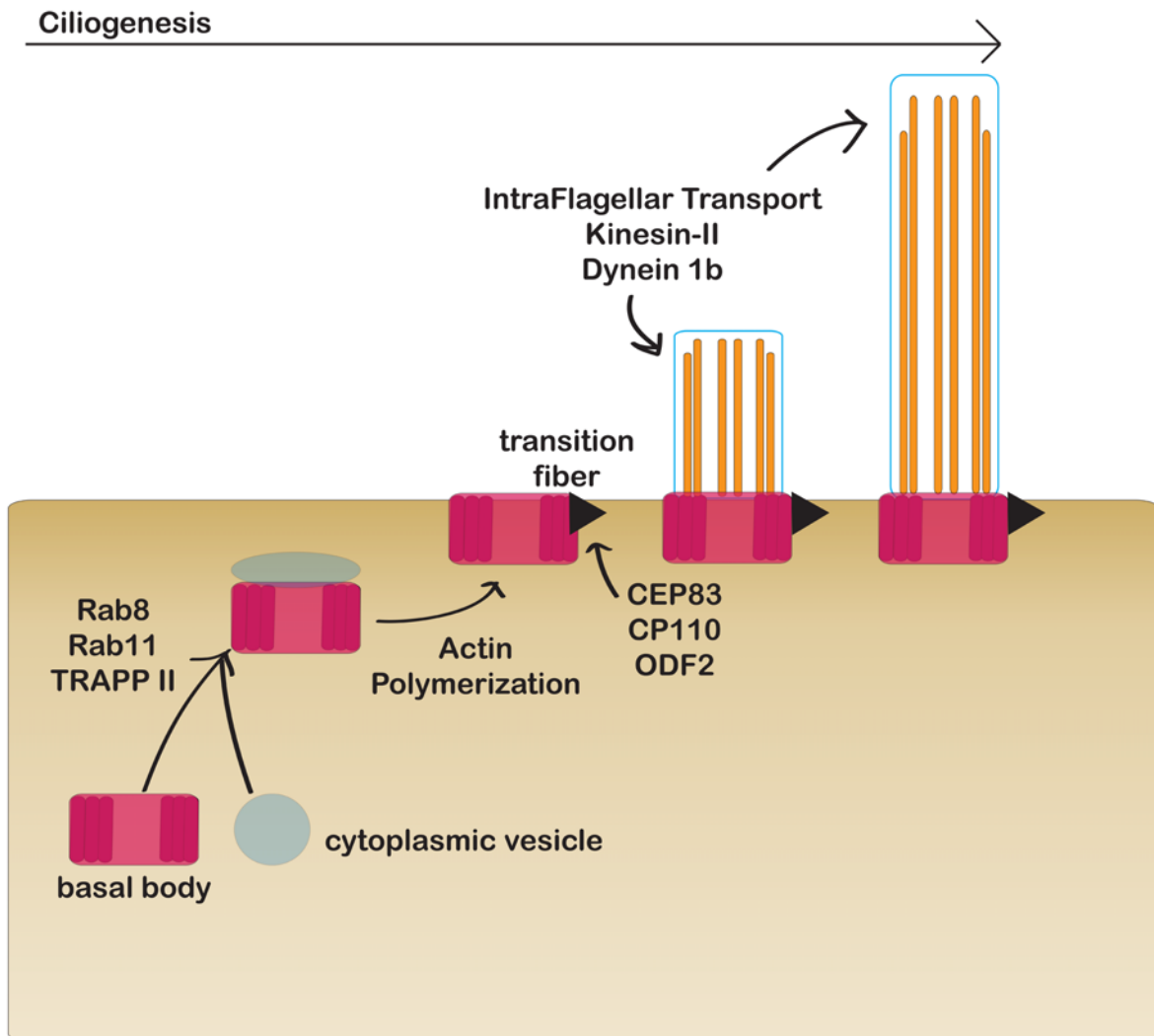


Figure 3: A highly schematized version of ciliogenesis is presented. The process begins when the mother centriole associates with a cytoplasmic vesicle in a Rab11-Rab8-TRAP II dependent manner. Subsequently, the basal body docks in a process that depends on the actin cytoskeleton. Simultaneously, the basal body elaborates distal appendages (also known as transition fibers) in a process controlled by Cep83. Once the basal body has docked, the axoneme is elaborated by the concerted action of Intraflagellar transport proteins.

loss of downstream members of the pathway only interferes with the later axonemal outgrowth (Tanos et al., 2013). These data suggest that Cep83 may control a number of events related to ciliogenesis. Indeed, Cep83 function is also required for the removal CP110/centriolin from the distal ends of mother centrioles (Tanos et al., 2013), a prerequisite for ciliary outgrowth (Spektor et al., 2007; Cao et al., 2012; Tsang and Dynlacht, 2013). In addition, Cep83 is required for the recruitment of Tau Tubulin Kinase 2, which in turn recruits of the Intraflagellar transport complexes required for axoneme outgrowth (Goetz et al., 2012).

A number of open questions remain about the earliest steps of ciliogenesis: how are proteins selectively localized in asymmetric manner to the mother centriole/basal body? What is the precise molecular mechanism for actin driven basal body migration (see the discussion of actin and ciliogenesis below) and how is it subsequently anchored? The application of emerging imaging (e.g. super-resolution microscopy) and proteomic technologies to these questions should yield exciting insights in the near future.

1.4.2: Cytoplasmic trafficking during ciliogenesis

Ciliary directed cytoplasmic traffic is a key process during ciliogenesis (Avasthi and Marshall, 2012). As mentioned above, one of the first

morphological indications of ciliogenesis, at least in fibroblasts, is the association of the mother centriole with the primary ciliary vesicle. This vesicle flattens as the nascent cilium extends and eventually fuses with the plasma membrane during basal body docking (Sorokin, 1962). Recruitment of this vesicle occurs via a molecular cascade that begins with recruitment of Rabin8 and Rab11 to the basal body via the TRAPP II intra-golgi trafficking complex (Fig. 3 (Knödler et al., 2010; Westlake et al., 2011)). Rabin8 is a guanine exchange factor (GEF) for Rab8, and interacts with the BBSome, a multi-protein complex whose components are mutated in the Bardet-Biedl syndrome ciliopathy. These proteins act together at the basal body to promote active Rab8-driven vesicle fusion into the cilium (Nachury et al., 2007). Together Rabin8, Rab8, and Rab11 recruit and activate components of the exocyst complex, which likely function to drive vesicle fusion into the ciliary compartment (Das and Guo, 2011; Feng et al., 2012; Zuo et al., 2009). Interestingly, however, Rab8 is not strictly required for ciliogenesis, as mouse mutants null for both Rab8a and Rab8b have normal cilia. Knockdown of Rab10 in Rab8 double null cells did lead to significant ciliation defects, however, suggesting a general requirement for Rab-directed cytoplasmic trafficking during ciliogenesis (Sato et al., 2007; 2014). Further, this data suggests that Rab8 function can be compensated for during exocyst activation, or that alternative pathways are sufficient for the delivery of ciliary vesicles. It is still unclear what percentage of the cargo required for ciliogenesis

is trafficked through this pathway, and the cytoplasmic controls on cilia-destined traffic remain one of the least understood aspects of ciliogenesis.

1.4.3: The actin cytoskeleton and ciliogenesis

The actin cytoskeleton plays an important, though complex, role in the process of ciliogenesis. Early pharmacological studies in multiciliated cells suggested that an apical actin network might be required for basal body localization (Boisvieux-Ulrich et al., 1990). More recently it has been demonstrated that this actin network is regulated, at least in part, by activation of the small GTPase Rho A (Park et al., 2006; 2008; Pan et al., 2007a). Recent studies have also found a role for the actin regulator Nubp1 and members of the focal adhesion complex in the coordination of actin during basal body docking in multiciliated cells (Ioannou et al., 2013; Antoniadou et al., 2014).

In contrast to the above data, several recent studies have suggested that actin polymerization is actually a negative regulator of ciliogenesis. One of the first indications of this came from a study of meckelin, the protein product of a gene mutated in many Meckle-Gruber ciliopathy patients. Meckelin was shown to be required for ciliogenesis via an interaction with the actin binding protein nesprin-2. Loss of meckelin in cultured cells caused nesprin-2 to aberrantly

localize to stress-fibers, led to reorganization of the actin cytoskeleton, and caused hyper activation of RhoA (Dawe et al., 2009).

More recently, a high-throughput screen for mediators of ciliogenesis in cultured retinal pigmented epithelium (RPE) cells uncovered a number of actin regulators. First, the actin severing proteins gelsolin and AVIL were found to be positive regulators of ciliogenesis, as siRNA mediated depletion of these proteins led to a decrease in the number of ciliated cells after serum starvation. In contrast, knockdown of ARP3, a member of the ARP2/3 complex that nucleates branched F-actin, led to increased average cilia length and high rates of ciliogenesis even in serum replete conditions (Kim et al., 2010a). Subsequent studies showed that other mediators of actin polymerization also negatively regulate ciliogenesis. Missing in metastasis (MIM), for example, is required for ciliogenesis by negatively regulating the Src-dependent phosphorylation of Cortactin, another positive regulator of branched actin. Loss of MIM, therefore, leads to increased Cortactin activity, increased branched actin polymerization, and a reduction in the number and length of cilia (Bershteyn et al., 2010). Another study found that the microRNA miR-129-3p is a regulator of ciliogenesis that acts multi-functionally to down-regulate several ciliogenesis-limiting factors, including CP110 (see above), and the branched actin regulators ARP2, TOCA, and ABLIM-1 and -3. Notably, this microRNA is highly expressed in ciliated tissues, but does not seem to affect multiciliation (Cao et al., 2012).

Together, these studies strongly suggest that a highly branched actin cytoskeleton is in some way inhibitory to the ciliogenic program, though the specific mechanism remains unclear. One proposed hypothesis is that branched actin networks inhibit ciliogenesis by blocking the formation of vesicular-tubular structures, termed pericentriolar preciliary compartments (PPCs), which act as reservoirs of the materials required for rapid ciliation. Therefore, in conditions where branched actin polymerization is inhibited, such as ARP2/3 knockdown, cilia form both more spontaneously and more rapidly than in controls (Kim et al., 2010a).

A further link between ciliogenesis and actin is the negative correlation between actin stress fibers and cilia. For example, loss of BBS-4 or -6 from cultured cells leads to an increased number and intensity of bundled actin stress fibers and a decrease in cilia number and length (Hernandez-Hernandez et al., 2013). Similar results are found upon loss of retinitis pigmentosa GTPase receptor (Gakovic et al., 2011), the tetraspan membrane protein TMEM216 (Valente et al., 2010), or the poorly characterized tetratricopeptide repeat protein TTC17 and its binding partner C2orf62 (Bontems et al., 2014). This phenotype of increased stress fibers and decreased ciliogenesis seems to correlate with hyperactivation of RhoA and failure of basal body docking.

While a great deal of data on the interplay between the actin cytoskeleton and ciliogenesis has been reported recently, there is still no unifying model for

these observations. In fact, the data from one study often seem to contradict data from others. The effect of cytochalasin D (cytoD), for example, varies from study to study; Boisvieux-Ulrich and colleagues in their early studies of the quail oviduct found cytoD to inhibit basal body docking and ciliogenesis (Boisvieux-Ulrich et al., 1990), whereas studies in cultured cells more recently have shown that it leads to longer cilia and more robust ciliation (Kim et al., 2010a; Cao et al., 2012). Further, *Xenopus* multiciliated cells treated with higher doses of cytoD showed no large-scale defects in ciliogenesis, though they did maintain apical actin (Werner et al., 2011). Another discrepancy is found in the role of focal adhesion (FA) complexes. The large scale screen from Kim et al. demonstrated that PARVA, a member of the FA complex is a negative regulator of ciliogenesis (Kim et al., 2010a); however, another recent study found that FA complex proteins, including FA kinase, are required for ciliogenesis in *Xenopus* multiciliated cells (Antoniades et al., 2014). Finally, while there is evidence in cell culture for a negative regulation of ciliogenesis by branched actin polymerization, recent studies *in vivo* have demonstrated that actin polymerizing agents are required for cilia formation. Cordon-bleu, a nucleator of non-branched F-actin is required for ciliogenesis in both mono- and multiciliated tissues of zebrafish (Ravanelli and Klingensmith, 2011; Schüller et al., 2013), and N-WASP, an activator of ARP2/3 branched actin polymerization, is

required in the neural tissues of mice to generate the cilia of ependymal cells (Jain et al., 2014).

The above discussion highlights the complex relationship between the actin cytoskeleton and the process of ciliogenesis. How can the data suggesting that actin polymerization is a negative regulator of cilia number and length be reconciled with the clear requirement for actin polymerization during the process of ciliogenesis? First, it is noteworthy that the data indicating that branched F-actin is a negative regulator of ciliogenesis comes entirely from studies in mono-ciliated cells in culture conditions. Ciliogenesis in these cells is studied largely in the context of the stress response to serum starvation, which induces cell cycle arrest and ciliary biogenesis. This suggests, that the observed negative regulation of ciliogenesis by branched actin might be a reflection of the cytoskeletal remodeling required when a cell undergoes a transition from cycling/growing to quiescence. Given that this transition likely requires extensive actin remodeling, cells with reduced actin polymerization potential, and as a result, sparser branched actin networks might be able to accomplish remodeling and centrosome repositioning more rapidly, due to decreased depolymerization requirements. The finding that branched actin inhibits formation of ciliogenic reservoirs in the cytoplasm (Kim et al., 2010a), strongly suggest that actin dynamics play a role in organizing cytoplasmic trafficking during ciliogenesis. Therefore, a commitment by the cell to the ciliogenic program

would require significant remodeling of the cytoskeleton. The problem is clearly one of actin dynamics, given the demonstrated role for both polymerization and de-polymerization of actin during ciliogenesis.

Other properties of actin networks may also play a role in ciliogenesis. Indeed, an elegant study by Pitaval et al. found that the spatial confinement and contractile tension of cells are critical regulators of both the actin cytoskeleton and ciliogenesis. Using micro-printed patterns of defined diameter, the authors of this study found that spatially constrained cells had actin networks of low contractility, as well as high incidences of ciliogenesis. Spread cells, conversely, exhibited highly contractile actin networks and reduced ciliation. To test if actin contractility levels and ciliogenesis were related, spread cells were treated with either Y27632 or Blebbistatin to reduce MyoII activity. Treated cells exhibited a marked increase in ciliation percentage and in the rate of ciliogenesis. The same effect was observed in spread cells plated on soft substrates (Pitaval et al., 2010). These observations are in line with the studies, mentioned above, which suggest that actin stress fibers and ciliogenesis are negatively correlated.

Increased actin contractility is also strongly correlated with failure in the correct positioning of basal bodies--the same defect observed in multiciliated cells with disrupted actin networks. It is tempting to speculate, therefore, that basal body positioning is the common thread, and that the dynamic remodeling of actin networks is required for this process. However, it should be noted that

while relaxation of actin contractility is sufficient to rescue basal body positioning it does not lead to the lengthened axonemes observed in cells with reduced branched actin polymerization (Pitaval et al., 2010). Truly dynamic studies of actin and basal body/centrosome positioning will be informative, as will a deeper understanding of how ciliogenic cargo interacts with the actin cytoskeleton. Such studies will be necessary to fully understand the link between actin dynamics and ciliogenesis.

1.4.4: Intraflagellar transport and axoneme extension

Early studies suggested that cilia grow from basal bodies by constant addition to the distal end of the axoneme (Rosenbaum and Child, 1967). Subsequent analysis of microtubule incorporation dynamics demonstrated that ciliary doublets are stable along the majority of their length, with tubulin subunit addition and turnover occurring only at the distal tip (Marshall and Rosenbaum, 2001; Marshall et al., 2005). Given that cilia are spatially constrained and lack ribosomes, they require the active trafficking of ciliary cargoes to the distal tip for continued outgrowth and maintenance. This trafficking is accomplished by the intraflagellar transport (IFT) system.

IFT was first observed as a “motility distinct from flagellar beating” in pioneering work from Kozminski and colleagues, who used differential interference

contrast microscopy to record bidirectional movement of granules along the flagella of the green alga *Chlamydomonas reinhardtii* (Kozminski et al., 1993). Shortly after that initial discovery, the same group reported that this motility required the action of a kinesin-like protein and a cytoplasmic dynein (Kozminski et al., 1995; Pazour et al., 1998). Subsequently, this kinesin was identified as a member of the heterotrimeric kinesin-II family (Cole et al., 1998). In addition, biochemical characterization linked IFT to a complex of polypeptides that co-sedimented at 16-17s (Cole et al., 1998; Piperno and Mead, 1997). It has since been demonstrated that IFT proteins are highly conserved across ciliated eukaryotic species, including vertebrates (Cole et al., 1998; Pazour et al., 2000; Briggs et al., 2004; van Dam et al., 2013).

The IFT system is now known to be composed of ~20 proteins, though the exact number differs between species (Bhogaraju et al., 2013a; Ishikawa and Marshall, 2011; Briggs et al., 2004). To be considered a *bona fide* member of the IFT system, a protein must physically interact with the original 16s-17s biochemical complex. Each protein in this complex is designated by its molecular weight, so that IFT80 stands for intraflagellar transport protein of 80 kD. The IFT proteins are known to form two sub-complexes, IFT-A (consisting of: IFT43, IFT121/IFT122B, IFT122/IFT122A, IFT139, IFT140, IFT144) and IFT-B (IFT20, IFT22, IFT25, IFT27, IFT46, IFT52, IFT54, IFT57, IFT70, IFT74/72, IFT80, IFT81, IFT88, and IFT172) (Ishikawa and Marshall, 2011). Evidence suggests that the IFT-A proteins are

predominately mediators of dynein-driven retrograde axonemal traffic, *i.e.* traffic from the distal tip of the axoneme to the cell body, whereas IFT-B proteins are important for kinesin-dependent anterograde movement to the distal tip (See below and (Ishikawa and Marshall, 2011)).

These IFT-A and IFT-B complexes, together, make up an IFT particle, and these particles multimerize to form large assemblies known as IFT trains, which are the functional unit of IFT driven axoneme growth (Fig. 4). The first microscopically observed IFT train is generally thought to be that seen in the electron microscopy of *Chlamydomonas* flagella published by Ringo in 1967, where, due to its unknown nature, it was simply called “opaque material next to the flagellar membrane (Ringo, 1967).” Since the discovery that these structures are composed of IFT proteins (Kozminski et al., 1993; 1995), significant inroads have been made into understanding the fine structure of these large molecular assemblies. These trains are generally on the order of hundreds of nanometers long, and seem to have some intrinsic periodicity (Kozminski et al., 1993; 1995; Dentler, 2005; Pedersen et al., 2006). A recent study by Piginio et al. quantified an impressively large number of trains by thin section electron microscopy in *Chlamydomonas* flagella and found that trains can be divided into two categories: short trains (~250 nm), and long trains (~700 nm). The short trains were more electron opaque and had an intrinsic periodicity of approximately 16 nm, whereas the long trains were less opaque and

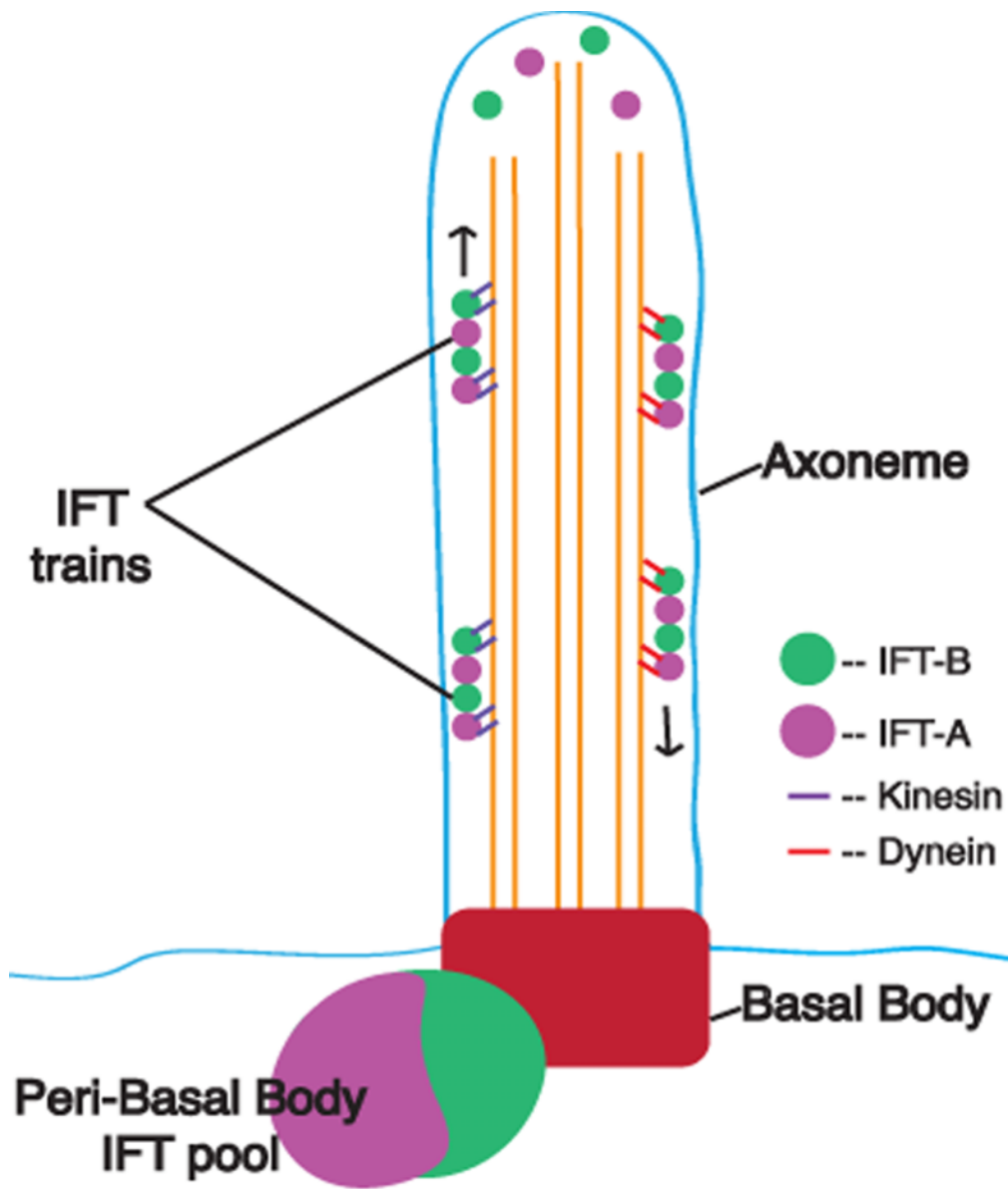


Figure 4: A schematic representation of IFT localization and dynamics. IFT proteins show two predominant localizations, large pools at the base of the cilia and a punctate distribution along the length of the axoneme. These puncta represent IFT trains, complex multi-protein assemblies that govern bi-directional transport within the axoneme. There are two classes of IFT proteins, anterograde IFT-B proteins, which mediate kinesin dependent transport to the distal tip, and retrograde IFT-A proteins which are necessary for the dynein-mediated return of trains to the deeper cytoplasm.

had a periodicity of about 40 nm (Pigino et al., 2009). These data suggest that these two categories of trains may represent different conformational states of IFT particles. The authors then analyzed IFT trains in *fla14* mutant *Chlamydomonas*, which lack the LC8 dynein light chain required for efficient retrograde IFT movement. In this context, there was a severe loss of short IFT trains, but an abundance of long trains (Pigino et al., 2009). One possible explanation for this shift in train abundance is that short and long trains might be responsible for retrograde and anterograde IFT movement respectively. Therefore, the loss of dynein activity could lead to a failure to form retrograde IFT trains. The loss of short trains could also be the result of non-specific defects in train assembly or maintenance (Pigino and Ishikawa, 2012). It has also been shown that IFT train length scales inversely with flagellar length (Engel et al., 2009), and given that the flagella of *fla14* mutants are approximately half length that of wild-type flagella, its possible that this loss of short trains simply reflects a scaling response. Finally, Pigino et al. used electron tomography to make 3D reconstructions of the longer IFT trains. This analysis showed that, as expected, IFT trains are made up of repeating units that make a series of connections to each other. One surprising result, however, is that instead of a single file train one particle wide, each repeating unit is actually made up of two IFT particles, such that the trains resemble a double column of repeating IFT particles (Pigino et al., 2009). It should be noted that the above data all come from *Chlamydomonas*, and it is therefore unclear how strictly these organizing principles

are conserved. However, the highly conserved nature of the IFT proteins themselves suggests that basic train organization, if not the length profile, is probably similar in other organisms, including vertebrates.

Within the axoneme IFT trains undergo a transport cycle consisting of several steps (Fig. 4). First, the train assembles from peri-basal body pools of IFT proteins in a poorly understood manner (Ludington et al., 2013; Deane et al., 2001; Ishikawa and Marshall, 2011). The train is subsequently injected into the axoneme in an uncharacterized manner, though it seems to depend on IFT concentration and actively overcomes diffusion barriers (Hu et al., 2010; Ye et al., 2013; Breslow et al., 2013; Dishinger et al., 2010). Next, the train undergoes a processive, kinesin-dependent anterograde movement from base of the cilia to the distal tip (Iomini et al., 2001). Once the train has reached the tip of the axoneme a series of poorly understood events occur. First the train unloads its cargos (tubulin dimers, for example) and picks up any ciliary turnover products, then it undergoes some kind of conformational or biochemical change, such that dynein is now the active motor and the train is in a retrograde conformation (Engel et al., 2009; Dentler, 2005). This switch between anterograde and retrograde modalities is thought to require the interaction between IFT172 and the EB1 and FAP256 capped microtubules of the distal ciliary tip (Pedersen et al., 2005; Schröder et al., 2011; Satish Tammana et al., 2013). Finally the train undergoes a processive retrograde motion to the ciliary base

and exits the cilium via an unclear mechanism (Engel et al., 2012; Iomini et al., 2009; Piperno et al., 1998).

While loss of a single IFT-B or IFT-A member is usually enough to halt anterograde or retrograde traffic respectively (Ishikawa and Marshall, 2011; Kozminski et al., 1995; Follit et al., 2006; Pedersen et al., 2005; 2006; Qin et al., 2011; Lucker et al., 2005), the functions of individual IFTs are not, on the whole, well characterized. Generally, IFT proteins are highly enriched for protein-protein interaction domains, e.g. coiled-coil, WD repeat, and tetratricopeptide repeat domains (Cole, 2003). This result is unsurprising, given that these proteins assemble into large trains and bind ciliary cargoes; it is also largely uninformative about the role of single IFT proteins within the assembly. Recent reports, however, have begun to parse this problem. IFT172, an IFT-B member, appears to be a regulator of the transition from anterograde to retrograde train conformations that occurs at the distal tip of the axoneme, though the mechanism of action for this process remains opaque (Pedersen et al., 2005). IFT27, another IFT-B has been recently characterized as a small GTPase with a role in the cell cycle (Qin et al., 2007), an interesting finding given the negative relationship between ciliogenesis and cell division (Ishikawa and Marshall, 2011; Garcia-Gonzalo and Reiter, 2012). IFT25 binds strongly to IFT27, and they seem to be obligate, as mice null for IFT25 also lack detectable IFT27 protein expression (Keady et al., 2012). Indeed, IFT27 is insoluble alone, but when co-expressed with IFT25, the two form a very stable

complex (Bhogaraju et al., 2011). This IFT27/25 complex is not required for IFT cycling dynamics in cilia, but is required for IFT-dependent Hedgehog signaling ((Keady et al., 2012), see below). The conservation pattern of IFT27 and IFT25 seems to reflect this Hedgehog functionality; they are present in vertebrates where they regulate Hedgehog signaling, but absent in *C. elegans* and *Drosophila*, which lack cilia-based Hedgehog signaling. Curiously, however, *Chlamydomonas* do have an IFT25/27 complex, suggesting that this explanation is incomplete (Keady et al., 2012). Other IFTs with known functions include: IFT70, an IFT-B required for the polyglutamylolation, and thus stabilization, of the B-tubule of ciliary doublets (Pathak et al., 2007; Fan et al., 2010), and IFT74 and IFT81 which cooperatively mediate tubulin binding and transport (Bhogaraju et al., 2013b).

When examined more generally, loss of anterograde IFT function leads to severe defects in ciliogenesis, as mutations in IFT-B components lead to very short or absent axonemes (Huangfu et al., 2003; Baker et al., 2003; Pazour et al., 2000; Friedland-Little et al., 2011; Ishikawa and Marshall, 2011). Loss of retrograde IFT-A components leads to generally milder, though still severe, ciliary phenotypes with half-length or shorter cilia with bulbous tips containing accumulated IFT-B machinery (Tsao and Gorovsky, 2008; Tran et al., 2008; Arts et al., 2011; Iomini et al., 2009). However, single null mutations in IFT144, or some IFT-A double mutants lead to an almost complete loss of the cilium (Liem et al., 2012). Recent work has

shown that the severity of structural outcomes is also reflected in the signaling functions of cilia, as detailed in the following section.

1.5: CILIA, IFT, AND HEDGEHOG SIGNALING

Members of the Hedgehog family of morphogens are potent developmental cues that must be processed in a heavily restricted spatiotemporal manner in order to achieve appropriate developmental outcomes. In the simplest representation of vertebrate Hedgehog signal transduction, the diffusible ligand Hedgehog binds to the cilia-resident receptor Patched, causing it to exit the cilium (Rohatgi et al., 2007) thus relieving its inhibition of Smoothened, which translocates into the cilium (Corbit et al., 2005). This leads to Smoothened-mediated repression of the proteolytic cleavage of the Gli transcription factors, which then undergo additional maturation into transcriptional activators (Niewiadowski et al., 2014), rather than becoming short-form repressors (McMahon et al., 2003; Scholey and Anderson, 2006; Eggenchwiler and Anderson, 2007). Forward mutagenesis screens in mice have revealed that vertebrate Hedgehog signals require cilia and IFT (Huangfu et al., 2003; Huangfu and Anderson, 2005; Tran et al., 2008; Qin et al., 2011; Ocbina et al., 2011), though their exact role remains unclear. Kathryn Anderson and colleagues have argued that IFT is not required for Hedgehog responsiveness by transport alone, but also as a result of its impact on ciliary structure, and by the

compartmentalization of the Gli transcription factors within the ciliary tip (Ocbina et al., 2011). However, they and others have also demonstrated that IFT-B is required for the localization of a number of Hh related proteins to the cilium (Ocbina et al., 2011; Liem et al., 2012; Keady et al., 2012; Haycraft et al., 2005; Tran et al., 2008).

One recent and counterintuitive finding stems from work from out of the Anderson and Eggenschwiler labs, where they have found that mutations in the retrograde IFT-A machinery lead to ligand-independent activation of the Sonic Hedgehog (Shh) pathway, and an expansion of Shh-dependent cell populations in the neural tube and limb of developing mice (Qin et al., 2011; Liem et al., 2012). Interestingly, this expansion of Shh-dependent fates is reversed in very strong alleles of IFT144, a core IFT-A retrograde component, and also in double mutants for other retrograde IFTs. In these cases, the Shh-dependent populations in the neural tube are absent (Liem et al., 2012). It is interesting that this phenotypic reversal is correlated with much stronger defects in cilia structure, especially given that it is the mutations in anterograde IFT resulting in very short or absent cilia which are also strongly deficient in Shh neural tube populations. Anderson and colleagues have argued that this is due to a gene-dose dependent depletion of ciliary integral membrane proteins, such as adenylyl cyclases, which are important in the transduction of Shh signals. (Liem et al., 2012) An alternative hypothesis is that strongly decreasing the retrograde IFT machinery leads to an increasing failure of

cycling dynamics and a resulting loss of Gli activation, or possibly a reduction in activated Gli translocation from the cilium to the nucleus, and thus results in greatly reduced Shh signal transduction.

Another direct link between IFT and Shh signaling comes from work out of the Yoder lab showing that the small IFT-B protein, IFT25 is required for Shh signaling. Interestingly, mice lacking IFT25 do not show any ciliary structural defects, and even appear to have normal IFT cycling. However, these mutants fail to appropriately localize Shh pathway members resulting in a failure of Shh signal transduction (Keady et al., 2012). Yoder and colleagues also show that IFT25 is found in vertebrates, but not in *Drosophila*, which uses a non-ciliary mechanism for Hedgehog transduction, or in *C. elegans* which does not seem to rely on Hedgehog signaling during development (Keady et al., 2012).

The link between IFT and Hedgehog signaling is well supported, but the precise nature of this link is still in dispute. As the above discussion highlights, the relationship is likely to be quite complex. A number of factors most likely feed into the transduction of Hedgehog, including localization of pathway members and the proximo-distal pattern of axonemes, both of which appear to be controlled by IFT.

1.6: MULTICILIATED CELLS

Multiciliated cells (MCCs) are a specialized population of post-mitotic cells that generate many dozens of cilia. These cilia are motile, and beat in a polarized and synchronized fashion to drive directed fluid flow across an epithelium. These cells are found in the ventricles and spinal cord of the vertebrate brain, in the mammalian airway, and in the oviduct/fallopian tubes. Therefore, dysfunction of MCCs is associated with defects in neural guidance, respiration, and fertility (Sawamoto et al., 2006; Wanner et al., 1996; Möller et al., 2004; Lyons et al., 2006). In addition, MCCs have recently been found to have some sensory and signaling functions (Shah et al., 2009). Despite their importance, MCCs are relatively poorly studied and we are only beginning to understand the mechanisms underlying their differentiation and maturation.

Mammalian models for the investigation of MCC biology face two difficulties: first, the generation of mammalian MCCs takes place during late embryonic and early postnatal development and the full articulation of ciliary tufts continues into adulthood. Second, these MCC populations are found in internal tissues, which prevents easy dynamic analysis. Despite these issues, a number of excellent studies of mammalian MCCs have been performed (see below and for e.g. (Tissir et al., 2010; Voronina et al., 2009)). In addition, You et al. developed an excellent primary culture model of the mouse tracheal epithelium (You et al., 2002), which has been used in a number of recent studies of MCC biology (see below and (Vladar et al., 2012; Vladar and Stearns, 2007)). An alternative model of basic MCC biology is the embryonic

epidermis of *Xenopus laevis*. Work from a number of labs has established *Xenopus* MCCs as a rapid and tractable experimental platform for the investigation of both the specification and basic cellular biology of MCCs (see below and (Werner and Mitchell, 2012)).

1.6.1: Transcriptional controls on multiciliogenesis

Given that the generation of dozens of cilia requires large populations of the basic machinery of ciliogenesis (e.g. tubulins, basal bodies, IFT proteins, dynein arms, etc.) it seems likely that there is a specialized transcriptional network activated during MCC specification and differentiation. The most upstream event of MCC biogenesis yet studied is the generation of MCC precursors. This process requires the activity of the Notch pathway in the *Xenopus* epidermis, the mouse airway, and the multiciliated cells of the zebrafish pronephros (Deblandre et al., 1999; Tsao et al., 2009; Rock et al., 2009; Liu et al., 2007). The lateral inhibition element of this pathway seems to be important, as overexpression of the Notch intracellular domain (ICD) leads to a reduction in the number of ciliated cells, and, conversely, repression of Notch signaling leads to an increased number of cells adopting an MCC fate (Deblandre et al., 1999; Stubbs et al., 2006; Tsao et al., 2009; Morimoto et al., 2010; Marcet et al., 2011). The upstream control of Notch in this context is still unknown, though a recent report suggests that the activity of the pathway is mediated in part by the micro RNA miR-449 (Marcet et al., 2011).

MCCs are often an intercalating population, *i.e.* they are specified in a deep layer of the epithelium and subsequently undergo an apical migration (sometimes referred to as radial intercalation) into the surface layer (Deblandre et al., 1999; Stubbs et al., 2006; Morimoto et al., 2010; Rock et al., 2009; Marcet et al., 2011). Control of intercalation and ciliogenesis appear to be tightly coordinated in MCCs. Recent evidence suggests that the Rfx2 transcription factor is involved in both of these processes, as knockdown of Rfx2 leads to failures in both intercalation and ciliogenesis (Chung et al., 2014). A screen for direct targets of Rfx2 uncovered several cytoskeletal regulators that potentially mediate radial intercalation. Many key players in ciliogenesis, including members of the IFT pathway, were also identified as targets of Rfx2 transcription (Chung et al., 2014). Unsurprisingly, Rfx2 was found to be required for ciliogenesis in a broad array of ciliated tissues in *Xenopus*, including the neural tube, the gastrocoel roof plate (analogous to the mammalian node), and the multiciliated cells of the embryonic epidermis (Chung et al., 2012). Other studies have shown that a number of Rfx family members are differentially required for ciliogenesis in many tissues and organisms (Piasecki et al., 2010). For example, Rfx3 is required broadly for motile multi-ciliogenesis in the mouse, including in the airway and in the ependymal cells lining the brain ventricles, and loss of Rfx3 function is associated with hydrocephalus (Didon et al., 2013; Zein et al., 2009; Baas et al., 2006). Rfx4 does not seem to be required for multiciliogenesis, but is required for the primary ciliogenesis in the neural tube, and

Rfx4 mutants have incorrect dorsoventral patterning as a result of defective Hedgehog signaling (Ashique et al., 2009).

Another key transcriptional effector of ciliogenesis is FoxJ1, which governs the articulation of motile cilia, including those of MCCs, in very evolutionarily distant organisms (Hagenlocher et al., 2013; Pan et al., 2007b; Vij et al., 2012; Gomperts et al., 2004; Yu et al., 2008; Stubbs et al., 2008). Strikingly, ectopic overexpression of FoxJ1 in the non-ciliated cells of the *Xenopus* embryonic epidermis leads to the generation of one or two motile cilia. FoxJ1 alone, however, is not capable of generating an ectopic MCC tuft, likely due to the fact that it does not lead to *de novo* production of basal bodies (Stubbs et al., 2008). However, multicilin, a recently discovered putative transcriptional co-activator, can generate an MCC like fate from non-MCC cells, and is required for ciliogenesis in fated MCCs (Stubbs et al., 2012). Additionally, the Myb transcription factor also has a role in the specification and/or elaboration of MCCs and appears to act downstream of multicilin (Tan et al., 2013). The overall regulatory cascade underlying the transcriptional control of MCC ciliogenesis remains unclear. It has been proposed that multicilin sits at the top of the cascade and activates Rfx2/3 and Myb, and that these in turn activate Foxj1. Together these factors then cooperate to transcribe the gene products necessary for ciliogenesis. However, this model awaits thorough experimental validation (Chung et al., 2014; Tan et al., 2013).

1.6.2: Cell biology of multiciliogenesis

While the developmental programs underlying MCC specification are becoming clearer, the cellular biology required for the generation and coordination of dozens of axonemes in a single cell is still a largely open question. One example is that of *de novo* basal body generation. Unlike cycling, mono-ciliated cells where one centriole gives rise to the cilium, terminally differentiated MCCs require the generation of many dozens of basal bodies (~150 on average in a *Xenopus* epidermal MCC) (Sorokin, 1968; Klos Dehring et al., 2013). The first insights to the process came from early electron microscopy work in various multiciliated tissues including the mammalian lung (Sorokin, 1968), the avian trachea (Kalnins and Porter, 1969), and oviduct (Dirksen, 1971). These studies revealed that many basal bodies could be synthesized in the cytoplasm. Further, these new basal bodies were not templated by the existing centrioles, but rather by an indistinct but electron opaque structure termed the deuterosome, the molecular nature of which has remained elusive. Recently, an exciting study from Klos Dehring et al. reported the first known deuterosomal molecule, the coiled-coil domain containing protein CCDC78. This protein localizes to acentriolar structures in the cytoplasm of *Xenopus* MCCs, and knockdown leads to a reduction in centriole number. Further CCDC78 is required to localize Cep152 to deuterosomes, which in turn activates polo-like kinase 4 to drive SAS-6 dependent basal body biogenesis (Klos Dehring et al., 2013). It remains to be seen how deuterosome formation and function is controlled at a

transcriptional level, though CCDC78, at least, appears to be downstream of multicilin (Klos Dehring et al., 2013). The identification of the first *bona fide* component of this long intractable structure opens the door to sophisticated proteomic and cell biological analysis of a process central to MCC function.

Once basal bodies have formed, they must undergo migration in order to dock with the apical surface of the MCC. Again, the precise mechanisms of this process have yet to be worked out. Early experiments in the quail oviduct using pharmacological agents to perturb cytoskeletal elements showed that basal body docking depended upon actin filament assembly but not microtubule polymerization (Boisvieux-Ulrich et al., 1990; Lemullois et al., 1988; Sandoz et al., 1988). More recently it has been shown that FoxJ1-mediated apical Rho activation is required to build an apical actin network that is necessary for basal body docking in airway epithelial cells (Brody et al., 2000; Pan et al., 2007a; You et al., 2004). Further evidence of a role for actin networks in basal body docking comes from a recent study of focal adhesion complex proteins in *Xenopus* MCCs, where knockdown of Focal Adhesion Kinase disrupts basal body to actin network connections and leads to a failure of basal body apical migration (Antoniades et al., 2014). In another recent study, Nucleotide binding protein 1 (Nubp1) was shown to regulate an internal actin network that anchored basal bodies to the cell cortex during MCC intercalation. Disruption of Nubp1 led to a disorganized actin mesh, and a failure of basal body migration without disrupting the localization or activation of Rho

(Ioannou et al., 2013). Finally, the planar cell polarity proteins Dishevelled and Inturned (see below) are required for actin organization and the apical activation of Rho in *Xenopus* MCCs (Park et al., 2008).

Another key aspect of MCC development is the polarization of cilia. In order for MCCs to effectively generate fluid flow, all of the axonemes within a cell must beat in a synchronized and polarized fashion. Newly intercalated MCCs show only a weak polarization, with many axonemes not yet properly oriented. As the MCC matures these axonemes are reoriented until all the axonemes of the cell beat in a single direction (Mitchell et al., 2007; Boisvieux-Ulrich et al., 1985). This reorientation of cilia is accomplished through a positive feedback mechanism, where the weak, but directional, flow of the early axonemal tuft directs the reorientation of axonemes into the correct conformation. This was experimentally demonstrated in an elegant study where fluid flow was externally reversed across explanted MCCs, which caused cilia to reorient opposite to their normal direction in response. Such reorientation only occurred when cilia were motile, as experimental ablation of dynein arms and other key motility components led to a general failure in axonemal polarization (Mitchell et al., 2007). The mature polarity is actively maintained, as demonstrated by a study of the coiled-coil containing protein Bbof1. Loss of Bbof1, a Foxj1 target gene, does not interfere with the initial weak polarization of immature MCCs, but does lead to a failure to refine cilia polarity. Further, Bbof1 knockdown cells are capable of undergoing flow-mediated

reorientation to achieve strong polarity similar to that of mature MCCs, however they are incapable of maintaining that polarity once artificial flow is no longer applied (Chien et al., 2013).

Cytoskeletal organization is also a key regulator of ciliary polarity in MCCs. Early electron microscopy work showed that basal bodies are closely associated with both actin and microtubule networks, and early Cytochalasin D experiments suggested that the actin network was important for ciliary polarity (Boisvieux-Ulrich et al., 1990; Lemullois et al., 1988; Sandoz et al., 1988). More recently, a careful set of pharmacological experiments demonstrated differential roles for actin and microtubule networks in the refinement of cilia polarity. In *Xenopus* MCCs, apical actin is localized in two distinct populations, an apical actin meshwork, and a sub-apical set of actin links between neighboring cilia. Doses of cytochalasin D that specifically perturb this sub-apical population were shown to lead to global defects in cilia polarity within an MCC. That is, the cilia of the MCC still exhibited an initially biased polarity, but failed to undergo refinement (Werner et al., 2011). Additionally, the Dishevelled/Active RhoA cassette mentioned above is required for actin meshwork establishment and polarization of cilia, in addition to its role in basal body docking (Park et al., 2008). In contrast to the global refinement defects resulting from disruption of actin networks, treatment of MCCs with the microtubule de-polymerizer nocadazole led to a disruption of local polarity; *i.e.*

neighboring cilia were oriented randomly with respect to one another, ablating even the modest polarization bias of early MCCs (Werner et al., 2011).

In addition to intracellular polarization, where the cilia of a single MCC establish a refined and unidirectional aspect, MCCs must also be polarized at the tissue level so that coordinated beating can lead to directed and productive fluid flow across the epithelium. In the *Xenopus* embryonic epidermis, MCCs polarize after they intercalate and do so in response to established polarity cues. Epidermal regions with disrupted planar cell polarity (PCP) organization, accomplished by knockdown or overexpression of the transmembrane proteins Frizzled 3 (Fz3) or Van Gogh Like 2 (Vangl2), showed non-autonomous defects in MCC orientation. Interfering with Dishevelled function, on the other hand, led to cell autonomous MCC polarization defects, as expected given its role in basal body orientation (Mitchell et al., 2009). This tissue-level planar cell polarity information seems to inform ciliary orientation via specialized microtubules linking the apical cytoskeleton of MCCs to the asymmetric protein domains delimited by PCP proteins (Vladar et al., 2012). The PCP proteins Vangl2, Dvl1, Celsr2, and Celsr3 all have a demonstrated requirement in MCC polarization in murine ependymal cells, suggesting a conservation of this polarization paradigm across tissues and vertebrate species (Guirao et al., 2010; Hirota et al., 2010; Tissir et al., 2010).

While many aspects of multiciliogenesis are becoming clearer, thanks to excellent work from a number of labs, there are still many open questions: How is

the transcriptional cascade of multiciliogenesis initiated? What proteins compose the deuterosome, and how is the biogenesis of this structure regulated? What aspects of actin regulation are important for basal body docking and migration? How is the basic machinery of axonemal outgrowth, IFT, regulated in multiciliated cells? These and many other questions provide exciting avenues into understanding the biology of MCCs, which are key players in neurogenesis, respiration and fertility (Sawamoto et al., 2006; Lyons et al., 2006; Afzelius, 1976).

1.7: PLANAR CELL POLARITY AND CILIOGENESIS

The term planar cell polarity (PCP) refers to a property of cells, whereby they exhibit differential pattern or activity within the plane of the tissue. In addition, PCP refers to a conserved set of proteins, initially discovered in forward screens in *Drosophila*, that govern this planar polarization in many—but not all—contexts (see (Wallingford, 2012; Gray et al., 2011; Bayly and Axelrod, 2011) for recent reviews).

The PCP proteins can be broadly divided into two groups. Core planar cell polarity proteins are asymmetrically localized and help differentiate the planar poles of the cell. These include the transmembrane proteins of the Frizzled (Fz), Celsr, and Van Gogh-like (Vangl) families, and the cytoplasmic proteins Dishevelled and Prickle. The second group of proteins includes downstream

effectors of the core PCP network. These include Fuzzy (Fuz), Inturned (Intu), and Fritz (also called WDPCP) (Wallingford, 2012).

Both core and effector PCP proteins seem to have roles in ciliogenesis. Frizzled and Dishevelled have been implicated in the assembly of the apical actin meshwork required for ciliogenesis in multiciliated cells (see above and (Oishi et al., 2006; Park et al., 2006)). The cadherins Celsr2 and Celsr3 appear to mediate apical docking of basal bodies, as well as the polarization of Frizzled3 and Vangl2 (Tissir et al., 2010).

Interestingly, the PCP effector proteins seem to play differential roles in the process of ciliogenesis. Inturned appears to cooperate with Dishevelled to coordinate apical RhoA activity and basal body docking (Park et al., 2006; 2008). The WD repeat containing protein Fritz (also known as WDPCP) seems to govern the assembly of a septin diffusion barrier at the base of cilia (Kim et al., 2010b). Finally, the novel protein Fuz appears to mediate both cytoplasmic and axonemal trafficking events during ciliogenesis (see Chapter 2 and (Park et al., 2006; Gray et al., 2009)).

While the unifying principles underlying PCP mediated ciliogenesis--if, indeed, any such exist--remain obscure, it is noteworthy that so many of the constituent components of the pathway converge on the biogenesis of this organelle. Future work utilizing unbiased proteomic approaches will hopefully provide insights into the logic of this phenomenon.

1.8: CONCLUDING REMARKS

The cilium is clearly a complex organelle, both structurally and functionally, and it is easy to see why it has fascinated generations of biologists. From early electron microscopic studies of the ultrastructure of the organelle (Sorokin, 1962; Sotelo and Trujillo-Cenóz, 1958b; Ringo, 1967), to the first genetic and biochemical mappings of the machinery involved in its outgrowth (Rosenbaum and Child, 1967; Kozminski et al., 1993; Piperno et al., 1977), to the discovery that it plays critical roles in developmental signal processing and human health (Huangfu et al., 2003; Waters and Beales, 2011), to the renewed flurry of interest in the molecular and transcriptional mechanisms underlying its biogenesis and maturation (Garcia-Gonzalo et al., 2011; Ludington et al., 2013; Engel et al., 2012; Baker et al., 2003; Follit et al., 2008), this small protrusive outgrowth continues to fascinate and surprise. While much has been learned about cilia, there are still any number of questions regarding every aspect of their structure and function.

Chapter 2: Control of vertebrate intraflagellar transport by the planar cell polarity effector Fuz

Portions of this chapter are modified with permission from: Brooks, ER and Wallingford, JB. Control of Vertebrate Intraflagellar Transport by the Planar Cell Polarity Effector Fuz. J Cell Biol. (2012) 198 (1) 37-45

2.1: THE PLANAR CELL POLARITY EFFECTOR FUZ IS REQUIRED FOR VERTEBRATE CILIOGENESIS

Initially discovered in screens for polarity mediators in *Drosophila* wing hairs (Collier and Gubb, 1997), Fuz is a protein that is conserved across vertebrates, and in flies, but with no apparent orthologue in *C. elegans* or *Chlamydomonas*. In vertebrates--including humans--Fuz is required for primary ciliogenesis and, therefore for appropriate Hedgehog signaling (Fig 5; and see (Gray et al., 2009; Park et al., 2006; Heydeck et al., 2009; Seo et al., 2011). In addition studies have shown that Fuz is required for the biogenesis of the multiple cilia of multiciliated cells (MCCs), indicating that Fuz is generally required for ciliogenesis (Fig. 5). However, the precise function of Fuz during ciliogenesis remains unclear (Park et al., 2006; Gray et al., 2009), though preliminary evidence suggests it localizes to basal bodies, indicating that it may function at the ciliary base (Michinori Toriyama, personal communication).

Primary sequence analysis of the Fuz protein revealed almost no known motifs, other than a short putative N-terminal trans-membrane region (Collier and

Gubb, 1997; Gray et al., 2009). However, predictive 3D structure analysis suggested that the C-terminus of Fuz may fold into a Longin domain, a motif of alpha-helices flanking beta sheets, which is conserved only at the tertiary level (Gray et al., 2009; Rossi et al., 2004), and are found in proteins that play a role in vesicular trafficking (e.g. SNAREs (Rossi et al., 2004; De Franceschi et al., 2014)). The observation of a putative Longin domain in Fuz, along with other predictive functional networking data suggest that Fuz may play a role in cytoplasmic trafficking functions (Gray et al., 2009). This hypothesis is supported by a failure in the exocytosis of mucous granules in the non-ciliated goblet cells of *Xenopus* with reduced Fuz function (Gray et al., 2009). Additionally the MCCs of Fuz exhibit defects in the cytoplasmic localization of the microtubule bundling protein CLAMP (Gray et al., 2009). However, the pathways influenced by Fuz during ciliogenesis remain obscure.

2.2: FUZ IS REQUIRED FOR APPROPRIATE PROXIMO-DISTAL PATTERNING OF AXONEMES

As mentioned in Chapter 1, the key axis of ciliogenesis is proximal-distal, with proximal indicating the cell body, and distal indicating the tip of the axoneme. Interestingly, cilia present with a highly ordered molecular pattern along this axis, with various dynein isoforms and motility factors distributed in a highly stereotyped manner (Panizzi et al., 2012; Tarkar et al., 2013; Guichard et al., 2001; Chung et al., 2014). Defects in this pattern in humans results in primary ciliary

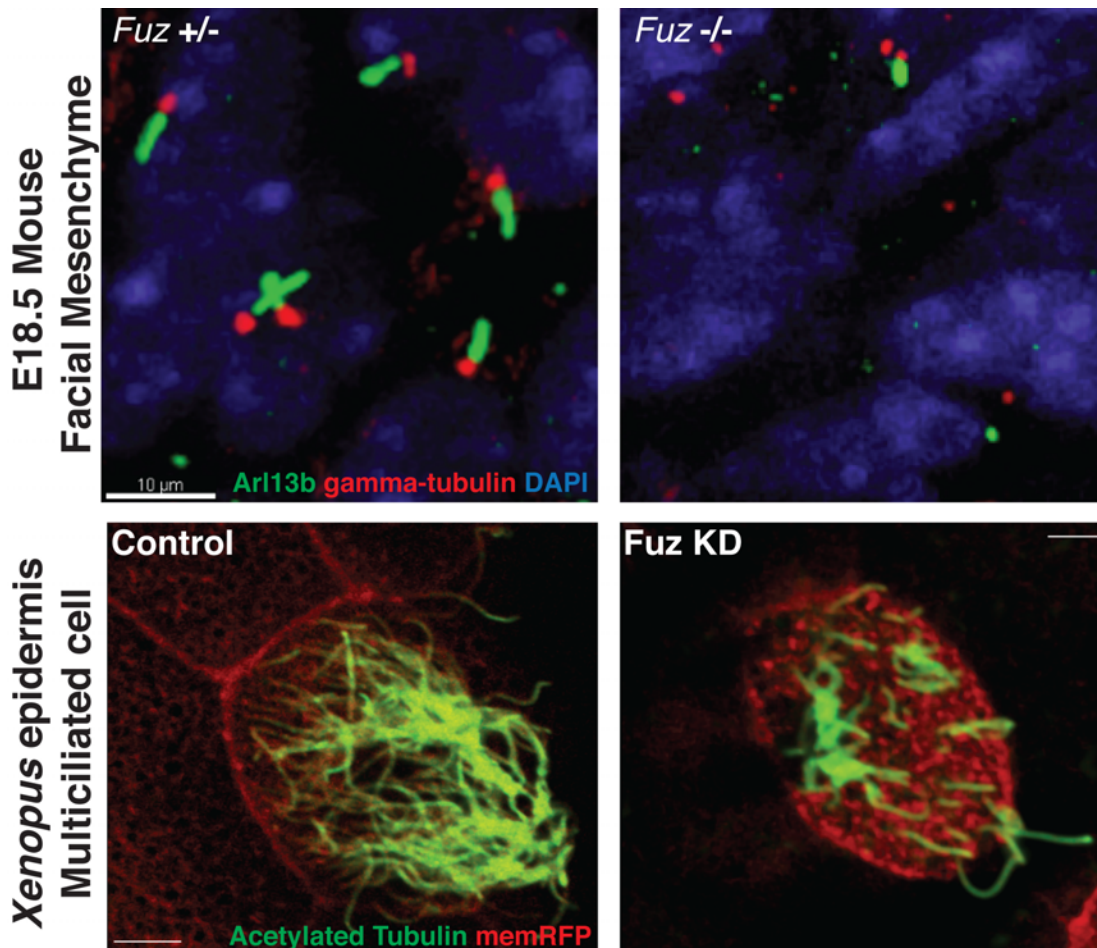


Figure 5: Fuz is required for ciliogenesis in multiple tissue types. The upper panels are representative slices of the facial mesenchyme of E18.5 mice stained with antibodies against the axonemal protein Arl13b, the basal body protein gamma-tubulin, and counterstained with DAPI. The panel on the left is from a heterozygous control animal, while the panel on the right is from a homozygous Fuz mouse with a gene trap that is predicted to result in null functionality. Notice the reduced number of ciliated cells, and the poor morphology of the residual cilia. The bottom panels are representative *Xenopus* epidermis multiciliated cells (MCCs) stained with acetylated tubulin, and using membrane-tethered RFP as an injection tracker. Notice the reduced number and impaired morphology of cilia in the Fuz KD MCC. Scale bars represent 10 µm in upper panels and 5 µm in lower panels.

dyskinesia, a disorder that presents with respiratory and fertility defects (Guichard et al., 2001; Panizzi et al., 2012; Sleight, 1981). In addition, it has been shown that ciliary outgrowth occurs exclusively at the distal tips of axonemes (Rosenbaum and Child, 1967; Marshall and Rosenbaum, 2001). Therefore, I set out to understand if Fuz function was required for appropriate proximal-distal patterning in axonemes.

Previous work established that Fuz governs the distal enrichment of the microtubule bundling protein CLAMP at the tips of cilia (Fig. 6a, b; (Gray et al., 2009)), reminiscent of the localization of microtubule end-binding proteins in cilia (Pedersen et al., 2005; 2003; Schröder et al., 2011). In order to further characterize the role of Fuz in ciliary patterning, I undertook a quantitative examination of CLAMP localization within the axonemes of control and Fuz knockdown multiciliated cells.

As demonstrated in Fig 6 and 7, RFP-CLAMP weakly decorates the entire length of the axoneme, but is very highly enriched in the distal most region. Given that this domain of enrichment was of a consistent length between axonemes and from cell to cell (~2µm; ~16% of total axoneme length; Fig 6a, 7a, 8a, Fig 9a), I refer to this enrichment as the CLAMP compartment.

I next quantified the effect of Fuz knockdown (KD) on this compartment using a previously validated Fuz anti-sense morpholino oligonucleotide (Gray et al., 2009). Fuz knockdown led to a significant reduction in the absolute length of the CLAMP compartment as compared to controls (~60% reduction, Fig 6a vs Fig 6b;

Fig 7a' vs Fig 7b', Fig 8a). Because Fuz KD also significantly disrupts axoneme length (Fig 8c), it was possible that this shortening of CLAMP enrichment simply reflected the reduction in axoneme length. However, when I examined the percentage of the axoneme occupied by this compartment, I found that it was significantly reduced in Fuz KD axonemes as compared to controls (~10% axoneme length in Fuz KD vs. ~16% in controls; Fig 6b' vs. 6a', and see Fig. 9a). Additionally, this compartment was completely absent in many Fuz KD axonemes (Fig. 6b; 7b, b'; 8a). Together these data suggest that Fuz function is required for the enrichment of CLAMP at the distal tip of axonemes, indicating that it may play a role in patterning distal axonemal identity.

I next asked if loss of distal enrichment was specific to CLAMP or if it represented a more general defect in the distal identity of the axoneme, and therefore a more general role for Fuz in patterning this axonemal compartment. To do so, I assayed the enrichment of another microtubule binding protein, EB3, which localizes to the distal tips of cilia and is required for normal cilia structure (Schröder et al., 2011). I found that GFP-EB3 is enriched in the same distal domain as RFP-CLAMP, and further, that the length of the GFP-EB3 compartment was reduced more than 60% upon Fuz KD (Fig. 8f).

These data could reflect a role for Fuz in the control of distal axoneme identity, or--alternatively--a more general role for Fuz in ciliary protein localization. To address this issue, I examined the localization of the microtubule-binding domain

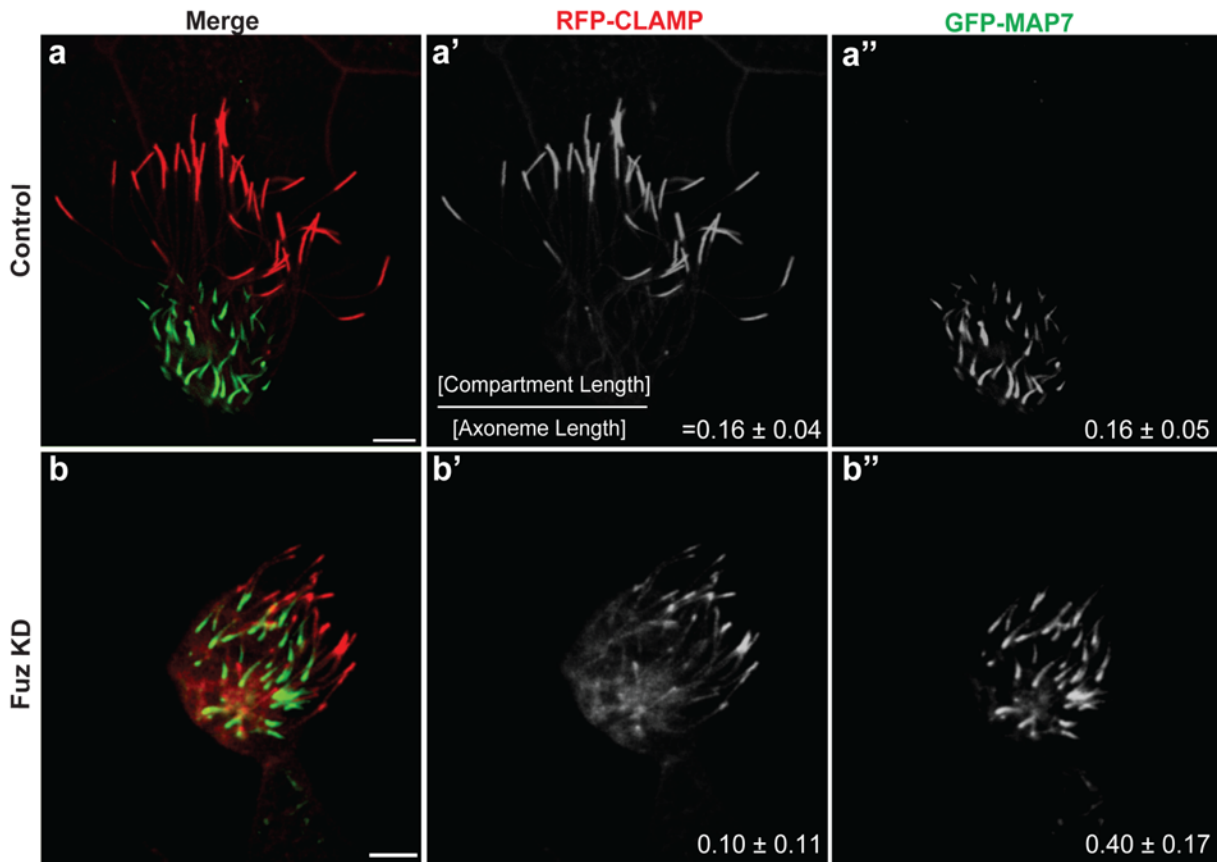


Figure 6: Axonemes in *Xenopus* MCCs display a highly stereotyped proximal-distal organization, and this organization is disrupted upon Fuz KD. **(a)** Cilia on a control multi-ciliated cell expressing CLAMP-RFP (red, **a'**) to label the distal axoneme and MAP7-GFP (green, **a''**) to label the proximal axoneme. **(b)** Cilia on a Fuz KD vertebrate multi-ciliated cell expressing CLAMP-RFP (**b'**) and MAP7-GFP (**b''**). See also Fig. 7a, b. The average percent axoneme length \pm SD occupied by the CLAMP or MAP7 domains are indicated in the bottom right of panels **a'** (n=54), **a''** (n=130), **b'** (n=52), **b''** (n=130) (see Fig. 9a, b for quantitation; only axonemes whose whole length was obvious were used for this analysis, the compartment analysis for this data set is shown in Suppl. Fig. 9c). Scale bars represent 3 μ m.

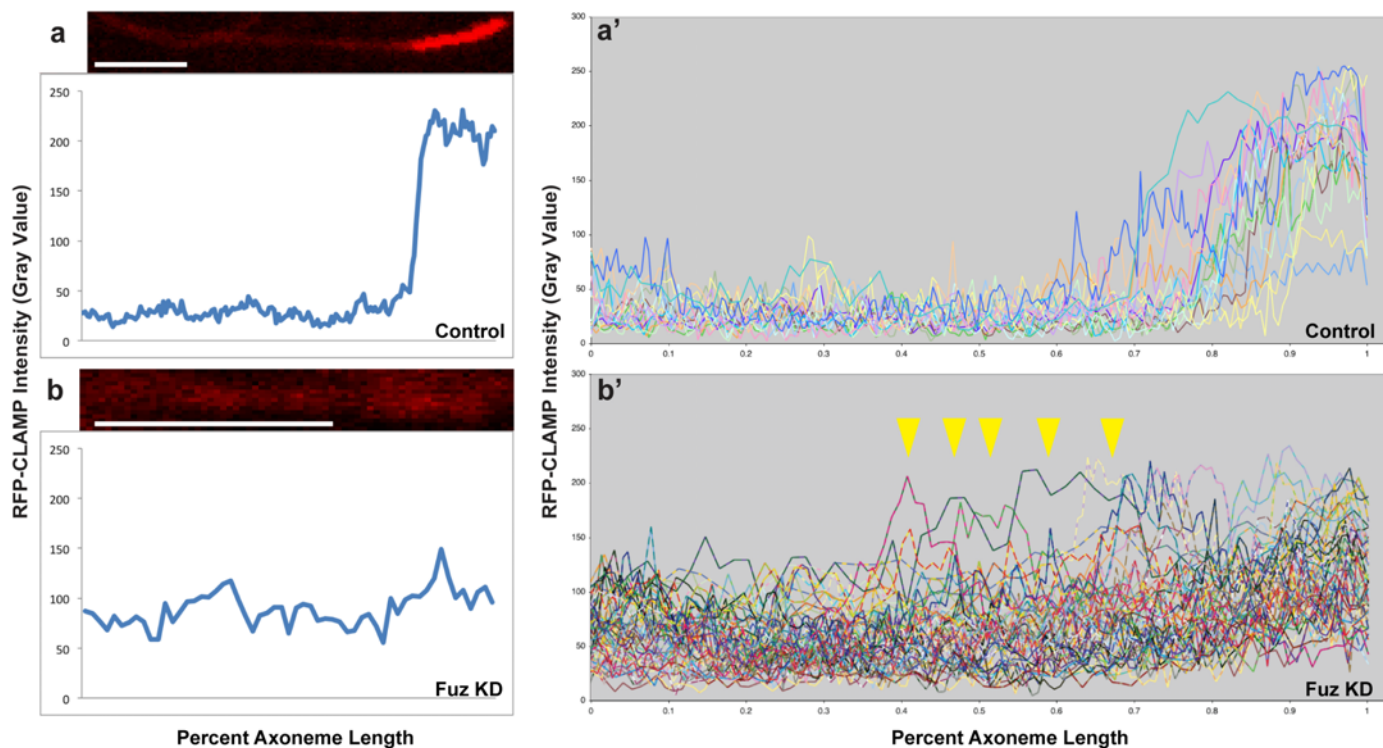


Figure 7: Intensity profiles of CLAMP-RFP along the length of axonemes reveal a role for Fuz in the distal enrichment of CLAMP. **(a)** An axoneme from a control multiciliated cell expressing CLAMP-RFP and its corresponding intensity profile, note the very sharp border between enriched distal axoneme, and un-enriched proximal axoneme. **(a')** A collection of CLAMP intensity profiles from control axonemes. Each profile is normalized as a percentage of length to allow for comparison between axonemes. **(b)** An axoneme from a Fuz KD multiciliated cell and its associated intensity profile, note the loss of distal enrichment. **(b')** A collection of intensity profiles from Fuz KD axonemes. Note the decreased tendency to be enriched distally, and the ectopic enrichments of CLAMP proximally. Scale bars represent 3 μm .

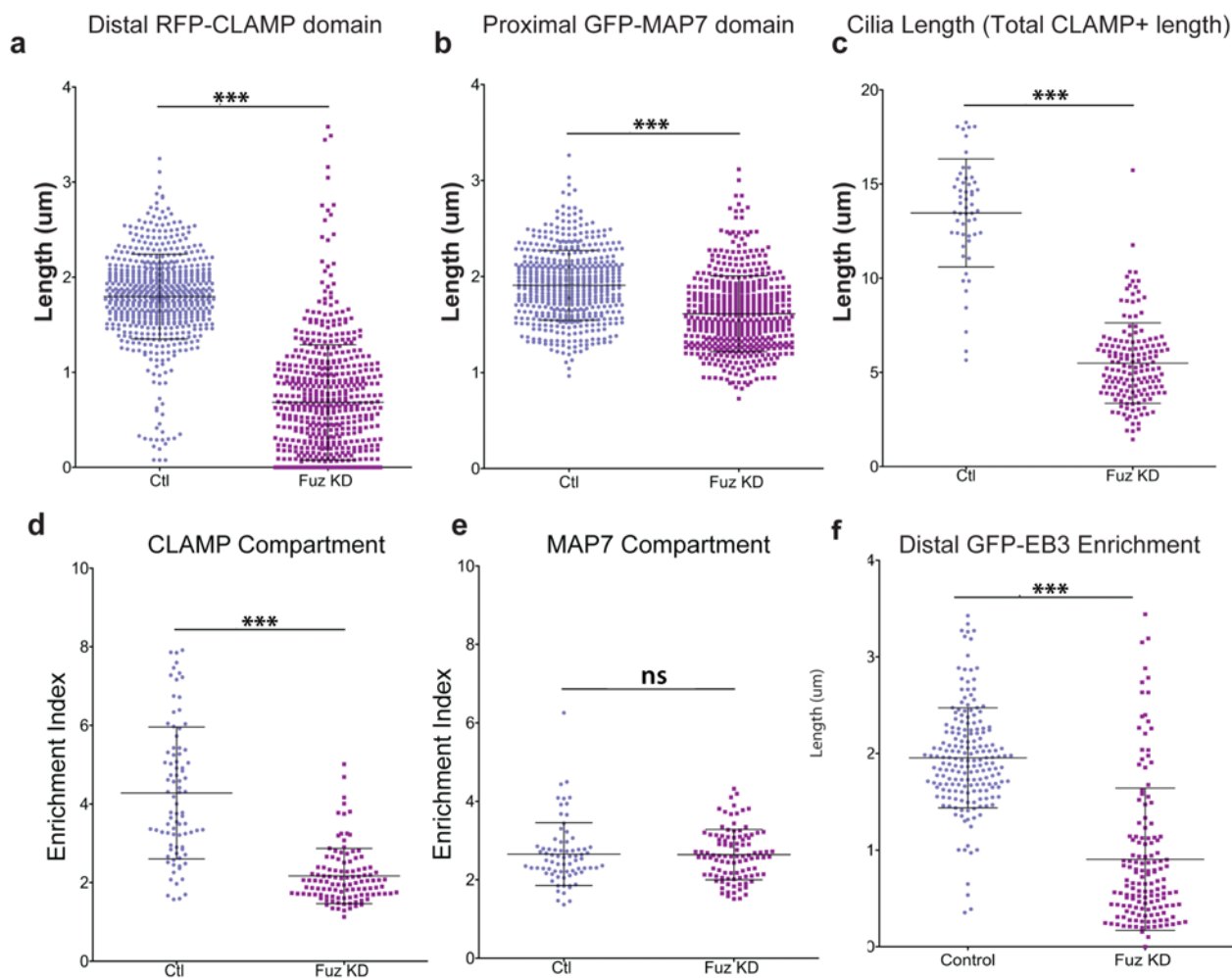


Figure 8: Quantification of ciliary compartments in control and Fuz KD axonemes. (a) Graph of distal RFP-CLAMP compartment length of control and Fuz KD cells. RFP-CLAMP compartment length is severely reduced in Fuz KD cells as compared to controls. (Fuz KD: mean \pm SD = 0.68 ± 0.61 , n=652 vs. Ctl: 1.80 ± 0.45 , n=582; $p < 0.0001$). (b) Graph of proximal GFP-MAP7 compartment length. GFP-MAP7 compartment length is only modestly reduced in Fuz KD cells as compared to controls (Fuz KD: mean \pm SD = 1.61 ± 0.39 , n=523 vs. Ctl: 1.91 ± 0.36 , n=516; $p < 0.0001$). (c) Total ciliary length (as measured by RFP-CLAMP) is reduced in Fuz KD axonemes as compared to controls (Fuz KD: mean \pm SD = 5.49 ± 2.14 , n=54 vs. Ctl: 13.46 ± 2.87 , n= 161; $p < 0.0001$). (d) Fuz KD axonemes show reduced enrichment of RFP-CLAMP signal in the distal domain over basal axoneme levels as compared to controls. Enrichment Index = (mean intensity compartment) / (mean intensity of an equivalent length of non-enriched axoneme, see Fig 9d). Fuz KD enrichment index: mean \pm SD = 2.17 ± 0.70 , n=113 vs. Ctl enrichment index: 4.28 ± 1.68 , n=87; $p < 0.0001$. Note that only axonemes with discernable distal RFP-CLAMP compartments were used for this analysis. (e) There is no change in the enrichment of the MAP7 compartment between control and Fuz KD axonemes (Fuz KD enrichment index: mean \pm SD = 2.64 ± 0.64 , n=102 vs. Ctl enrichment index: 2.65 ± 0.80 , n=75; $p = 0.6508$). (f) EB3, another marker of the distal compartment is also severely reduced (54% average reduction; Fuz KD: mean \pm SD = 0.91 ± 0.74 , n=146 vs. Ctl: 1.96 ± 0.52 , n=189; $p < 0.0001$).

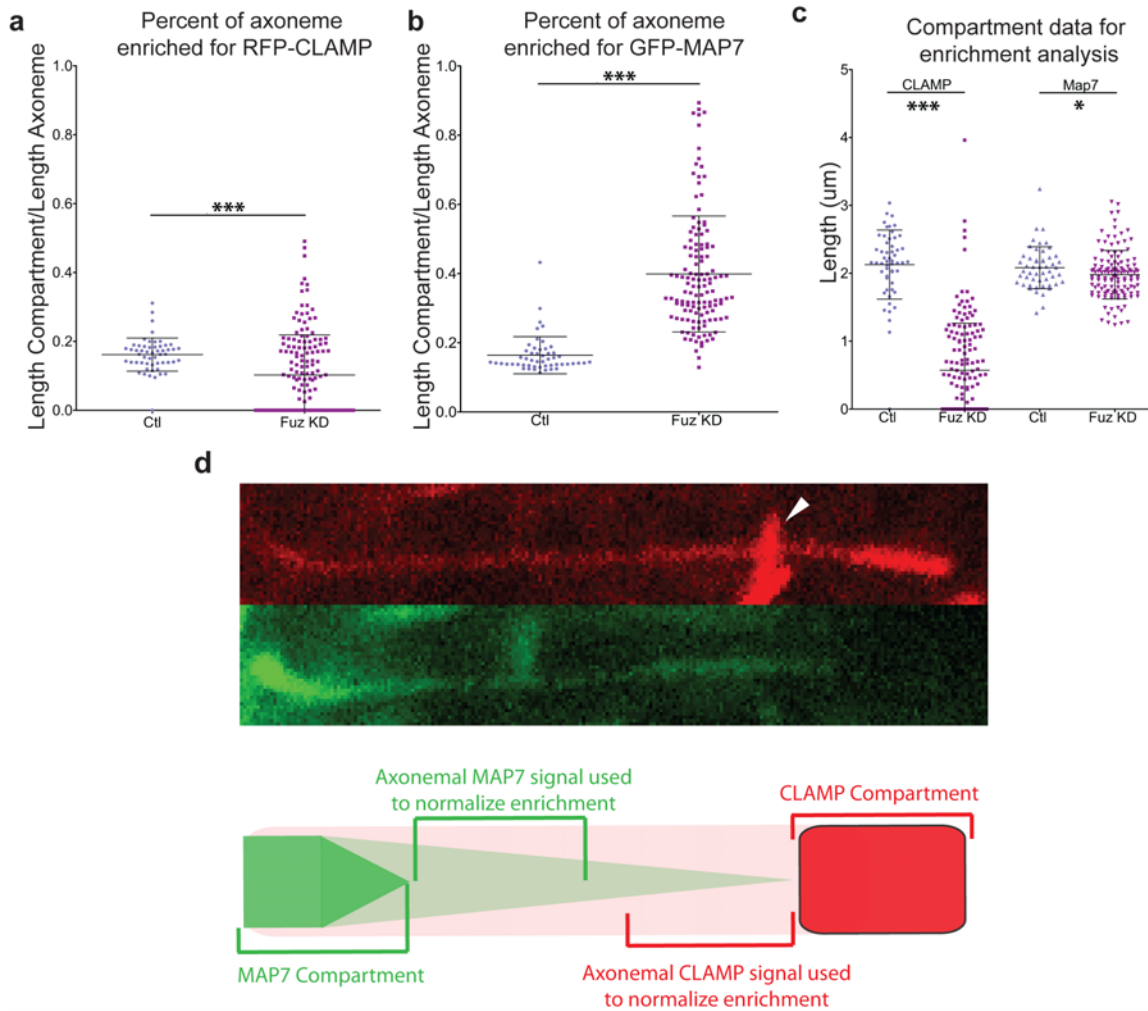


Figure 9: Quantification of compartment occupancy of axonemes. **(a)** The percentage of the axoneme occupied by the enriched CLAMP compartment is decreased upon Fuz KD (37% reduction, Fuz KD: mean \pm SD = 0.10 ± 0.12 , $n=161$ vs. Ctl: 0.16 ± 0.05 , $n=54$; $p<0.0001$). **(b)** The percentage of the axoneme occupied by the enriched MAP7 domain is increased upon Fuz KD (59% increase, Fuz KD: mean \pm SD = 0.40 ± 0.18 , $n=130$ vs. Ctl: 0.16 ± 0.05 , $n=52$; $p<0.0001$). Note that this increase is not caused by a lengthening of the MAP7 compartment in absolute terms (Fig 9c). **(c)** A plot of the compartment lengths of the subset of CLAMP and MAP7 data where it was possible to also measure the full length of the axoneme (by RFP-CLAMP). These data were used to calculate the percent of axoneme length occupied by the compartments. I was unable to accurately measure the full length of short axonemes in control cells, as their signal was lost in the ciliary tuft. Therefore, the average length of the CLAMP domain is slightly elevated in this data set as compared to the whole data set presented in Fig 8. **(d)** Localization of RFP-CLAMP and GFP-MAP7 in a single axoneme. Note that each marker is highly enriched in a subset of the axoneme, but that both markers are also found at low levels outside of these enriched areas. The white arrowhead in the CLAMP panel indicates the tips of other cilia overlying the axoneme (note that in this case the intensity was measured proximal to these tips). The bottom panel schematizes this localization and describes how enrichment of the compartments was calculated.

of MAP7 fused to GFP, which strongly labels a domain in the proximal axoneme of *Xenopus* multi-ciliated cells (Fig 6a, a''; Fig 9d). MAP7-GFP was enriched in a consistent region from axoneme to axoneme and I designated this enrichment the MAP7 domain ($\sim 2\mu\text{m}$ and $\sim 16\%$ axoneme length, Fig. 6a'', 9b). In contrast to the CLAMP domain, the absolute size of the MAP7 domain was only slightly perturbed upon Fuz KD (Fig. 6b'' vs. a'', and see Fig. 8b and Fig. 9b). Due to the shortening of Fuz KD axonemes, however, the relative occupancy of the MAP7 domain was significantly increased ($\sim 40\%$ axoneme length in Fuz KD, compared to 16% in controls). Thus, disruption of Fuz appears to specifically perturb the distal ends of axonemes in multi-ciliated cells (Fig 6a vs. b), and the loss in axoneme length appears to reflect a specific loss of the more distal axoneme.

The loss of distal identity may reflect a defect in delivery of cargo destined for the CLAMP domain. In this case, a reasonable prediction is that the distal compartments in Fuz KD axonemes would be both shorter and contain a reduced amount of CLAMP. To test this prediction, I exploited the fact that RFP-CLAMP is enriched distally but also weakly labels the entire axoneme, and measured the intensity of the distal CLAMP domain normalized against the weaker signal in the proximal axoneme. The CLAMP domain in controls was enriched greater than four-fold on average over the more proximal axoneme (Fig. 8d; and see Fig. 9d for methodology). Strikingly, in Fuz KD cilia this value was reduced by roughly half (Fig.

8d). Importantly, a similar analysis of MAP7 enrichment showed no change between control and Fuz KD axonemes (Fig. 8e).

A trafficking defect within Fuz KD cilia might be expected to lead to ectopic CLAMP accumulations in the proximal axoneme. Indeed, examination of CLAMP-RFP intensity profiles along the length of control and Fuz KD axonemes reveals exactly this phenotype, with many KD axonemes exhibiting ectopic enrichments of CLAMP in areas proximal to the compartment (Fig. 7b'). Together, these data support a role for Fuz in maintaining ciliary trafficking to the distal axoneme and led me to propose that Fuz mediates axonemal trafficking during ciliogenesis, a process largely controlled by intraflagellar transport (IFT).

2.3: DEVELOPMENT OF AN *IN VIVO* SYSTEM FOR ANALYSIS OF IFT DYNAMICS IN MULTICILIATED CELLS

One of the key processes in ciliogenesis is intraflagellar transport (IFT, see above), and to date it has not been studied in an MCC context. Here, I report the development of a novel platform for *in vivo* imaging of IFT in the MCCs of the *Xenopus laevis* embryonic epidermis.

IFT is a highly dynamic, and processive transport system within ciliary axonemes (Fig. 10, and see, for e.g., (Kozminski et al., 1993; Besschetnova et al., 2010; Tran et al., 2008). Therefore, I used high-speed confocal microscopy to

directly observe GFP-labeled IFT trains in the MCCs of the *Xenopus* epidermis (Fig 10a; see materials and methods for a description of this technique).

Using GFP-IFT20--which labels trains moving in both directions--I found that IFT in the axonemes of *Xenopus* MCCs has a mean velocity of 0.84 $\mu\text{m}/\text{sec}$ in the anterograde direction, and 0.87 $\mu\text{m}/\text{sec}$ in the retrograde direction (Fig 10b; see Materials and Methods for a description of how rates were determined). While these velocities are far slower than in the green algae *Chlamydomonas* (~ 2 $\mu\text{m}/\text{sec}$ anterograde; ~ 4 $\mu\text{m}/\text{sec}$ retrograde) where IFT dynamics are best studied (Dentler, 2005; Kozminski et al., 1993; Ishikawa and Marshall, 2011), they are well in line with studies in *C. elegans* and vertebrate cell culture systems where IFT proceeds at ~ 0.7 $\mu\text{m}/\text{sec}$ in both anterograde and retrograde conformations (Besschetnova et al., 2010; Tran et al., 2008; Ou et al., 2005; Pan et al., 2006).

GFP-IFT20 also labels a pool at the the basal body, the site train assembly and disassembly (Ishikawa and Marshall, 2011), and I was able to visualize the injection of new anterograde IFT trains from the basal body pool into the axoneme and the return of retrograde particles into the basal body pool (Fig 11a, a'). I also observed a few cases of IFT trains pausing mid-axoneme before undergoing retrograde clearance (Fig 11b). While this behavior has been previously observed in *Chlamydomonas* (Dentler, 2005), it is a low-frequency behavior and its import is not understood. While these behaviors are not the focus of the studies reported here,

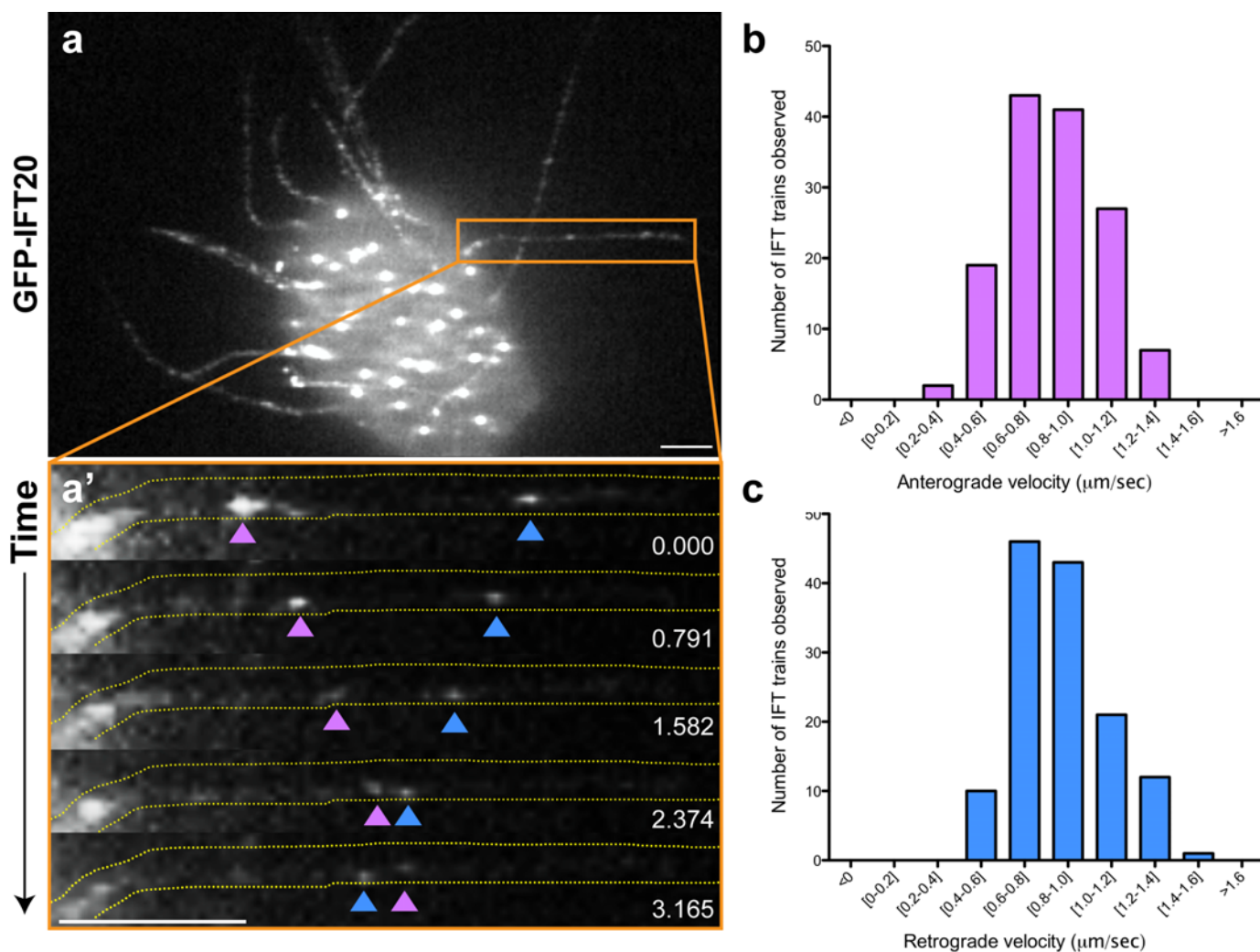


Figure 10: Analysis of Intraflagellar transport (IFT) dynamics in the multiciliated cells (MCCs) of the *Xenopus* epidermis. **(a)** A representative MCC of the Stage 26 *Xenopus* epidermis expressing GFP-IFT20 via targeted injection. Orange box indicates the region shown in **a'**. **(a')** A time series of bidirectional IFT movements within a single axoneme. Pink and blue arrowheads track a single anterograde and retrograde IFT train, respectively. **(b)** Histogram of anterograde rates of IFT in *Xenopus* multi-ciliated cells. **(c)** Histogram of retrograde rates. Mean velocities \pm SD are $0.84 \pm 0.22 \mu\text{m}/\text{sec}$ anterograde ($n=143$ trains from 24 cells, 6 embryos) and $0.87 \pm 0.22 \mu\text{m}/\text{sec}$ retrograde ($n=125$ trains from 25 cells, 6 embryos). Velocities ranged from 0.36 - $1.35 \mu\text{m}/\text{sec}$ anterograde and 0.42 - $1.43 \mu\text{m}/\text{sec}$ retrograde. Velocities were calculated as the average of three independent instantaneous velocities for each reported particle. Scale bars represent $3 \mu\text{m}$.

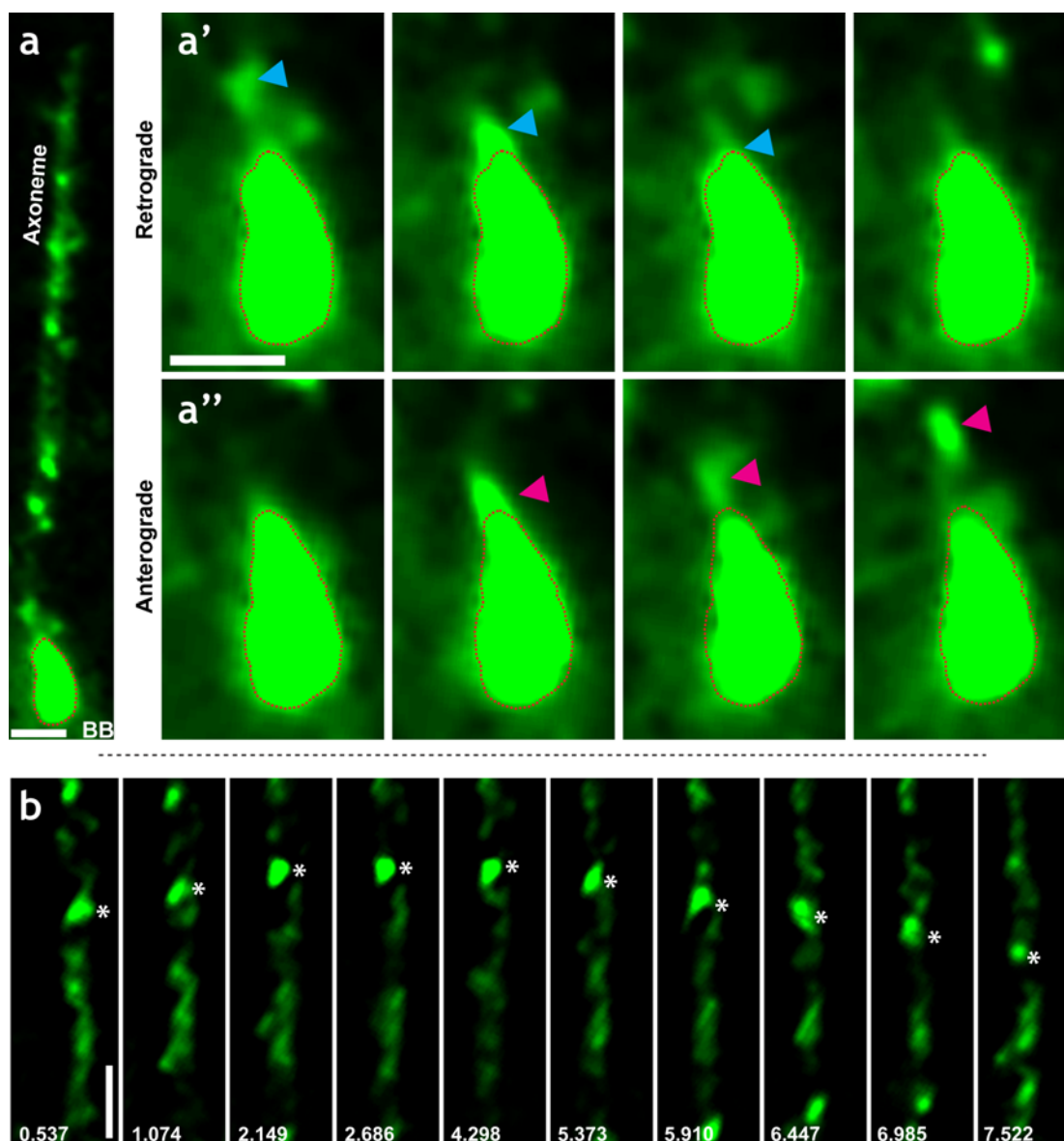


Figure 11: GFP-IFT20 behavior at the base and tips of axonemes. **(a)** Still frame from a high-speed confocal movie of a single axoneme from a GFP-IFT20 expressing cell. Red outline indicates peri-basal body IFT signal. **(a')** Still frames from a high-speed time-lapse movie showing the transition of a retrograde particle of GFP-IFT20 (blue arrowhead) from the axoneme into the basal body IFT pool (red outline). **(a'')** Still frames from the same movie showing the entry of an anterograde GFP-IFT20 particle (pink arrowhead) into the axoneme from the basal body (red outline). See also Movie 4. **(b)** Still frames from a time-lapse movie showing a GFP-IFT20 labeled particle moving anterograde, pausing, and beginning to move in a retrograde fashion. Distal is up in the figure; note that additional GFP-IFT20 signal is present distal to the point of reversal.

they do serve as examples of the power of the *Xenopus* MCC as an imaging platform for high-resolution studies of IFT dynamics.

2.4: FUZ IS REQUIRED FOR APPROPRIATE ANTEROGRADE IFT DYNAMICS

IFT controls both trafficking within cilia and the integrity of the ciliary distal tip (Marshall and Rosenbaum, 2001; Marshall et al., 2005)—both of which appear to be defective in Fuz KD conditions. Therefore, I hypothesized that Fuz might modulate IFT dynamics. In order to test this hypothesis, I used the system for *in vivo* imaging of IFT in *Xenopus* multiciliated cells (MCCs) described above. Using this imaging platform, I found that Fuz knockdown resulted in profound defects in IFT. Fuz KD cilia, contained areas of high GFP-IFT20 signal along the length of the axoneme (Fig 12a). These labeled areas were much larger than the IFT trains observed in controls (Fig. 10a), suggesting that they represent an accumulation of IFT trains. Time-lapse imaging revealed that these accumulations of GFP-IFT20 were entirely static and such large, non-motile IFT signals were never observed in control axonemes. Controls IFT trains did often pause for short periods (2-4 sec.), however, the large IFT trains in Fuz KD axonemes remained static during the entire course of my high-speed movies (15-30 sec.; Fig. 12a'). Moreover, when I made longer movies with conventional confocal microscopy, the accumulations of GFP-IFT20 in Fuz KD axonemes were found to remain static for over 4 minutes, at which

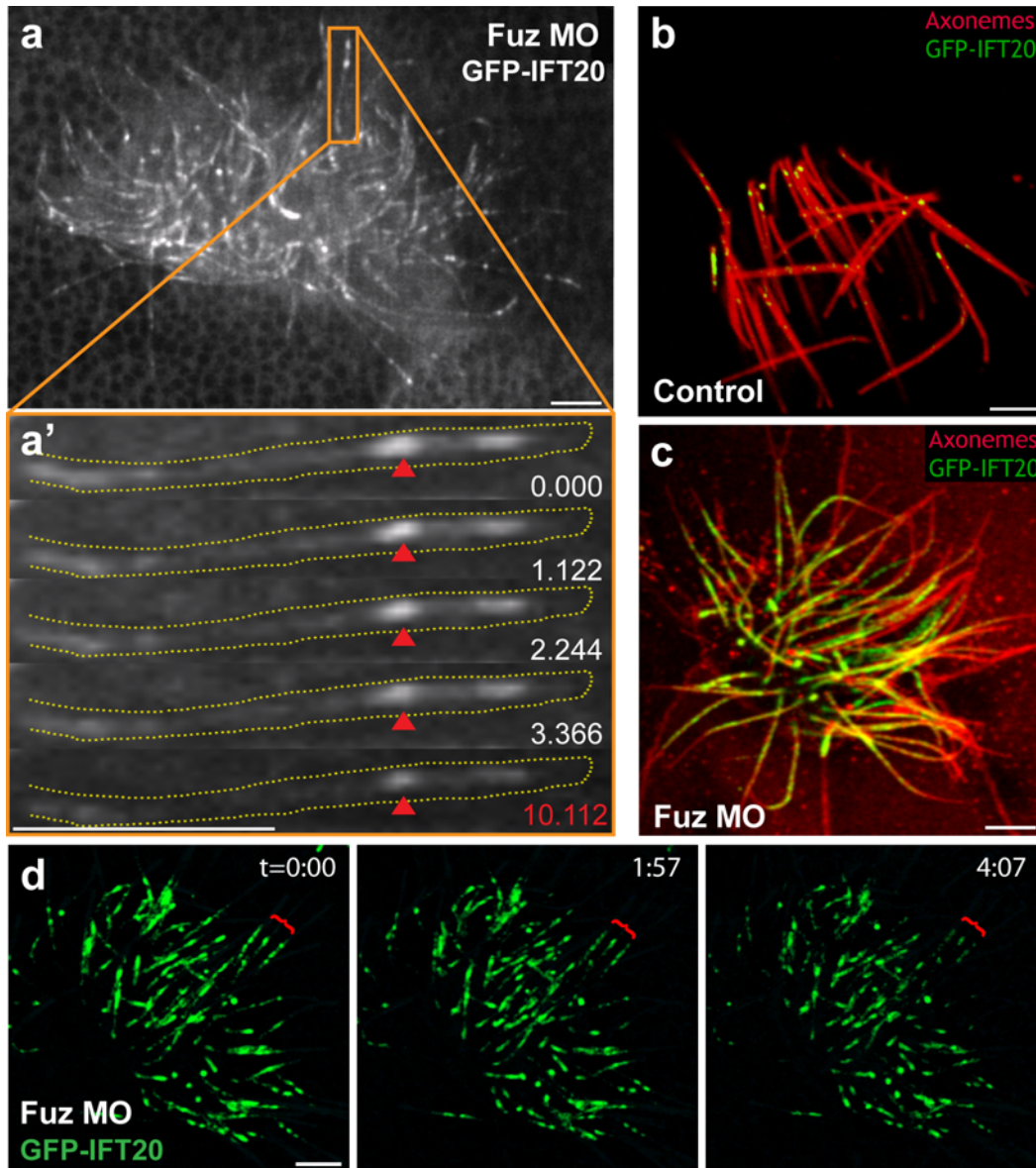


Figure 12: Loss of Fuz leads to disrupted anterograde IFT. **(a)** Still frame from a movie of GFP-IFT20 in a Fuz KD cell (Movie 5). **(a')** Still frames from a time-lapse movie reveal abnormally large and immotile IFT particles (red arrowhead) in a Fuz KD axoneme. The final frame is taken from the end of the time-series (Movie 6). **(b)** In a fixed control embryo, IFT particles (green) can be seen at low density in the axonemes of a multi-ciliated cell (red). **(c)** In a mildly affected Fuz KD embryo, IFT particles accumulate at high density throughout the axonemes. **(d)** GFP-IFT20 particles are static for over four minutes in Fuz KD axonemes. Red brackets indicate especially clear examples. Scale bars = 4 μm.

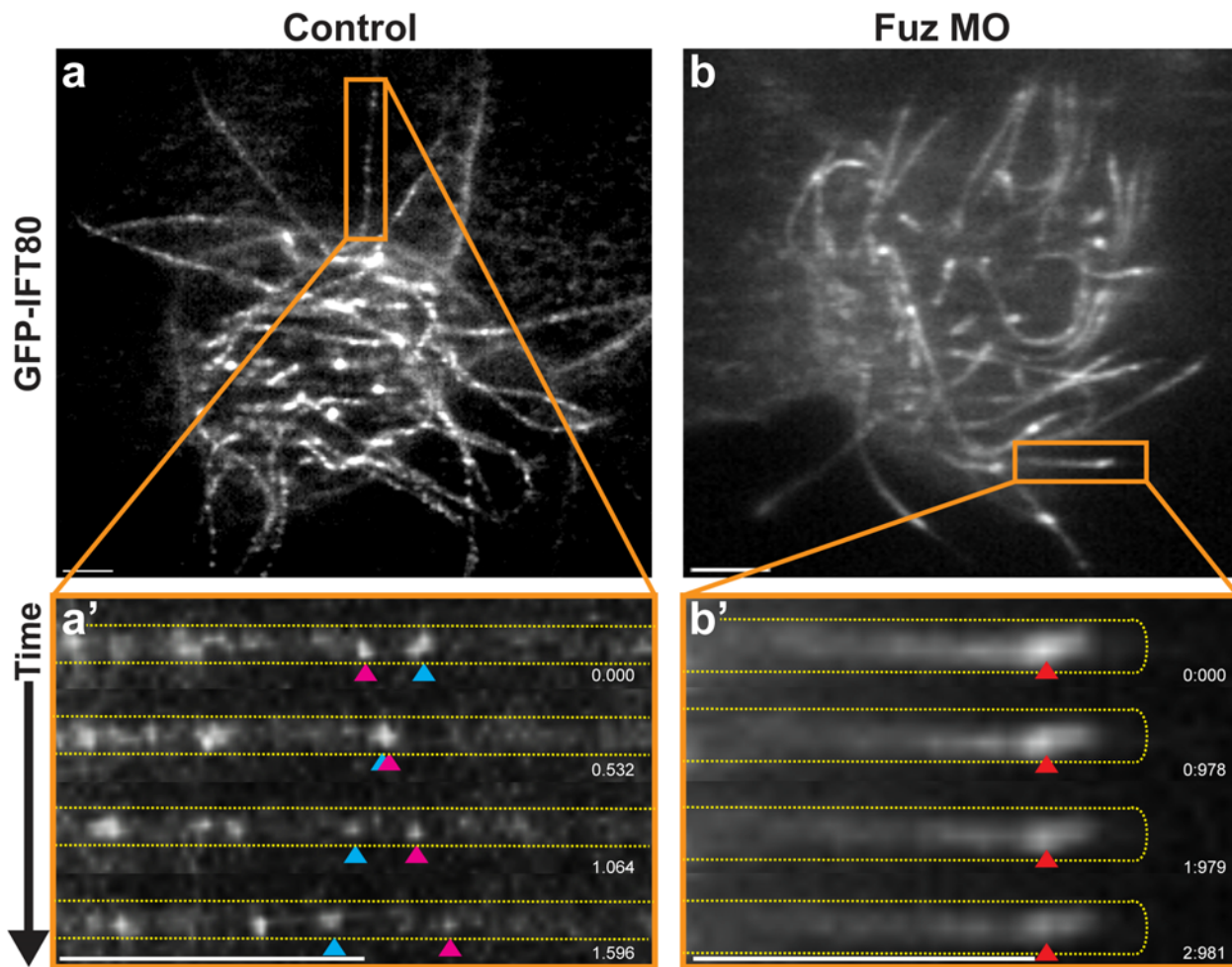


Figure 13: Fuz is required for IFT80 cycling dynamics. **(a)** Still frame from a confocal movie showing a GFP-IFT80 in a control multi-ciliated cell (Movie 7). Orange box represents region shown in a'. **(a')** Successive still frames from a time-lapse movie show the processive movement of GFP-IFT80 labeled particles. Time is indicated in seconds; pink arrowhead indicates an anterograde particle; blue arrowhead indicates a retrograde particle. **(b)** Still frame from a high-speed confocal movie of GFP-IFT80 in a Fuz KD cell (Movie 8). **(b')** Still frames from a time-lapse movie reveal abnormally large and immotile IFT80 labeled particles (red arrowhead). Scale bars indicate 3 μm

point photobleaching precluded further analysis (Fig. 12d).

I next asked if this defect was specific to IFT20, or if it was generalizable to another anterograde IFT-B, IFT80. IFT trains labeled by GFP-IFT80 behaved identically GFP-IFT20 trains (Fig. 13a, a'). Moreover, I also observed enlarged, non-motile GFP-IFT80 accumulations upon Fuz KD (Fig. 13b, b'). Together, these data suggest that the accumulatory phenotype is a likely to be a general outcome for anterograde IFT-B proteins in cells with compromised Fuz function.

2.5: FUZ IS REQUIRED FOR THE LOCALIZATION OF THE RETROGRADE IFT PROTEIN IFT43 TO AXONEMES

My analysis of IFT-B proteins in Fuz KD axonemes suggests a failure of processive anterograde trafficking. In general, loss of anterograde IFT function (e.g. by loss of an IFT-B member) leads to an absence of cilia (Ishikawa and Marshall, 2011; Pazour et al., 2000; Huangfu et al., 2003); Fuz KD, however, results in only shortened cilia. This short cilia phenotype is similar to that observed in retrograde IFT mutants (Tran et al., 2008; Qin et al., 2011; Ocbina et al., 2011). Additionally, the presence of anterograde IFT proteins within the axonemes of Fuz KD MCCs suggests that IFT-B is at least partially functional upon loss of Fuz function. Photo-bleached GFP-IFT20 accumulations in Fuz KD axonemes recover some fluorescence over time, suggesting that there is at least residual anterograde IFT, and indicating that the defects in anterograde IFT-B traffic may be indirect.

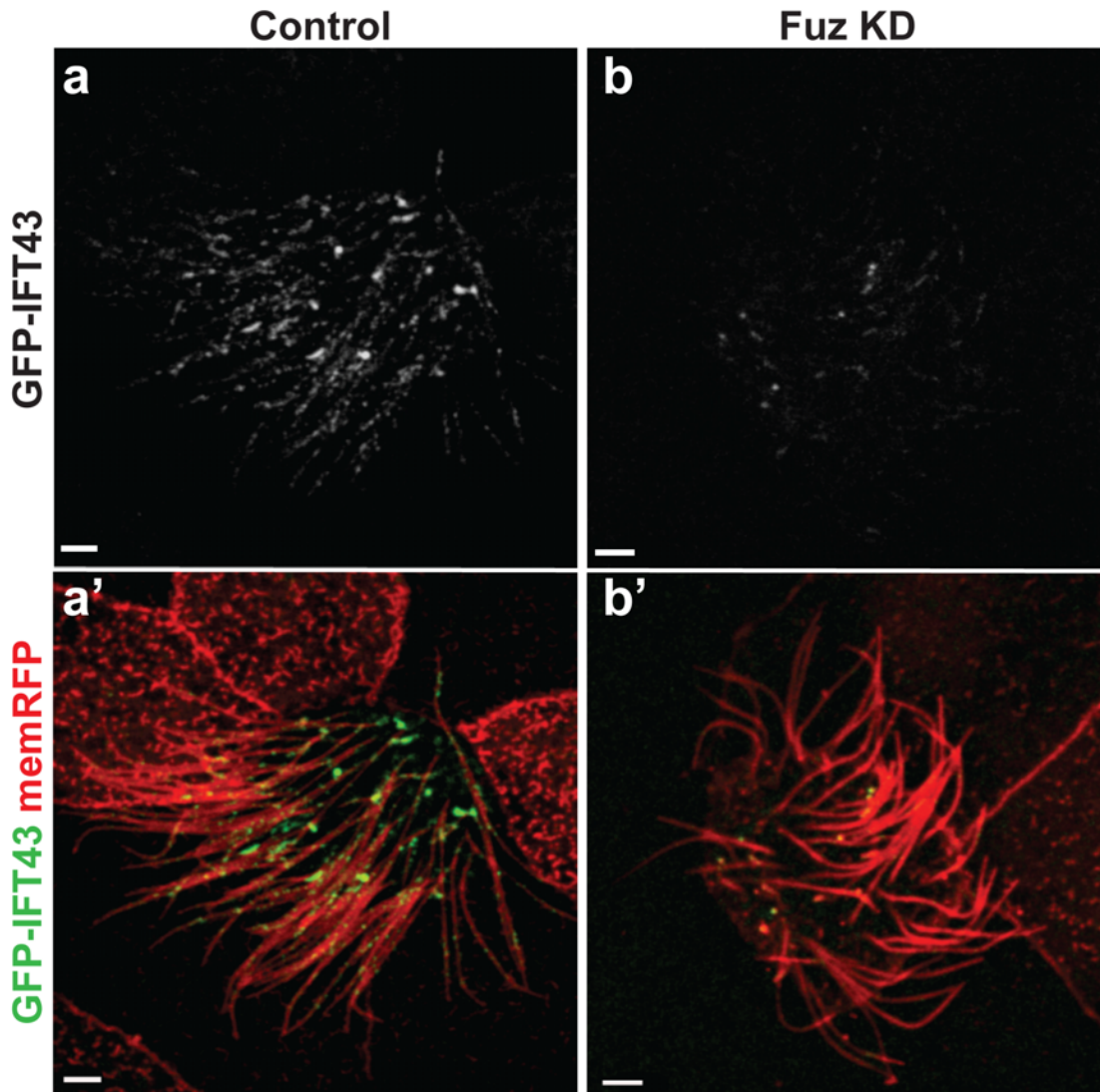


Figure 14: Reduced IFT43 localization in the axonemes of Fuz KD MCCs. **(a)** Punctate localization of the IFT-A component GFP-IFT43 in control multi-ciliated cell axonemes (marked by memRFP in **a'**). **(b)** Reduced GFP-IFT43 in the axonemes of Fuz KD multiciliated cells.

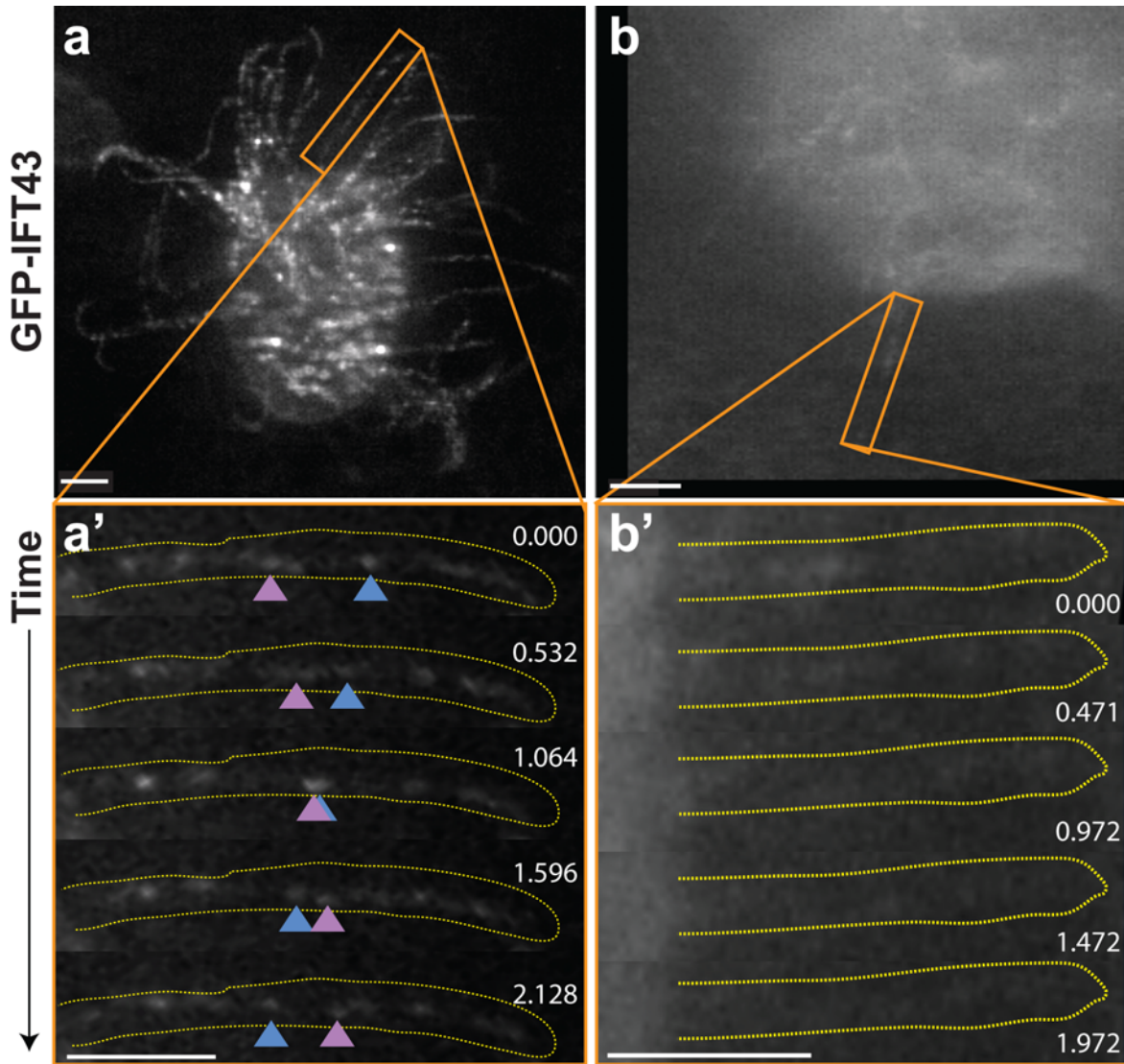


Figure 15: Loss of dynamic retrograde machinery from cycling axonemal IFT trains. **(a)** Still frame from a movie of a control multi-ciliated cell expressing GFP-IFT43 (Movie 9). Orange box indicates region shown in **(c')** **(c')** Still frames from a movie showing processive bi-directional transport in a single control cilium (Movie 10). Time is indicated in seconds; pink arrowhead indicates an anterograde particle; blue arrowhead indicates a retrograde particle. **(d)** A single frame from a time-lapse movie of a Fuz KD multi-ciliated cell expressing GFP-IFT43. The image has been intentionally over-exposed to bring out the faint background fluorescence of the axonemes. Orange box indicates region shown in **d'**. **(d')** Still frames from a movie showing loss of GFP-IFT43 dynamics in a single cilium from a Fuz KD multi-ciliated cell. Scale bars = 3 μm .

I therefore asked if Fuz might more directly impact the retrograde IFT-A subcomplex. I fused GFP to IFT43, whose human orthologue is mutated in Sensenbrenner Syndrome (Arts et al., 2011). This construct localized in a punctate distribution in control cilia, similar to IFT-B members (Fig. 14a, a'), and high-speed analysis of GFP-IFT43 in control cilia revealed highly processive bi-directional axonemal traffic (Fig. 15c, c'). In Fuz KD cilia I observed a severe loss of axonemal GFP-IFT43 localization (Fig. 14b, b'), and was unable to detect processive movement of GFP-IFT43 in either direction by high-speed confocal microscopy (Fig. 15d, d'). These findings suggest that the observed accumulation of IFT-B proteins in Fuz KD axonemes can be attributed to a failure in retrograde IFT caused by the failure of IFT43 and possibly other IFT-A proteins to incorporate into axonemal trains.

2.6: FUZ IS REQUIRED FOR THE LOCALIZATION OF IFT43 BUT NOT IFT20 TO PERI-BASAL BODY POOLS

The specific loss of IFT-A from Fuz KD axonemes was an interesting finding, and I wanted to understand the cellular basis of this phenotype. Given the previously identified role for Fuz in trafficking of ciliary proteins from the deeper cytoplasm to the apically localized basal bodies (Gray et al., 2009), I hypothesized that Fuz may be necessary for the localization of IFT43 to the apical pools of peri-

basal body IFT—where trains are thought to be assembled before they are injected into axonemes (Deane et al., 2001; Ishikawa and Marshall, 2011).

To test this hypothesis, I examined the recruitment of IFT43 to basal bodies by co-expressing GFP-IFT43 and the basal-body marker Centrin-RFP, and collecting confocal slices just below the apical surface of multi-ciliated cells. Quantification revealed a dramatic loss of normalized GFP-IFT43 signal from basal bodies in Fuz KD cells as compared to controls (Fig. 16a vs. b, 17, 18a, see Materials and Methods). I also observed a reduction in the number of IFT43-GFP labeled foci per multi-ciliated cell (normalized to the number of Centrin-RFP labeled basal bodies) (Fig. 16a, b, Fig. 18c). Importantly, a similar analysis of GFP-IFT20 recruitment to basal bodies revealed no significant change in either enrichment or number of foci between control and Fuz KD cells (Fig 16c, d; Fig 18b, d).

Together, these data suggest that Fuz is a key regulator, specifically of retrograde IFT. Further, Fuz performs this function by controlling the localization of IFT43 and possibly other retrograde IFT-A proteins to the peri-basal body pools where IFT trains are assembled before they are injected into the axoneme.

2.7: MODEL FOR FUZ FUNCTION DURING CILIOGENESIS

The findings reported here suggest that the observed defect in IFT-B in Fuz KD axonemes can be attributed to a failure of IFT43, and possibly other retrograde

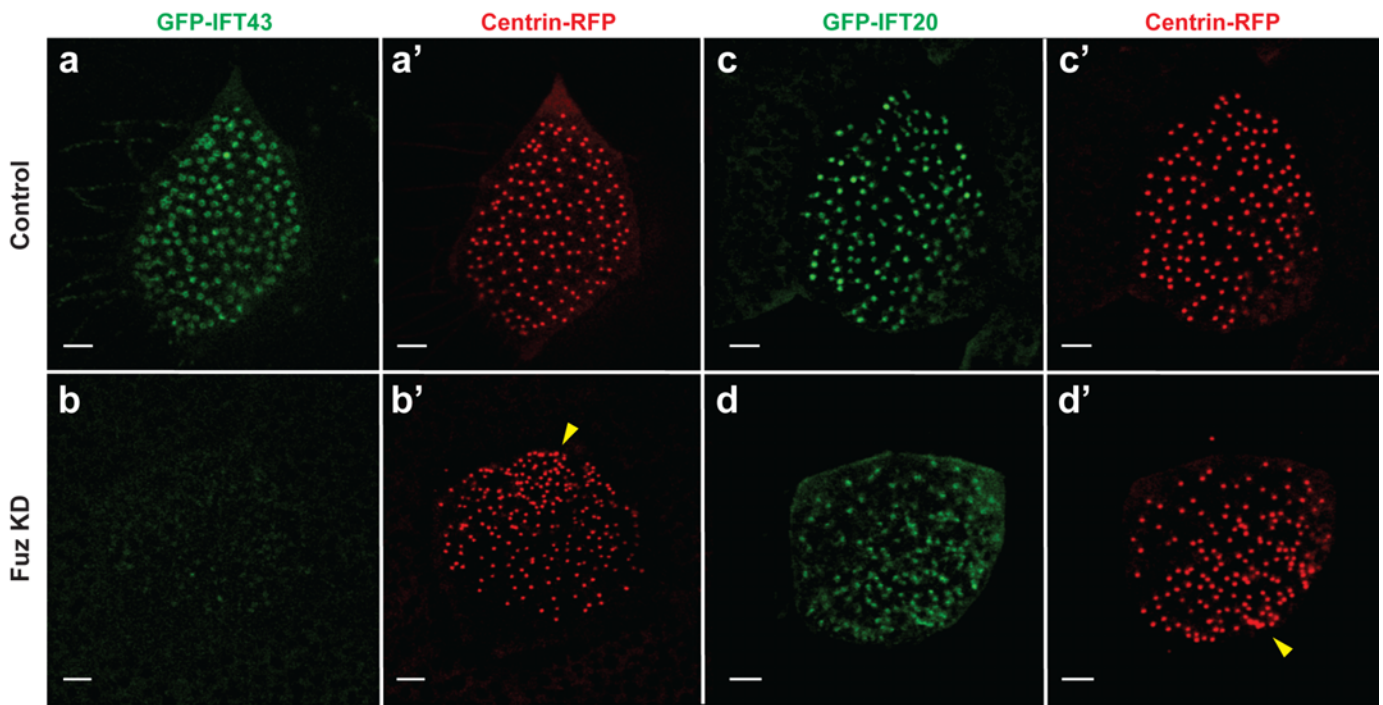


Figure 16: Fuz is required for the localization of GFP-IFT43, but not GFP-IFT20 to peri-basal body IFT pools. **(a)** Pools of GFP-IFT43 surrounding basal bodies marked by Centrin-RFP **(a')** in a control cell. Similar pools are observed for GFP-IFT20 **(c, c')**. GFP-IFT43 pools show reduced enrichment at basal bodies in Fuz KD cells **(b, b')**. However, GFP-IFT20 is still appropriately localized under the same conditions **(d, d')**. Note that Fuz KD cells exhibit a second phenotype of basal-body clustering (yellow arrowheads in **c', d'**; see also Gray et al., 2009). Scale bars represent 3 μ m.

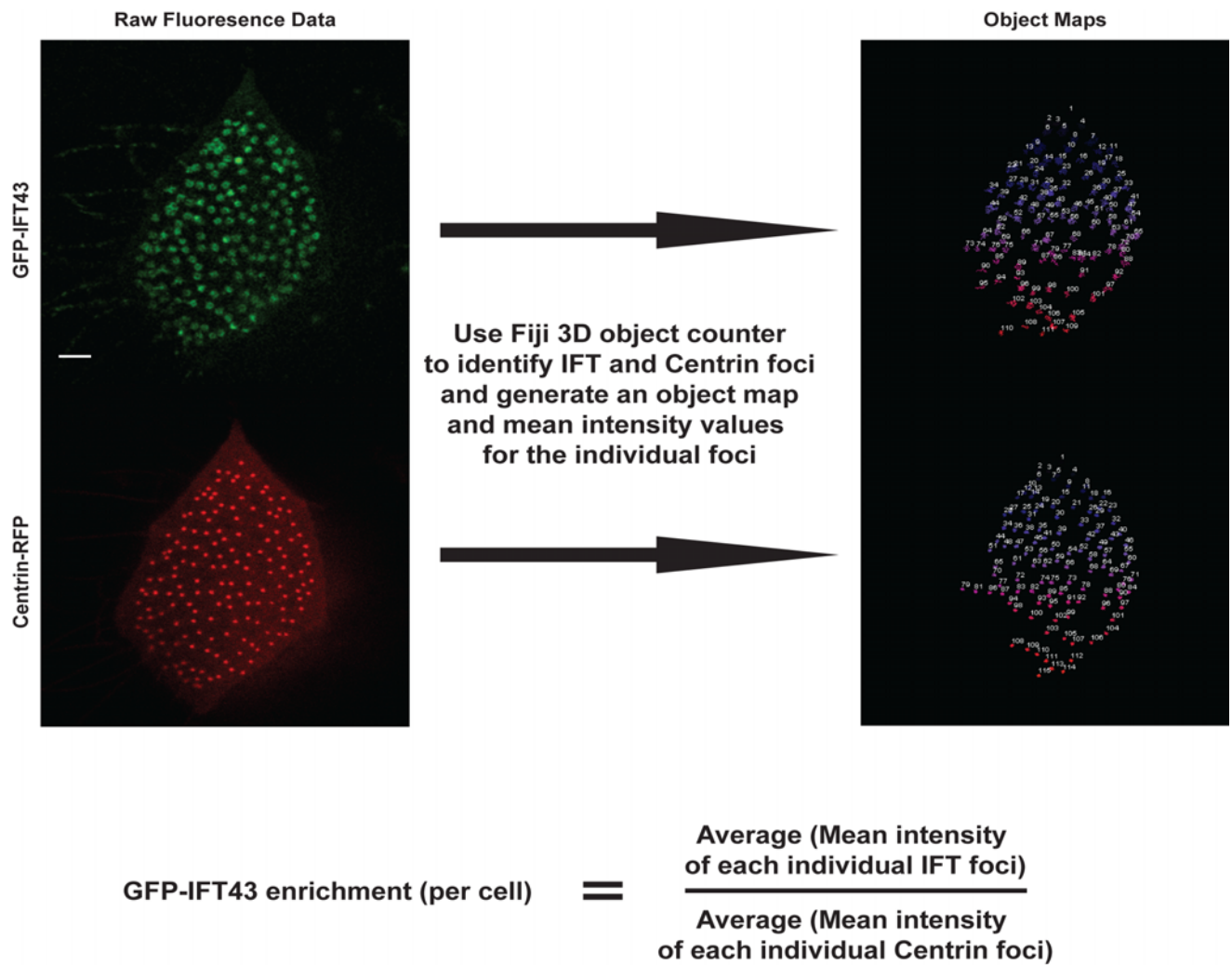


Figure 17: Schematic explanation of quantification methodology used for assessing enrichment of IFT at apically localized basal bodies. To quantify GFP-IFT recruitment, an object detection algorithm was used to identify foci of GFP-IFT and Centrin-RFP. The mean intensities of all detected GFP-IFT foci in a single cell were then averaged together and normalized to the averaged mean intensities of all Centrin-RFP foci in the same cell. Scale bars represent 3 μm .

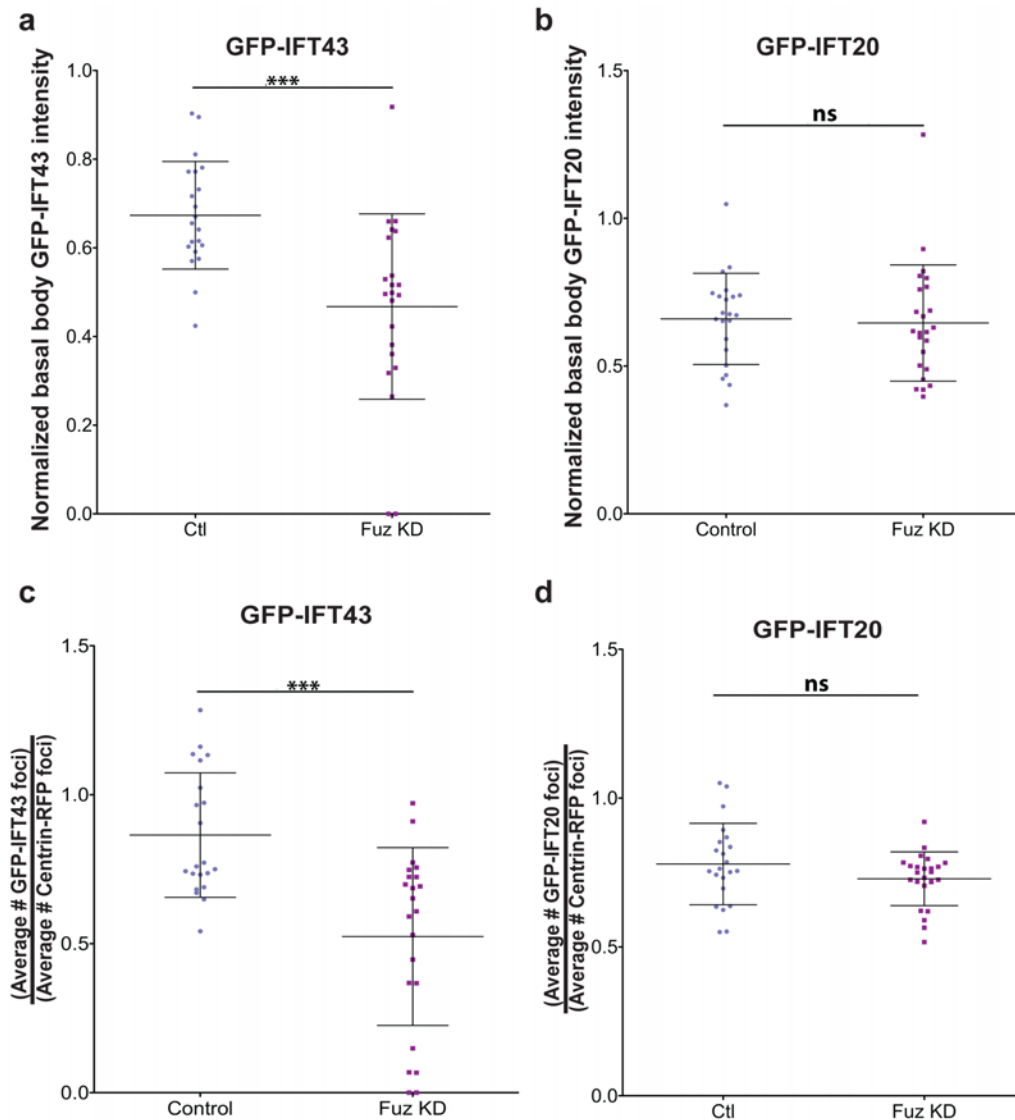


Figure 18: Quantitative analysis of GFP-IFT localization to basal bodies. **(a)** Quantitative comparison of GFP-IFT43 localization in control and Fuz KD cells. Each data point represents the average of the mean intensities of all GFP-IFT43 pools in a cell normalized to the average of the mean intensities of all Centrin foci. Fuz KD leads to a significant reduction in GFP-IFT43 localization to apical pools (Fuz KD: mean \pm SD = 0.47 ± 0.20 ; n=21 cells, 6 embryos vs. Control: mean \pm SD = 0.67 ± 0.12 ; n=21 cells, 6 embryos; p=0.0003). **(b)** A similar analysis of GFP-IFT20 shows no significant difference in localization between control and Fuz KD cells (Fuz KD: mean \pm SD = 0.65 ± 0.20 ; n=24 cells, 6 embryos vs. Ctl: mean = 0.66 ± 0.15 ; n=22 cells, 6 embryos; p=0.5308). **(c)** Quantification of the number of GFP-IFT43 foci detected per Centrin-RFP foci per cell. Fuz KD led to a significant reduction in this value (Fuz KD: mean \pm SD = 0.52 ± 0.30 , n=21 cells, 6 embryos vs. Ctl: 0.86 ± 0.21 n=21 cells, 6 embryos; p<0.0001). **(d)** There is no significant difference in the number of GFP-IFT20 foci per Centrin-RFP foci in control vs. KD conditions (Fuz KD: mean \pm SD = 0.73 ± 0.09 , n=24 cells, 6 embryos vs. Ctl: 0.78 ± 0.14 , n=22 cells, 6 embryos; p=0.2021)

IFT-A complex proteins, to localize appropriately to the peri-basal body pool of IFT proteins. This results in a failure to incorporate functional retrograde IFT-A machinery into trains injected into the axoneme (Fig. 19). In this scenario, anterograde IFT will function uni-directionally, facilitating the initial assembly of the axoneme. However, IFT trains will be unable to effect a processive retrograde transition and will become stuck in the axoneme, resulting in the observed accumulations of static IFT-B proteins in the axonemes (Fig. 12; Fig. 13). Further, as more IFT-B dominated trains are injected into the axoneme, they will begin to block transit to the distal tip in a scenario reminiscent of a traffic jam, and prevent the delivery of key cargoes (e.g. tubulin dimers, etc.). Because these cargoes are required to maintain cilia length by counterbalancing steady-state disassembly at the tip (Ishikawa and Marshall, 2011; Marshall and Rosenbaum, 2001; Kozminski et al., 1995), impaired delivery can explain both the observed defects in the distal axonemal pattern and the resulting ciliary shortening (Fig. 6 and Fig. 8).

The observed accumulation of IFT-B proteins upon Fuz KD is similar to the phenotype observed upon direct loss of retrograde IFT function (Qin et al., 2011; Tsao and Gorovsky, 2008; Tran et al., 2008). In these contexts, however, IFT-B proteins seem to accumulate preferentially at the distal tip of axonemes, while loss of Fuz leads to a more stochastic pattern of IFT accumulations along the entire length of the axoneme (Fig. 12). This stochastic positioning might be explained by partial function of residual IFT-A in Fuz KD axonemes. For example, residual

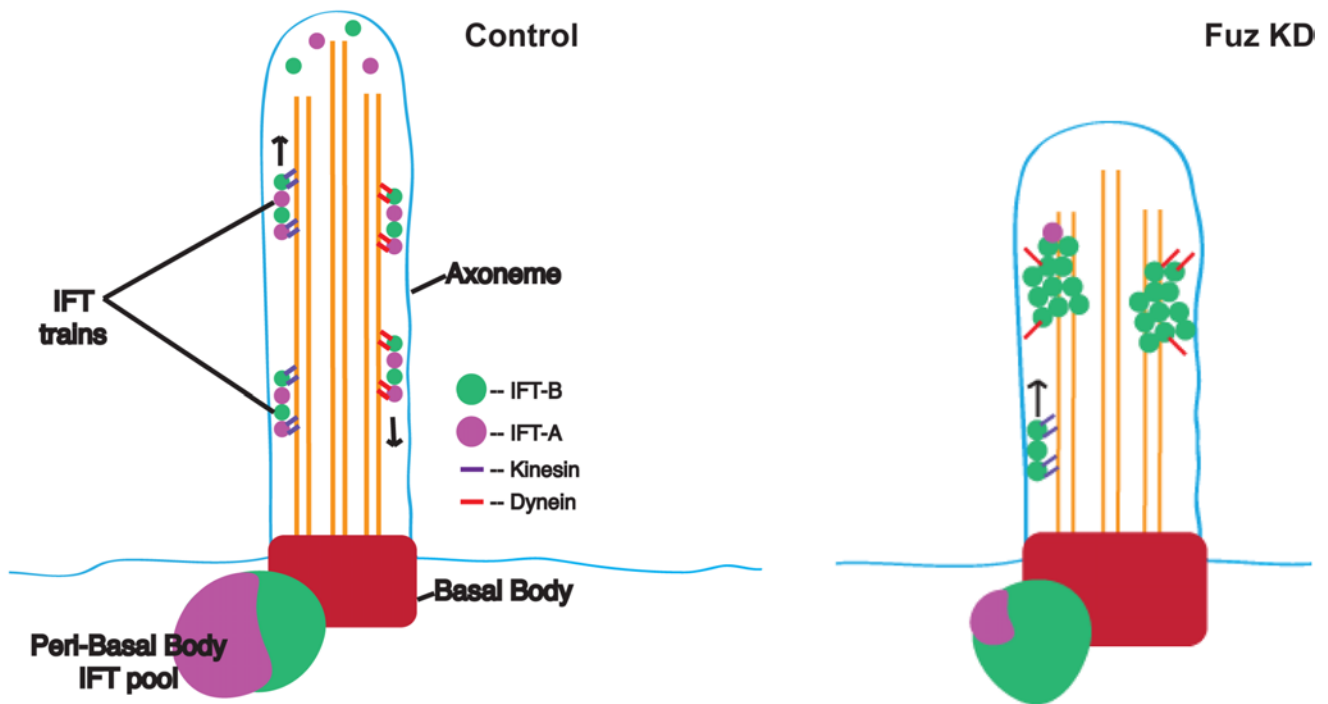


Figure 19: Model for Fuz function during ciliogenesis. Fuz functions to control the localization of IFT43, and possibly other retrograde IFT-A members to the peri-basal body pool of IFT proteins. Loss of Fuz function, therefore, results in greatly reduced retrograde IFT-A machinery at the basal bodies, and, as a result, in the assembled IFT trains. The impaired, anterograde heavy trains can be injected into axonemes, but can only function unidirectionally. As more trains are injected into the axoneme, without any retrograde clearance, a traffic-jam like scenario occurs, inhibiting delivery of key cargos to the distal tip (e.g. tubulin dimers). In the absence of new cargos, the steady-state depolymerizing kinesins at the tip take over and result in progressively shorter axonemes.

retrograde complexes may allow for only inefficient coherence with dynein, leading trains to disengage and stall randomly along the retrograde trajectory.

2.8: DISCUSSION

My data place Fuz as an effector of IFT that falls outside of the core biochemical complex of IFT proteins. Only a handful of other factors outside of the core machinery have been found to influence IFT. These include the Bardet-Biedel Syndrome proteins BBS-7 and -8, required for motor coordination in *C. elegans* (Blacque et al., 2004; Ou et al., 2005; Pan et al., 2006), Arl13b, a small GTPase required for cohesion of IFT-B and -A subcomplexes (Li et al., 2010; Cevik et al., 2010), Elipsa, which is required for localization of both IFT subcomplexes to basal bodies (Omori et al., 2008), and Ofd1, required to localize IFT88, but not other IFT-B proteins, to basal bodies (Singla et al., 2010). Additionally, the apparent selectivity of Fuz for retrograde IFT place it in the even smaller list of molecules exerting control over a specific subset of IFT proteins. Finally, the data presented here are also the first direct link between a PCP protein and the core, highly conserved machinery of ciliogenesis.

It is also of note that Fuz function in this context is evolutionarily restricted; neither *Chlamydomonas* nor *C. elegans*, possess an apparent orthologue of Fuz; and, while the *Drosophila* genome does contain a Fuz orthologue, it does not appear to

function in ciliogenesis. Thus, Fuz may be a vertebrate-specific effector of retrograde IFT function.

These findings substantially expand our understanding of the function of Fuz, a critical regulator of ciliogenesis and developmental signaling (Dai et al., 2011; Gray et al., 2009; Heydeck et al., 2009). Given that recent studies have linked mutation in the locus encoding Fuz with human pathologies (Seo et al., 2011), it will be important to understand how these mutations compromise Fuz function.

Deep analyses of vertebrate IFT dynamics are the critical next step in clarifying poorly understood aspects of this transport, including: events at the transition zone, loading and unloading of IFT trains, and low frequency axonemal behaviors. Such dynamic analysis will be required to understand the molecular etiology of ciliopathic mutations that present without obvious cilia morphology defects (Davis et al., 2011; Rix et al., 2011). The platform underlying the studies presented here allows for the generation of rich data sets at single train resolutions and will be valuable in elucidating IFT dynamics in both the cell body and the axoneme. Additionally, it is the first platform for IFT analysis in vertebrate multiciliated cells, a population with significant roles in respiration, fertility, and neural morphogenesis, and about which we know comparatively little (Wanner et al., 1996; Lyons et al., 2006; Banizs et al., 2005; Sawamoto et al., 2006).

Finally, it is tempting to speculate that dynamic spatio-temporal expression of Fuz may be one mechanism by which cells differentiate between ciliated and non-

ciliated outcomes. Further, it is likely that cytoplasmic control of IFT localization and function—likely including sequestering of IFT proteins in the deeper cytoplasm, as well as regulated assembly of IFT trains—is an important regulatory motif underlying the dynamics of cilia biogenesis, maintenance, and disassembly.

Chapter 3: The small GTPase Rsg1 is important for the cytoplasmic localization and axonemal dynamics of intraflagellar transport proteins

Portions of this chapter are modified with permission from: Brooks, ER and Wallingford, JB. The small GTPase Rsg1 is important for the cytoplasmic localization and axonemal dynamics of Intraflagellar transport proteins. Cilia (2013) 2: 13

3.1: THE PUTATIVE SMALL GTPASE RSG1 PHYSICALLY INTERACTS WITH FUZ AND IS REQUIRED FOR CILIOGENESIS

Small GTPases are key mediators of several aspects of ciliogenesis. As detailed in Chapter 1, a cascade of Rab small GTPases is required for trafficking ciliary membrane and cargos. Rhodopsin, a key component of modified photoreceptor cilia, is initially bound by the small GTPase Arf4 as it is sorted out of the *trans*-Golgi Network. Binding by Arf4 recruits Rab11 which directs Rhodopsin to the basal body (Mazelova et al., 2009a; b; Wang et al., 2012). The Rab11-Rab8 cascade has been shown to be important for vesicle tethering and fusion at the basal body in the context of many cargos (Mazelova et al., 2009a; Nachury et al., 2007; Knödler et al., 2010). Intraflagellar transport itself can be regulated by the action of GTPases, including IFT22 and in some cases IFT27 (Silva et al., 2012; Adhiambo et al., 2009; Qin et al., 2007). Additionally, the ciliary resident Arl13 and Arl3 GTPases have been shown to control coherence of the IFT-A and IFT-B subcomplexes (Cevik et al., 2010; Li et al., 2010).

Previous work in the Wallingford lab demonstrated that the putative small GTPase Rsg1 (Rem/Rab similar GTPase 1) physically interacts with Fuz and is required for ciliogenesis (Gray et al., 2009). Therefore, I hypothesized that it might be required for the cytoplasmic localization and axonemal dynamics of intraflagellar transport proteins, given that these are among the functions of its binding partner Fuz. To test this hypothesis I used the system for *in vivo* IFT imaging at basal bodies and in axonemes detailed in Chapter 2.

3.2: RSG1 FUNCTION IS REQUIRED FOR THE CORRECT ORGANIZATION OF THE AXONEMAL PROXIMO-DISTAL AXIS

Little is known about how the axoneme is patterned along its proximal-distal axis. It has recently been demonstrated that specific dynein isoforms are distributed in a restricted fashion along this axis in motile respiratory cilia, and that this pattern is functionally important (Fliegauf et al., 2006; Panizzi et al., 2012). In addition, a recent report has suggested that proximodistal pattern in primary cilia is important for modulating Sonic Hedgehog signaling (Ocbina et al., 2011). I showed in Chapter 2 that the microtubule binding protein CLAMP tagged with RFP is enriched in a specific compartment in the distal ~2 μ m of the axoneme, and that it also weakly decorates the entire proximal axoneme (Fig 20a'). Further, I demonstrated that this

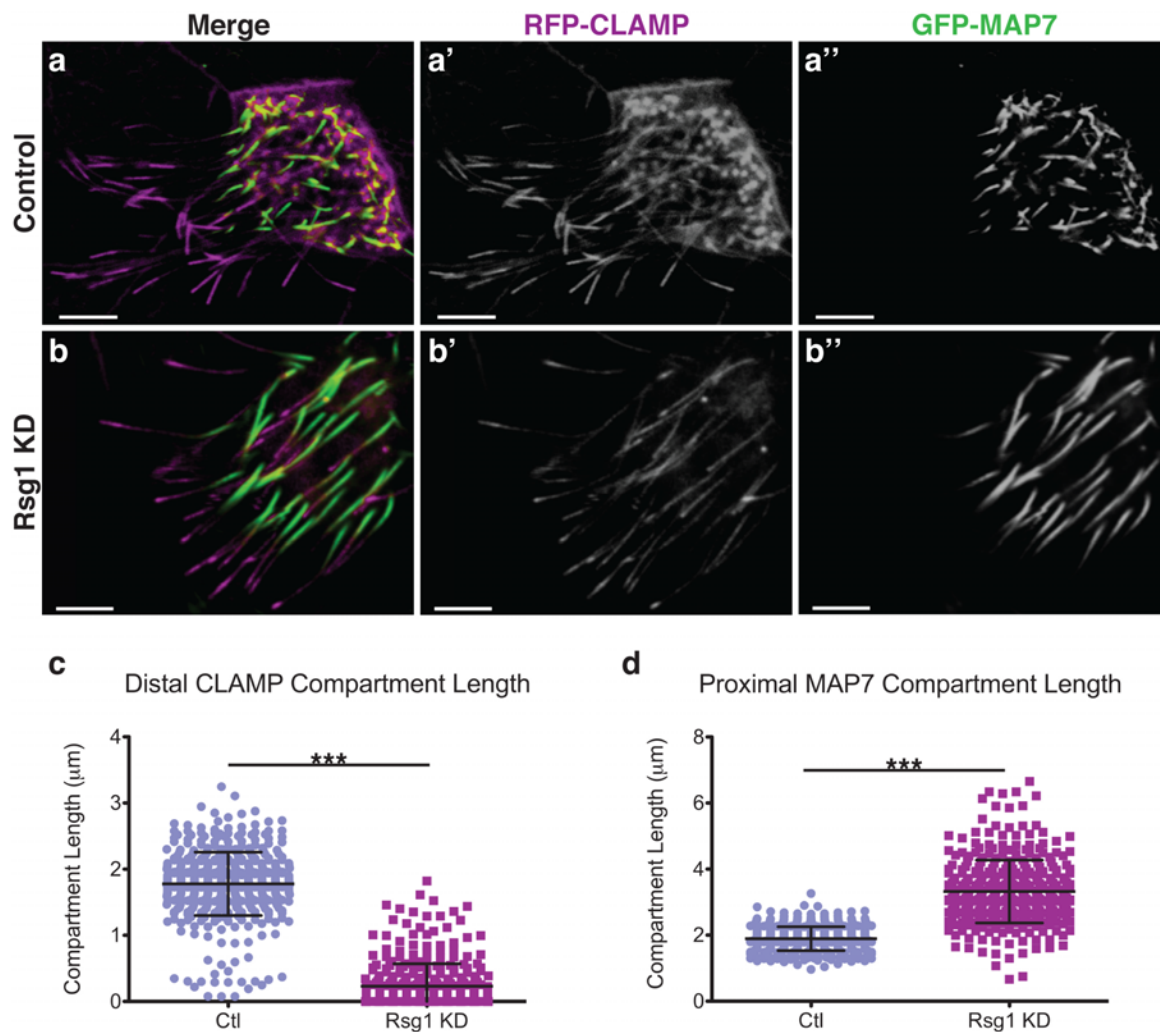


Figure 20: The putative small GTPase Rsg1 is required for correct proximal-distal axoneme patterning in *Xenopus* MCCs. **(a-a'')** A representative *Xenopus* multiciliated cell (MCC), co-expressing GFP-MAP7, a marker of proximal ciliary identity, and RFP-CLAMP, a marker of the distal-tips of cilia. **(b-b'')** A MCC co-expressing GFP-MAP7 and RFP-CLAMP, and in which the function of the small GTPase, Rsg1 has been knocked-down by a translation-blocking antisense morpholino oligonucleotide. Note the significantly shortened or absent distal compartments of RFP-CLAMP as compared to controls. In addition, the proximal compartment marked by GFP-MAP7 is significantly expanded in these axonemes. This cell exhibits a moderate Rsg1 KD phenotype, and was chosen to facilitate direct comparison with the control cell. **(c)** Quantification of axonemal RFP-CLAMP compartments reveals a severe reduction in distal identity upon Rsg1 KD. (Ctl [mean \pm SD]: $1.78 \pm 0.48 \mu\text{m}$, $n= 517$ axonemes, 29 cells, 5 embryos vs. Rsg1 KD: $0.23 \pm 0.34 \mu\text{m}$, $n= 361$ axonemes, 28 cells, 5 embryos. *** $p<0.0001$). **(d)** Quantification of GFP-MAP7-positive compartments reveals a significant increase in proximal identity. (Ctl: $1.90 \pm 0.36 \mu\text{m}$, $n= 452$ axonemes, 29 cells, 5 embryos vs. Rsg1 KD: $3.32 \pm 0.95 \mu\text{m}$, $n= 364$ axonemes, 39 cells, 5 embryos. *** $p<0.0001$). Scale bars represent $5 \mu\text{m}$.

distal compartment was specifically compromised upon Fuz KD (Chapter 2). I also demonstrated that proximal ciliary identity, marked by a construct consisting of GFP fused to the microtubule-binding domain of MAP7 (GFP-MAP7, Fig 20a''), was only minimally perturbed in Fuz KD axonemes.

To begin exploring the role of Rsg1 in ciliogenesis, I analyzed proximodistal axoneme patterning by knocking down Rsg1 with a previously validated antisense morpholino oligonucleotide (Rsg1 KD; (Gray et al., 2009) and see Materials and Methods) and analyzing the distribution of RFP-CLAMP and GFP-MAP7. Generally, axonemes were shorter in Rsg1 KD cells, and I found a very significant reduction in the length of the CLAMP-positive distal compartment in Rsg1 KD cilia (Fig. 20a' vs. b', c), a more severe variant of the phenotype observed in Fuz KD MCCs (See Chapter 2). Surprisingly, however, there was a significant increase in MAP7-positive proximal ciliary identity upon Rsg1 KD, a phenotype not observed in Fuz KD cilia (Fig 20a'' vs. b'', d; Chapter 2). This result suggests that Rsg1 may have functions in proximodistal patterning that are independent of Fuz, or that their functional relationship may not simply be one-to-one. Alternatively, these results could indicate that the Fuz and Rsg1 morpholinos used in these studies have different efficacies of knockdown, or that the two proteins have different abundances in MCCs. In this case the elongation of the MAP7 compartment could be the result of a more severe reduction in the common function of Fuz and Rsg1.

3.3: RSG1 IS REQUIRED FOR NORMAL INTRAFLAGELLAR TRANSPORT DYNAMICS WITHIN AXONEMES

The reduction in distal axonemal identity in Rsg1 KD MCCs was reminiscent of that observed in Fuz loss of function conditions (Chapter 2). This observation led me to hypothesize that Rsg1 function might be important for appropriate Intraflagellar transport (IFT) dynamics, as is the case for Fuz. Therefore I applied high-speed confocal imaging approaches to analyze IFT (Chapter 2 and Materials and Methods) in *Xenopus* MCCs lacking Rsg1 function. High-speed imaging of axonemes from control cells expressing GFP-IFT20—an anterograde IFT-B member (Follit et al., 2006; 2008; Baker et al., 2003; Jonassen et al., 2008)—showed highly dynamic and processive bi-directional IFT trains, as previously observed (Fig 21a; See Chapter 2). However, axonemes from Rsg1 KD MCCs showed disruption of these dynamics (Fig 21b). IFT trains could not be reliably tracked in most Rsg1 KD axonemes, as the entire length of the axoneme seemed to be filled with a low level of GFP-IFT20 (Fig 21b' vs. Fig 21a'), greatly reducing the signal to noise ratio. While some dynamic, train-like movement was occasionally observed, tracking and quantification of this behavior was impaired due to the increased background. Alternatively, it is possible that the IFT trains are misformed in Rsg1 KD axonemes, being either smaller or containing fewer IFT sub-complexes, and leading to a reduced signal, and a reduced ability to track these objects.

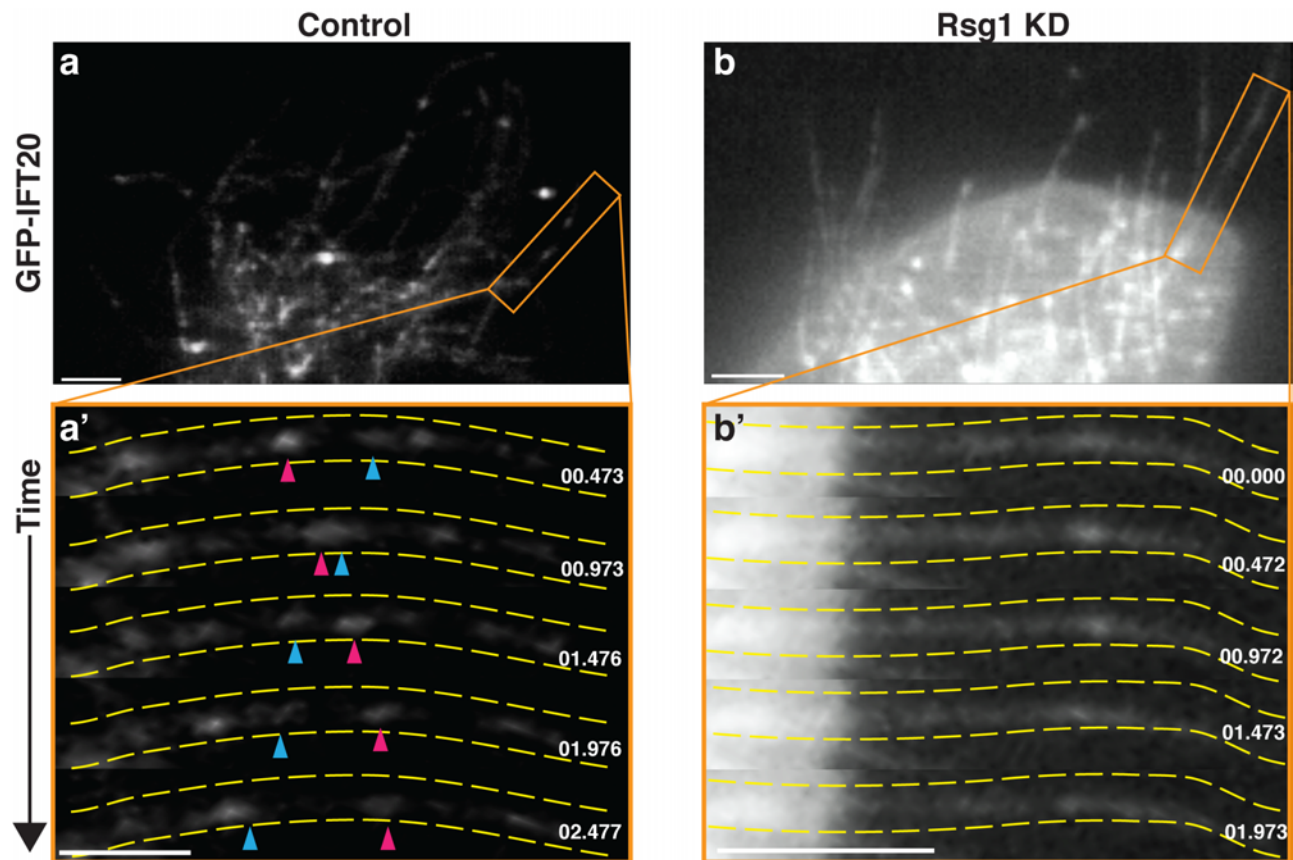


Figure 21: Rsg1 is required for appropriate IFT dynamics within the axonemes of MCCs. **(a)** High-magnification confocal image of axonemes from a control MCC expressing GFP-IFT20. The orange box indicates the region shown in **a'**. **(a')** A time series of a single axoneme from a control cell. Yellow dashed lines outline the axoneme and distal is to the right. Pink and blue arrowheads indicate an anterograde train and a retrograde train, respectively. **(b)** High-magnification confocal image of axonemes from an Rsg1 KD MCC expressing GFP-IFT20. Orange box represents the region shown in **b'**. **(b')** A time series from a single axoneme from an Rsg1 KD MCC. Yellow dashed lines outline the axoneme and distal is to the right. No IFT trains are visible during the course of the movie. Scale bars represent 3 μm

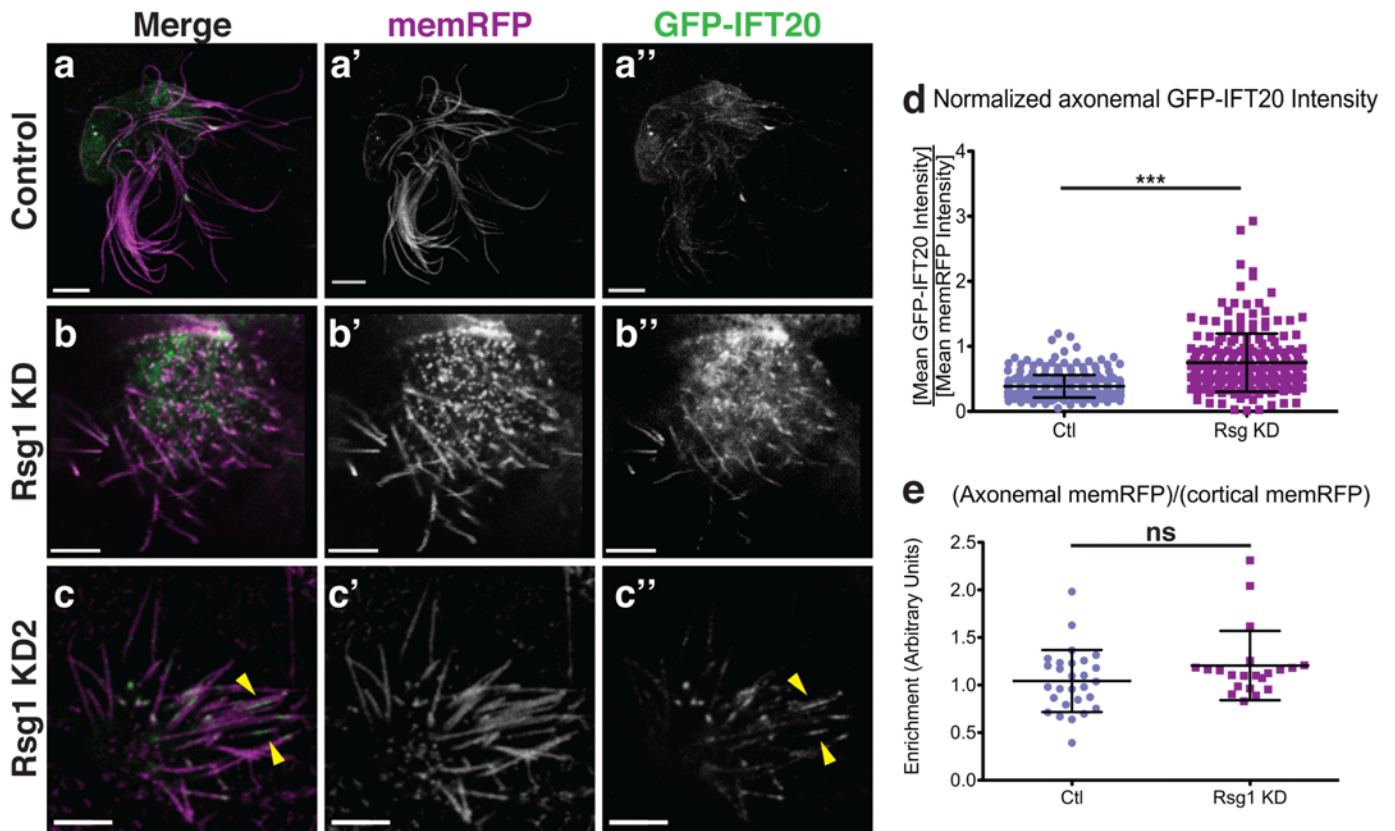


Figure 22: IFT20 accumulates in the axonemes of Rsg1 KD MCCs. **(a-a'')** A single confocal slice of an control MCC co-expressing membraneRFP and GFP-IFT20. **(b-b'')** A single confocal slice of an Rsg1 KD MCC co-expressing membraneRFP and GFP-IFT20. **(c-c'')** A single confocal slice of an Rsg1 KD2 (second-site morpholino) MCC co-expressing membraneRFP and GFP-IFT20. Yellow arrowheads indicate large GFP-IFT20 accumulations in distal axonemes **(d)** Quantification of mean GFP-IFT20 signal along control and Rsg1 KD axonemes, as normalized to membrane RFP intensity along the same length. Note the increase in normalized IFT20 signal in Rsg1 KD axonemes (Ctl (mean \pm SD): 0.39 ± 0.17 , $n = 304$ axonemes, 36 cells, 7 embryos vs. Rsg1 KD: 0.75 ± 0.45 , $n = 223$ axonemes, 31 cells, 6 embryos. $***p < 0.0001$). **(e)** There is no significant difference in axonemal average membraneRFP signal as normalized to cortical membraneRFP signal from the same cell, between control and Rsg1 KD conditions (Ctl (mean \pm SD): 1.04 ± 0.33 , $n = 28$ cells, 6 embryos vs. Rsg1 KD: 1.21 ± 0.36 , $n = 21$ cells, 6 embryos. $p = 0.2607$). Scale bars represent $5 \mu\text{m}$.

The high GFP-IFT20 background levels observed in Rsg1 KD axonemes might represent a more diffuse form of the IFT accumulation phenotype observed in Fuz KD MCCs (Chapter 2). To test this hypothesis, I took single confocal slices of control and Rsg1 KD MCC ciliary tufts co-expressing GFP-IFT20 and membrane RFP. I then normalized the mean intensity of GFP-IFT20 along the length of axonemes to the mean intensity of membrane RFP along the same length, and compared this value in control and Rsg1 KD conditions. This value was significantly increased on average in Rsg1 KD axonemes (Fig 22a'' vs. b'', d), supporting an expanded accumulation of anterograde IFT proteins in these cilia. It is possible that memRFP localization to cilia itself was effected by Rsg1 KD, which would result in changes in this normalized value. To control for this possibility I normalized axonemal RFP intensity against cortical memRFP signal in MCCs. When I compared this value in control and Rsg1 KD MCCs, I saw no significant difference (Fig 22e). Additionally, to rule out MCC specific memRFP trafficking defects, I normalized cortical MCC signal against the cortical signal of neighboring goblet cells. Again, I saw no change in this value between control and Rsg1 KD conditions (Ctl (mean \pm SD): 1.13 \pm 0.29, 15 cells, 6 embryos vs. Rsg1 KD: 1.06 \pm 0.31, 19 cells, 6 embryos. $p=0.8082$). Together, these data suggest that the observed increase in normalized GFP-IFT20 signal is not due to a change in memRFP localization.

To further control for the specificity of the previously validated Rsg1 morpholino (Gray et al., 2009), I used a second, completely non-overlapping

morpholino (designated Rsg1 KD2) to confirm that these phenotypes were due to a specific loss of Rsg1 function. As expected, injection of Rsg1 KD2 led to shorter axonemes and to elevated IFT20 signal in axonemes as compared to controls (Fig 22c-c'', Ctl (mean \pm SD): 0.23 ± 0.14 , n = 200 axonemes, 30 cells, 3 embryos vs. Rsg1 KD2: 0.35 ± 0.16 , n= 195 axonemes, 25 cells, 4 embryos. $p < 0.0001$). In addition, a small number of cells from embryos injected with Rsg1 KD2 contained axonemes exhibiting large IFT20 accumulations, reminiscent of those I observed upon Fuz KD (Fig 22, e'', Chapter 2).

These data suggest that the Rsg1 is required for appropriate axonemal IFT dynamics, and Rsg1 KD phenotypes may be a variant of the IFT phenotypes previously observed in Fuz KD MCCs. I therefore predicted that retrograde IFT axonemal localization would be reduced or absent upon Rsg1 KD. To test this prediction I first used high-speed confocal microscopy of MCCs expressing GFP-IFT43, an IFT-A protein associated with Sensenbrenner syndrome (Arts et al., 2011). Control axonemes showed processive bi-directional trafficking, as expected (Fig 23a vs. a'). However, axonemes from Rsg1 KD MCCs showed faint levels of GFP-IFT43, and I could not readily observe train-like dynamics (Fig23b vs. b'). In my previous experiments Fuz KD led to a severe and obvious reduction of axonemal IFT43 levels, but IFT43 was still apparent in Rsg1 KD axonemes. To directly test IFT43 localization to axonemes, I normalized mean GFP-IFT43 levels to mean membrane RFP levels as above. Rsg1 KD axonemes showed a significant decrease in average

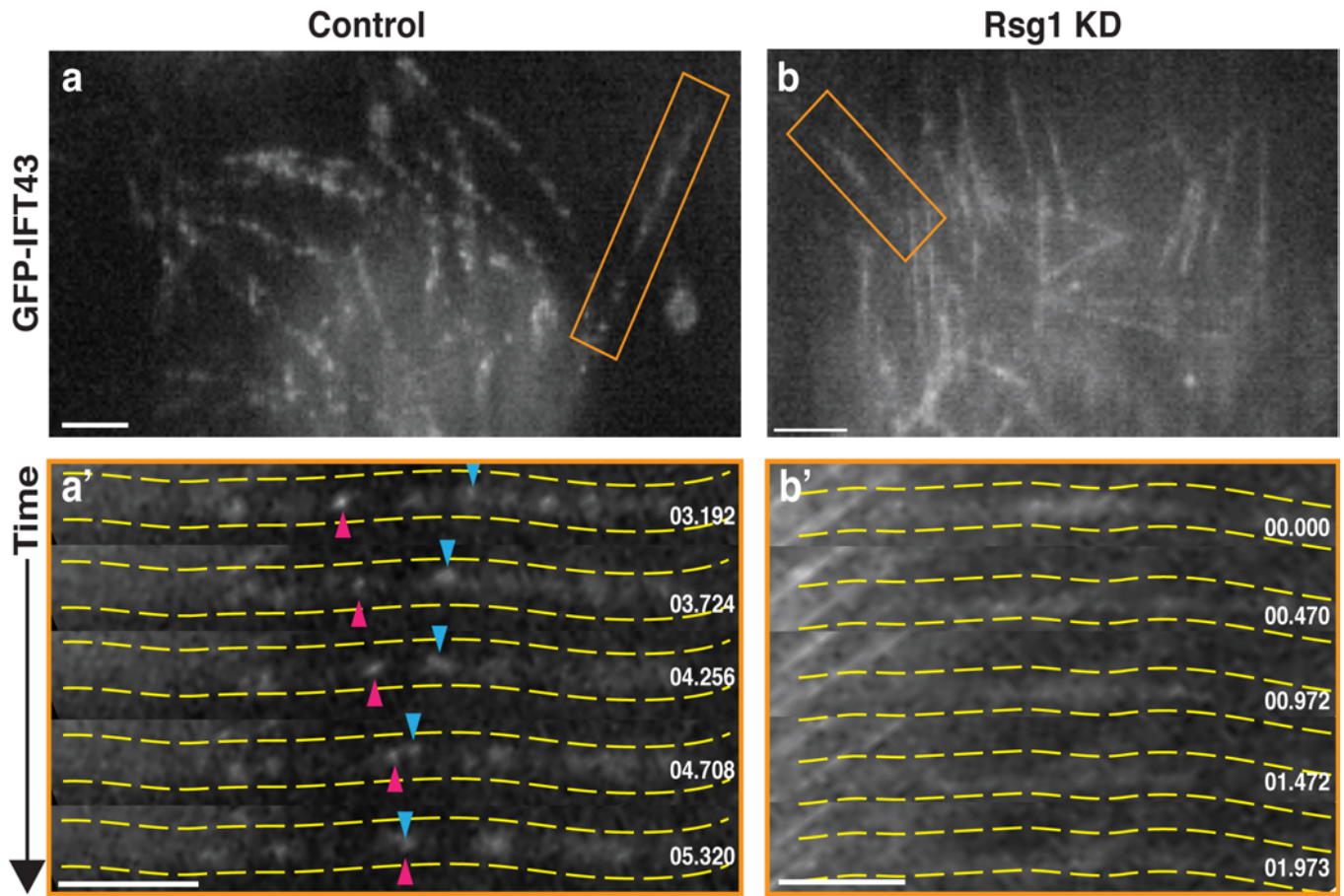


Figure 23: Axonemes from Rsg1 KD MCCs have reduced dynamic IFT43 signal. **(a)** High-magnification confocal image of axonemes from a control MCC expressing GFP-IFT43. The orange box indicates the region shown in **a'**. **(a')** A time series of a single control axoneme. Yellow dashed lines outline the axoneme, and distal is to the right. Pink and blue arrowheads indicate an anterograde train and a retrograde train, respectively. **(b)** High-magnification confocal image of axonemes from a Rsg1 KD MCC expressing GFP-IFT43. Orange box represents the region shown in **b'**. **(b')** A time series of a single axoneme from an Rsg1 KD MCC. Yellow dashed lines outline the axoneme, and distal is to the right. No IFT trains are visible during the course of the series. Note that the entire axoneme still exhibits a faint uniform background signal. Scale bars represent 3 μm .

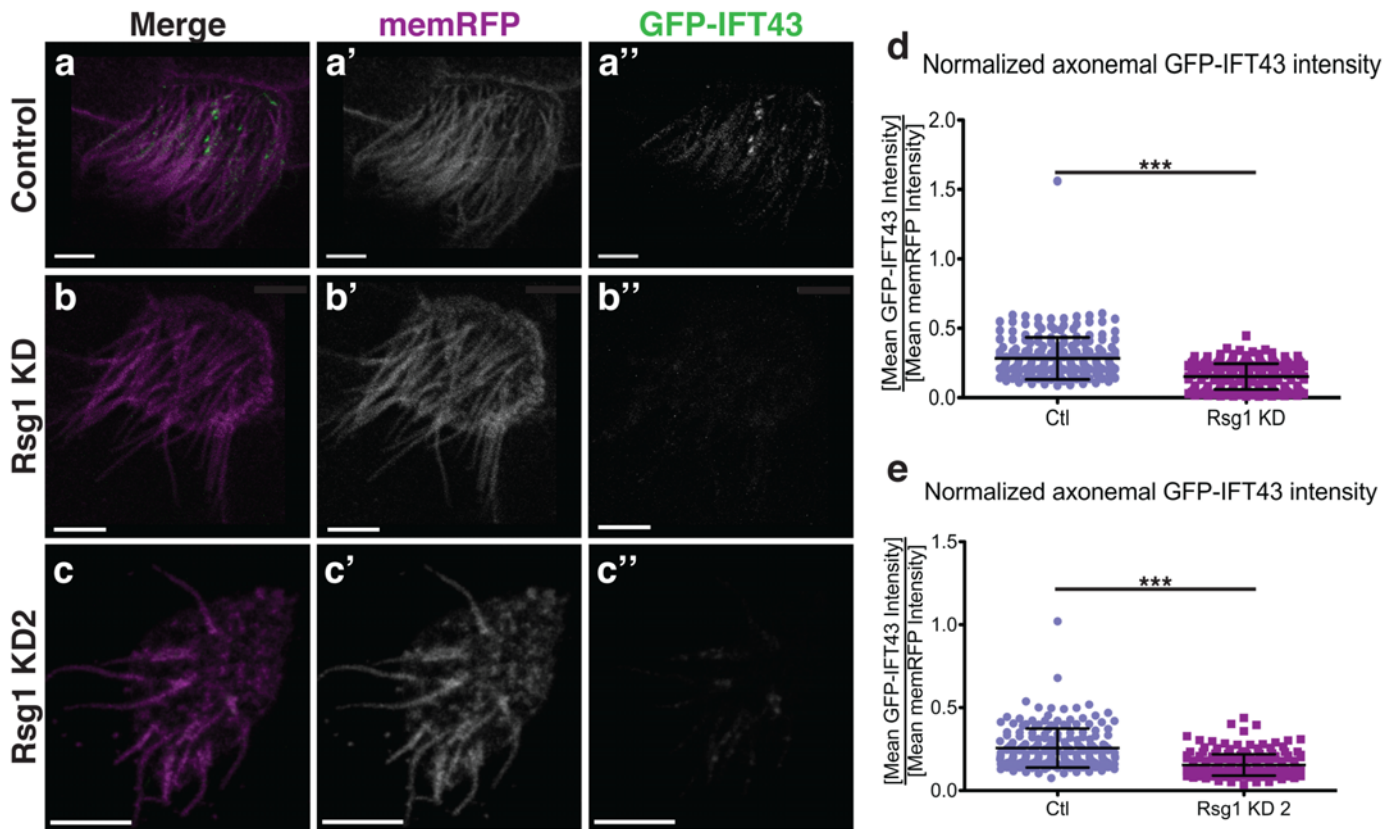


Figure 24: Loss of GFP-IFT43 from axonemes of Rsg1 KD MCCs. **(a-a'')** A single confocal slice of a control MCC co-expressing membraneRFP and GFP-IFT43. **(b-b'')** A single confocal slice of an Rsg1 KD MCC co-expressing membraneRFP and GFP-IFT43. **(c-c'')** A single confocal slice of an Rsg1 KD2 MCC co-expressing membraneRFP and GFP-IFT43 **(d)** Quantification of mean GFP-IFT43 signal along control and Rsg1 KD axonemes, as normalized to membrane RFP intensity along the same length. Note the decrease in normalized IFT43 signal in Rsg1 KD axonemes (Ctl (mean \pm SD): 0.28 ± 0.15 , $n = 225$ axonemes, 28 cells, 5 embryos vs. Rsg1 KD: 0.15 ± 0.09 , $n = 250$ axonemes, 32 cells, 6 embryos. $***p < 0.0001$). **(e)** Quantification of mean GFP-IFT43 signal along control and Rsg1 KD2 axonemes, as normalized to membrane RFP intensity along the same length (Ctl (mean \pm SD): 0.26 ± 0.12 , $n = 200$ axonemes, 44 cells, 6 embryos vs. Rsg1 KD: 0.15 ± 0.06 , $n = 223$ axonemes, 52 cells, 6 embryos. $***p < 0.0001$). Scale bars represent $5 \mu\text{m}$.

normalized IFT43 intensity (Fig 24a vs. b, d). I also performed the same analysis after injection of the Rsg1 KD2 morpholino and obtained similar results (Fig 24c-c'', e). Together these data suggest that loss of Rsg1 function leads to a failure of IFT43 localization to axonemes, though to a lesser extent than Fuz KD (Chapter 2).

Taken in whole, my analysis of IFT localization and dynamics within the axonemes of *Xenopus* MCCs suggests that Rsg1 is required for localization of the retrograde IFT43, and possibly other retrograde IFT-A proteins within axonemal IFT trains. Further, this failure of IFT43 incorporation leads to a failure of retrograde IFT transit, and an accumulation of anterograde IFT machinery along the length of the axoneme. It is interesting to note the differences in the accumulatory phenotype of anterograde IFT between Fuz knockdown and Rsg1 knockdown conditions. However, given the intrinsically variable nature of morpholino-mediated knockdown, it is impossible to determine if these differences are meaningful, or simply a result of different strengths of knockdown in the two conditions.

3.4: RSG1 FUNCTION IS REQUIRED FOR THE LOCALIZATION OF IFT43 BUT NOT IFT20 TO PERI-BASAL BODY POOLS OF IFT IN XENOPUS MULTICILIATED CELLS

In Fuz KD MCCs, IFT43, but not IFT20, fails to localize to cytoplasmic pools at basal bodies, and this is likely the cause of the axonemal IFT defects (Chapter 2). Given that Rsg1 KD axonemal phenotypes are so categorically similar to those of Fuz KD, I asked if the same failure to localize IFT43 to basal bodies also occurred in Rsg1

KD MCCs. To do this, I took single confocal slices of the apical surface of control and Rsg1 KD MCCs co-expressing either GFP-IFT20 or GFP-IFT43 along with the basal body marker Centrin-RFP (Fig 16a-f). I then used computational approaches to quantify various properties of basal bodies and their associated IFT pools.

First, I took the mean of the mean intensities of all GFP-IFT20 foci in a cell and normalized against the same value for Centrin-RFP. This value was statistically equivalent between control and Rsg1 KD MCCs, as expected from my studies on Fuz (Fig 26a; Chapter 2). Applying the same measure to GFP-IFT43 showed a modest, but significant decrease of GFP-IFT43 localization in Rsg1 KD conditions (Fig 26b). In addition, while some IFT43 foci are detectable by eye in Rsg1 KD MCCs (Fig 25e), they seem smaller and misshapen as compared to the controls. To further explore this defect, I normalized the average size of detected GFP-IFT43 foci in a cell against the average size of Centrin-RFP foci (which do not vary significantly between control and Rsg1 KD conditions; Fig 26h). As expected, this value is reduced in Rsg1 KD MCCs as compared to controls (Fig 26d). A similar analysis of GFP-IFT20 average foci area showed no significant difference between control and Rsg1 KD1 (Fig 16c). I also compared the number of detected IFT foci in a cell to the number of detected Centrin foci. There was no significant change in the number of GFP-IFT20 foci per Centrin-RFP foci between control and Rsg1 KD cells (Fig 26e). However, this value was significantly reduced in GFP-IFT43 expressing MCCs (Fig 26f). These analyses were repeated for Rsg1 KD2 MCCs and yielded similar results (Fig 27).

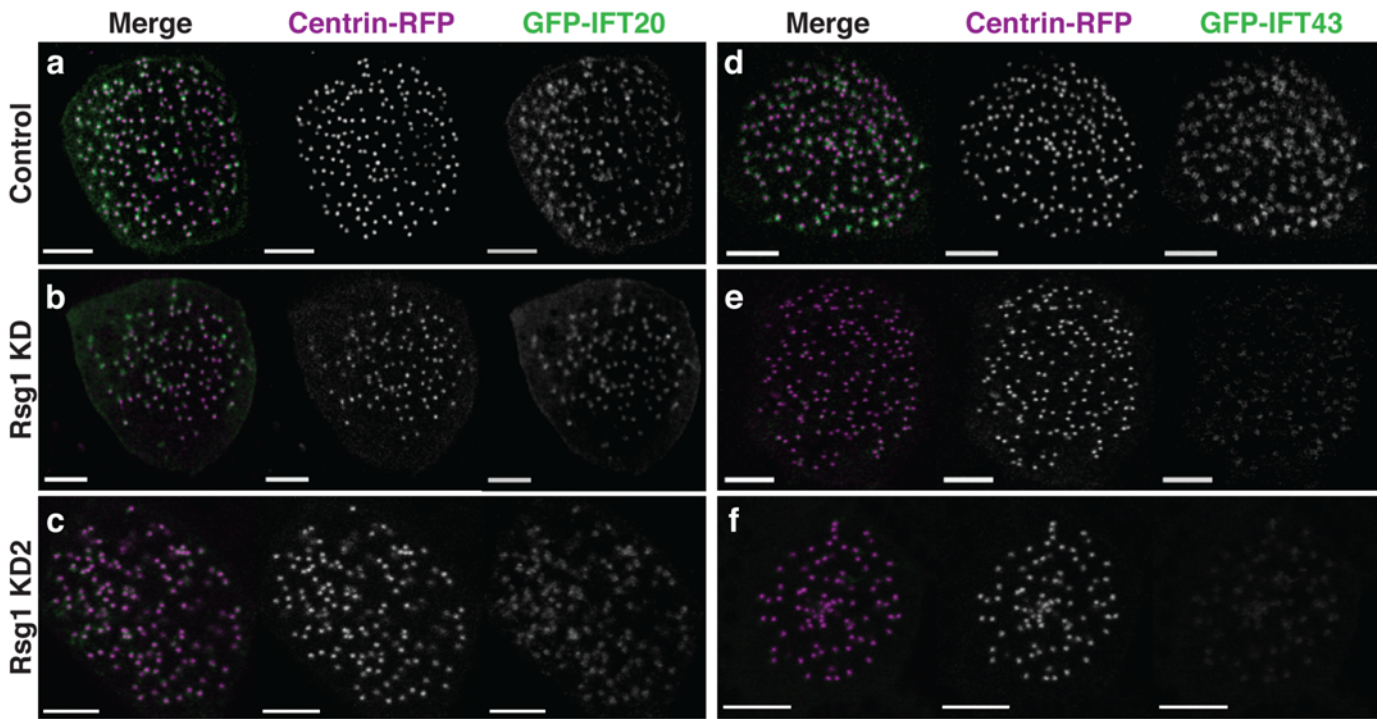


Figure 25: Rsg1 controls the localization of GFP-IFT43, but not GFP-IFT20 to basal bodies. **(a)** A single confocal slice of the apical surface of a control MCC expressing GFP-IFT20 and Centrin-RFP. **(b)** A single confocal slice of a representative Rsg1 KD MCC co-expressing GFP-IFT20 and Centrin-RFP. Note that despite the decreased density of Centrin-RFP foci there is still a strong correlation between the Centrin-RFP and GFP-IFT20 localization patterns. **(c)** A single confocal slice of a representative Rsg1 KD2 MCC co-expressing GFP-IFT20 and Centrin-RFP. **(d)** A representative control MCC expressing GFP-IFT43 and Centrin-RFP. **(e)** A representative Rsg1 KD MCC expressing GFP-IFT43 and Centrin-RFP. Notice the impaired localization of GFP-IFT43 to Centrin-RFP foci. **(f)** A representative Rsg1 KD2 MCC expressing GFP-IFT43 and Centrin-RFP.

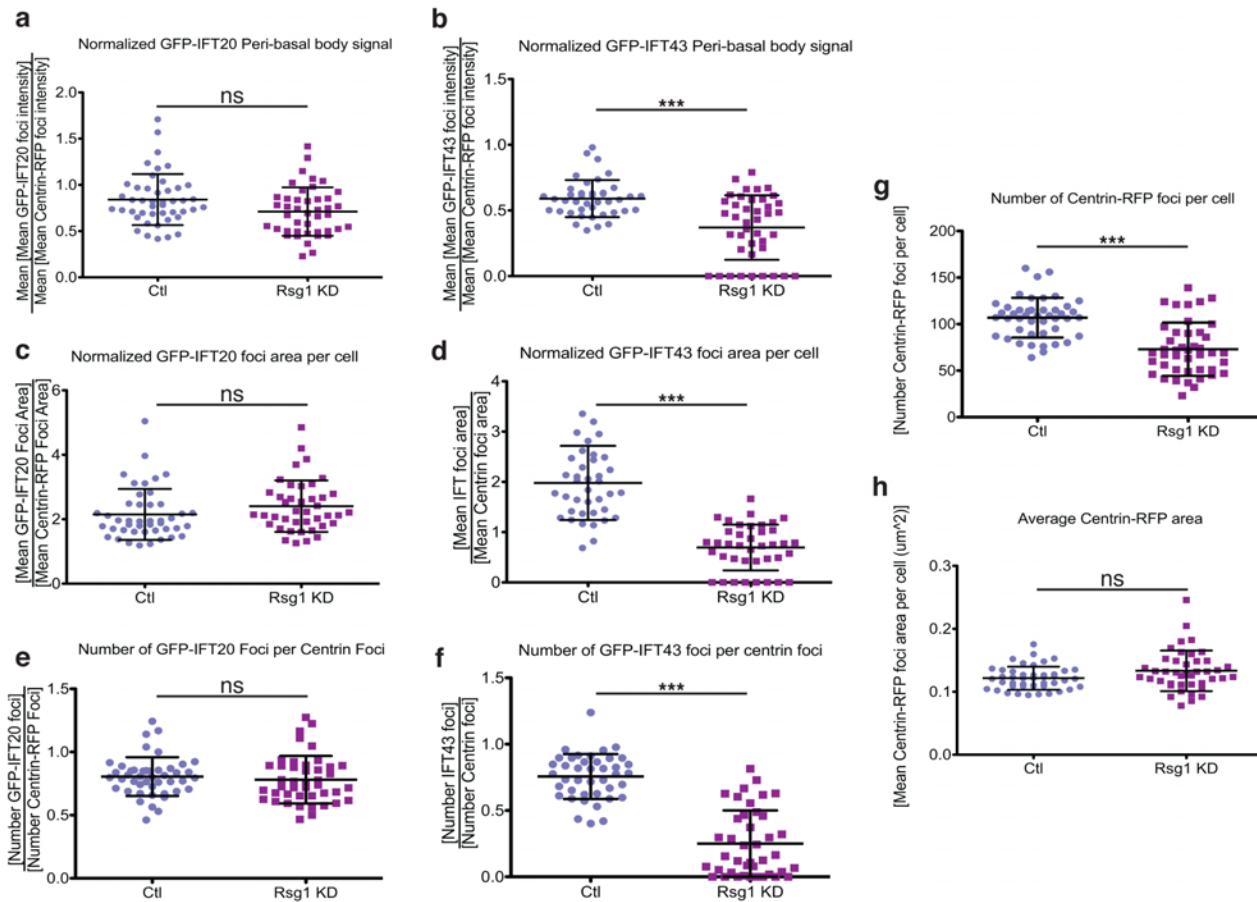


Figure 26: Quantification of GFP-IFT localization in control and Rsg1 KD MCCs. **(a)** Quantification of the mean of GFP-IFT20 foci mean intensities, as normalized to the same value for Centrin-RFP, shows no significant change between control and Rsg1 KD MCCs (Ctl (mean \pm SD): 0.84 ± 0.28 , n= 45 cells, 8 embryos vs. Rsg1 KD: 0.71 ± 0.26 , n= 43 cells, 8 embryos, p=0.042). **(b).** Quantification of the mean of GFP-IFT43 foci mean intensities, as normalized to the same value for Centrin-RFP, shows a significant decrease between control and Rsg1 KD MCCs (Ctl: 0.59 ± 0.14 , n=41 cells, 8 embryos vs. Rsg1 KD: 0.37 ± 0.25 , n=41 cells, 8 embryos. ***p<0.0001). **(c)** Quantification of the mean area of GFP-IFT20 foci in a cell normalized against the same value for Centrin-RFP shows no significant change between control and Rsg1 KD conditions (Ctl: 2.14 ± 0.79 , n=44 cells, 8 embryos vs. Rsg1 KD: 2.41 ± 0.80 , n=41 cells, 8 embryos. p= 0.3477). **(d)** Quantification of the mean area of GFP-IFT43 foci in a cell normalized against the same value for Centrin-RFP shows a significant decrease in Rsg1 KD MCCs as compared to controls (Ctl: 1.98 ± 0.74 , n=39 cells, 8 embryos vs. Rsg1 KD: 0.69 ± 0.46 , n=39 cells, 8 embryos. ***p<0.0001). **(e)** There is no significant change in the number of GFP-IFT20 foci detected per Centrin-RFP foci between control and Rsg1 KD MCCs (Ctl: 0.81 ± 0.15 , n=45 cells, 8 embryos vs. Rsg1 KD: 0.78 ± 0.19 , n=43 cells, 8 embryos. p=0.062). **(f)** There is a significant reduction in the number of GFP-IFT43 foci detected per Centrin-RFP foci between control and Rsg1 KD MCCs (Ctl: 0.76 ± 0.17 , n=41 cells, 8 embryos vs. Rsg1 KD: 0.25 ± 0.25 , n=41 cells, 8 embryos. ***p<0.0001). **(g)** There is a reduction in the number of Centrin-RFP foci detected on average in Rsg1 KD MCCs as compared to controls (Ctl: 106.90 ± 21.39 , n=45 cells, 8 embryos vs. Rsg1 KD: 72.95 ± 28.63 , n=43 cells, 8 embryos. ***p<0.0001). **(h).** The average area of detected Centrin-RFP foci is not significantly different between control and Rsg1 KD MCCs, indicating that there are no gross abnormalities in apically docked basal bodies upon Rsg1 KD (Ctl: 0.12 ± 0.02 , n=45 cells, 8 embryos vs. Rsg1 KD: 0.13 ± 0.03 , n=43 cells, 8 embryos. p=0.685).

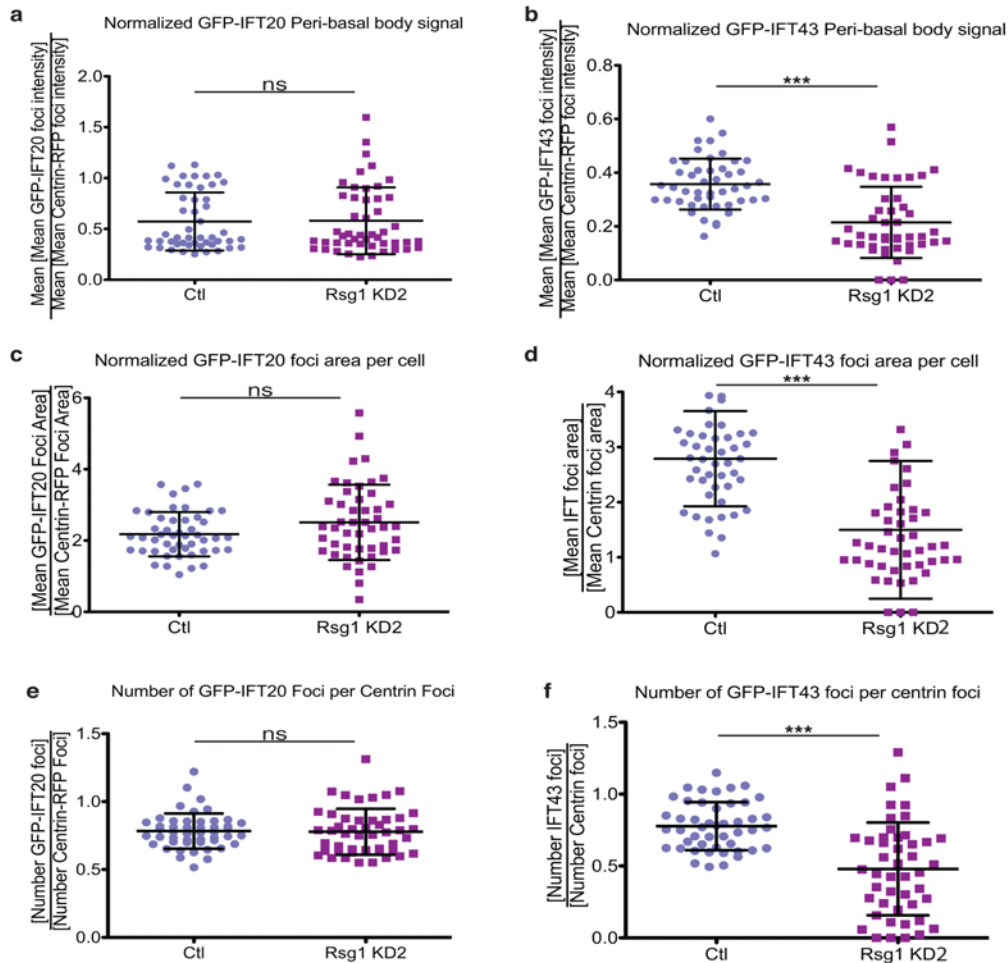


Figure 27: Quantification of GFP-IFT localization in control and Rsg1 KD2 MCCs. **(a)** Quantification of the mean of GFP-IFT20 foci mean intensities, as normalized to the same value for Centrin-RFP, shows no significant change between control and Rsg1 KD2 MCCs (Ctl (mean \pm SD): 0.57 ± 0.29 , $n = 48$ cells, 7 embryos vs. Rsg1 KD2: 0.57 ± 0.33 , $n = 48$ cells, 7 embryos, $p = 0.8980$). **(b)** Quantification of the mean of GFP-IFT43 foci mean intensities, as normalized to the same value for Centrin-RFP, shows a significant decrease between control and Rsg1 KD MCCs (Ctl: 0.36 ± 0.09 , $n = 47$ cells, 5 embryos vs. Rsg1 KD2: 0.21 ± 0.17 , $n = 46$ cells, 5 embryos. $***p < 0.0001$). **(c)** Quantification of the mean area of GFP-IFT20 foci in a cell normalized against the same value for Centrin-RFP shows no significant change between control and Rsg1 KD2 conditions (Ctl: 2.17 ± 0.62 , $n = 48$ cells, 7 embryos vs. Rsg1 KD2: 2.51 ± 1.06 , $n = 48$ cells, 7 embryos. $p = 0.1212$). **(d)** Quantification of the mean area of GFP-IFT43 foci in a cell normalized against the same value for Centrin-RFP shows a significant decrease in Rsg1 KD2 MCCs as compared to controls (Ctl: 2.79 ± 0.86 , $n = 47$ cells, 5 embryos vs. Rsg1 KD2: 1.50 ± 1.25 , $n = 46$ cells, 5 embryos. $***p < 0.0001$). **(e)** There is no significant change in the number of GFP-IFT20 foci detected per Centrin-RFP foci between control and Rsg1 KD2 MCCs (Ctl: 0.78 ± 0.13 , $n = 48$ cells, 7 embryos vs. Rsg1 KD2: 0.78 ± 0.17 , $n = 48$ cells, 7 embryos. $p = 0.5504$). **(f)** There is a significant reduction in the number of GFP-IFT43 foci detected per Centrin-RFP foci between control and Rsg1 KD2 MCCs (Ctl: 0.78 ± 0.17 , $n = 47$ cells, 5 embryos vs. Rsg1 KD2: 0.48 ± 0.32 , $n = 46$ cells, 5 embryos. $***p < 0.0001$).

Finally, I noticed that the apical basal body array seemed less densely populated in Rsg1 KD MCCs (Fig 25a-f). To test this I quantified the number of Centrin-RFP foci per MCC. While this value is variable even in control cells, I found that on average, there were fewer Centrin-RFP foci per cell between control and Rsg1 KD conditions (Fig 26g). However, the average absolute size of Centrin-RFP foci was not significantly different upon Rsg1 KD, suggesting that detected basal bodies are likely appropriately formed (Fig 26h).

The above data suggest that Rsg1 is required for the localization of IFT43 and possibly other retrograde IFT-A proteins to basal bodies, a role shared with Fuz. They also indicate that Rsg1 function may be shared with required for basal body biogenesis or docking.

3.5: RSG1 LOSS OF FUNCTION LEADS TO DEFECTS IN BASAL BODY APICAL MIGRATION

The reduced number of apically localized basal bodies could indicate that there is an apical trafficking defect of these basal bodies. To test this possibility, I took three-dimensional confocal stacks of single MCCs expressing Centrin-RFP and analyzed the distribution of Centrin foci. Control MCCs exhibit a stereotypical pattern whereby Centrin-RFP foci are arrayed at the apical surface (Fig 28a). In Rsg1 KD MCCs this pattern is variably perturbed, with either mild or severe

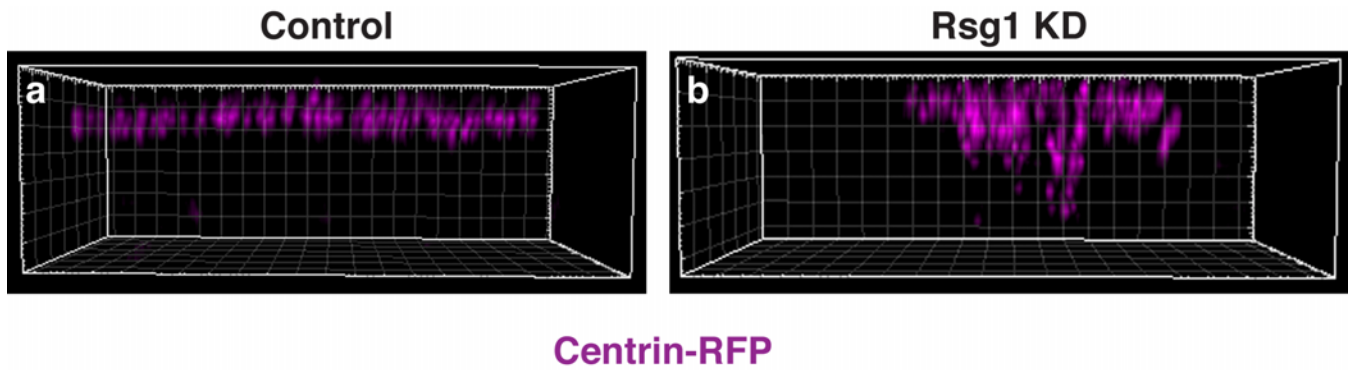


Figure 28: Rsg1 controls apical trafficking of basal bodies. **(a)** A 3D-reconstruction of the long axis of a control MCC shows a consistent localization of Centrin-RFP foci to the apical surface. **(b)** A 3D-reconstruction of the long axis of a Rsg1 KD MCC, shows a disorganization of Centrin-RFP foci, and a failure of some foci to localize apically. The grid-boxes in **a** and **b** are in 1 μm increments.

disruption of the apical array, as well as clumps of Centrin-RFP foci sitting below the apical surface (Fig 28b). When the total number of centrin-RFP foci in 3D reconstructions of MCCs was quantified, a modest, though significant, decrease was observed in Rsg1 KD MCCs (Ctl (mean \pm SD): 147.4 ± 12.47 basal bodies, $n = 21$ cells, 4 embryos vs. Rsg1 KD: 124.6 ± 24.36 basal bodies, $n = 21$ cells, 6 embryos. $p = 0.0012$). There are at least two interpretations of this result. First, Rsg1 KD MCCs often have a large closely-knit clump of sub-apical centrin-RFP foci (Fig 28b), which makes accurate quantification difficult and could lead to the observed reduction. A second interpretation is that there is a small defect in basal body generation, which might also be consistent with the observed sub-apical mass of centrin foci, as in *Xenopus* MCCs basal bodies are generated from sub-apical structures known as deuterosomes (Sorokin, 1968; Klos Dehring et al., 2013). Thus, the observed mass of centrin foci could be centered on a deuterosome undergoing defective basal body formation or failing to allow newly formed basal bodies to undergo appropriate trafficking. Therefore, there may be a defect in the latter steps of *de novo* basal body production (Sorokin, 1968; Klos Dehring et al., 2013).

3.6: DISCUSSION

One question that remains is how--or even if--Fuz and Rsg1 are coupled in the process of IFT localization to basal bodies. One hypothesis is that one of these

proteins is reliant on the other for its localization and/or function. Several lines of evidence suggest that Rsg1 may be the regulator if this is the case: First, its nature as a putative GTPase already suggests a mechanism for regulation of binding and/or localization. Second, the basal body docking phenotype in Rsg1 KD MCCs suggests that Rsg1 may be playing a role in the earliest localization events of ciliogenesis, while Fuz acts only later. Third, while the ciliogenic phenotypes in Rsg1 KD MCCs appear more severe than those of Fuz KD MCCs--overall shorter axonemes and far sparser ciliary tufts on average--axonemal IFT dynamics do not appear as perturbed as those in Fuz KD MCCs. One potential explanation for this is that Rsg1 controls the localization of a large number of ciliary proteins, including Fuz, while Fuz controls the localization of IFT43 and possibly other IFT-A proteins. Therefore, the partial loss of Rsg1 expected from incomplete knockdown would still allow some functional Fuz localization to basal bodies, which would--in turn--allow for the formation of a small number of appropriately assembled IFT trains. As a result IFT cycling dynamics might occur at a rate greater than allowed for by direct Fuz KD.

It is also interesting that there is a basal body docking phenotype in Rsg1 KD MCCs, but not in Fuz KD MCCs. This observation supports the notion that Fuz and Rsg1 may have partially non-overlapping functional profiles during ciliogenesis. Further, it suggests that Rsg1 might be involved in the Dishevelled/Inturned or Celsr2/3 mediation of basal body docking (Park et al., 2008; Tissir et al., 2010). If this is the case, then Rsg1 may sit at the nexus of many PCP dependent ciliogenic

processes. If so it will be interesting to discover if the GTPase activity of Rsg1 has some role in the regulation of ciliogenesis.

Chapter 4: Control of Intraflagellar transport by the novel Rfx2 target TTC29

4.1: INTRODUCTION

Rfx2 is a key transcriptional regulator of ciliogenesis in many tissues, including the embryonic *Xenopus* epidermis (Chung et al., 2012). Recent work demonstrated that it controls the transcription of a large subset of the ciliogenic machinery, including structural and motility factors that reside in the mature axoneme, as well as several intraflagellar transport proteins (Chung et al., 2014). This study additionally characterized a large number of proteins of unknown or poorly studied function as targets of Rfx2 transcription. These proteins were then functionally clustered by networking approaches using sophisticated guilt-by-association algorithms as functional predictors (Chung et al., 2014; Lee et al., 2011). One of the genes characterized in this way was the tetratricopeptide repeat containing protein of 29 kD (TTC29). This protein is poorly characterized but appears to be a dynein light chain of the LC8 family that interacts with the dynein arms of flagella (Hom et al., 2011). Interestingly, LC8 itself is required for retrograde IFT (Pazour et al., 1998).

Predictive networking suggested a strong functional link between TTC29 and the machinery of IFT, including a cluster of largely anterograde IFT-B proteins. Knockdown experiments in *Xenopus* MCCs demonstrated that TTC29 is

required for appropriate ciliogenesis. Further, TTC29-GFP was shown to localize along the length of axonemes, but not in the punctate distribution that would be expected from an IFT particle resident protein (see, for *e.g.*, the localization of IFT20 in Chapters 1 and 2) (Chung et al., 2014). I set out to directly test if TTC29 was important for IFT using *in vivo* imaging to examine IFT dynamics in the axonemes of TTC29 knockdown MCCs.

4.2: TTC29 IS REQUIRED FOR NORMAL ANTEROGRADE, BUT NOT RETROGRADE IFT DYNAMICS

Using high-speed confocal imaging, I analyzed the cycling dynamics of GFP-IFT20 labeled trains in the axonemes of *Xenopus* MCCs. Generally, TTC29 knockdown does not appear to effect IFT train morphology, and IFT trains continue to move bi-directionally without apparent stalling in these axonemes (Fig 29a vs. b). Interestingly, however, knockdown of TTC29 does result in a significant reduction in the average anterograde velocity of IFT trains (Fig 30a). This defect was specific to anterograde IFT, as retrograde velocity was unperturbed by loss of TTC29 (Fig 30b).

This specific disruption of anterograde IFT is very interesting, especially in light of the molecular identification of TTC29 as a dynein light chain, and given that the IFT dynein itself governs retrograde movement of trains. In addition, the

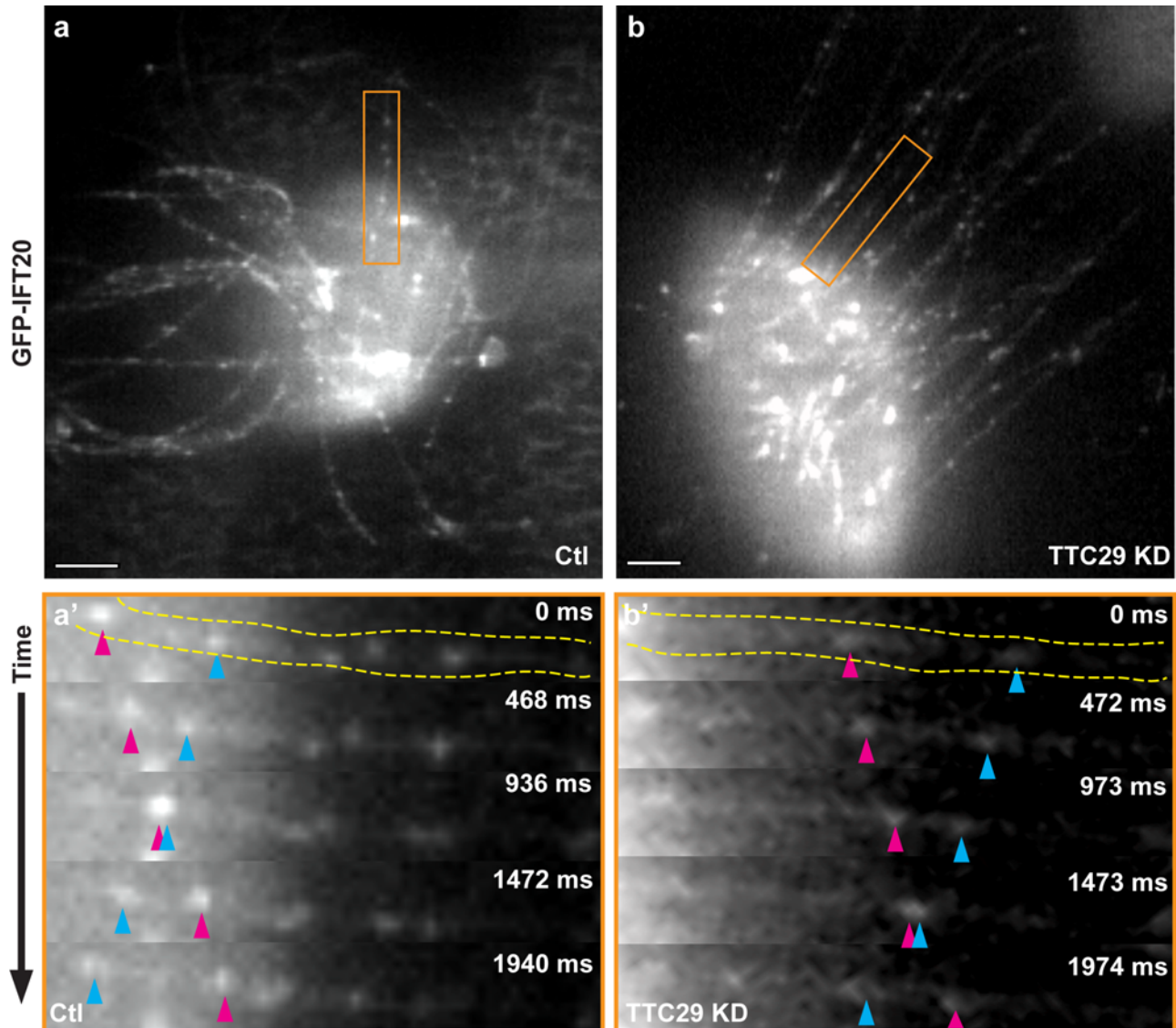


Figure 29: Loss of TTC29 does not lead to gross defects in IFT cycling dynamics. **(a)** Single frame from a high-speed confocal time-lapse data set of a control *Xenopus* MCC expressing GFP-IFT20. The orange box highlights the region shown in **a'**. **(a')** A series of stills of a single axoneme from a control MCC showing bidirectional IFT. Pink and blue arrowheads indicate a single anterograde and retrograde train respectively. **(b)** Single frame from a high-speed confocal time-lapse data set of a TTC29 KD *Xenopus* MCC expressing GFP-IFT20. The orange box highlights the region shown in **b'**. **(b')** A series of stills of a single axoneme from a TTC29 KD MCC showing no gross abnormalities in bidirectional axonemal traffic. Pink and blue arrowheads indicate a single anterograde and retrograde train respectively.

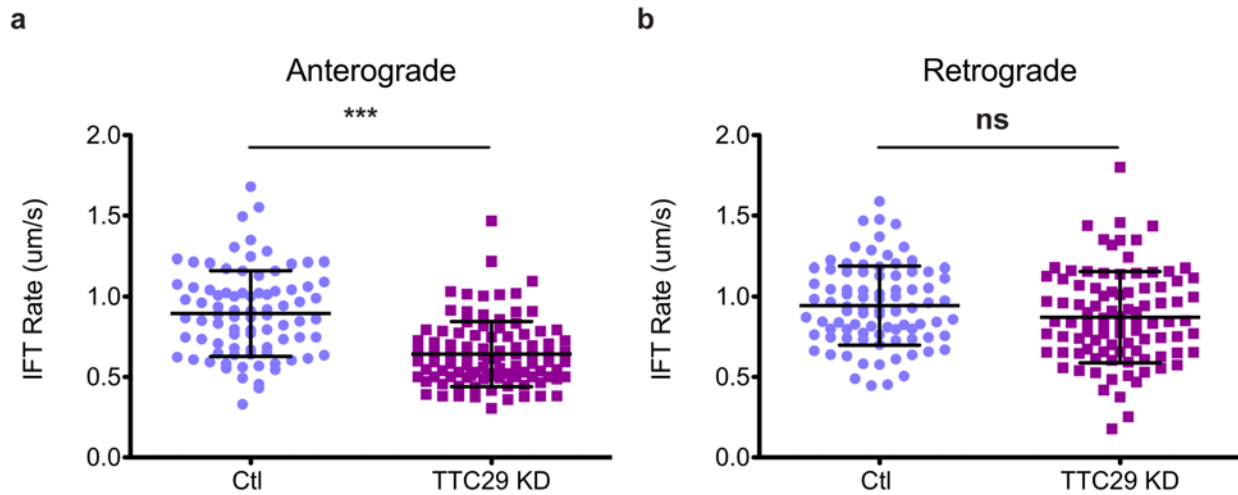


Figure 30: TTC29 KD leads to a reduction in the average anterograde, but not retrograde velocity of IFT trains. **(a)** Quantification of anterograde IFT train velocity in control and TTC29 KD conditions. IFT trains move at a significantly reduced rate in TTC29 KD axonemes (Control: $0.88 \pm 0.25 \mu\text{m/s}$, $n = 97$ IFT trains, 40 axonemes, 21 Cells, 6 embryos. TTC29 KD: $0.66 \pm 0.21 \mu\text{m/s}$, $n = 100$ IFT trains, 53 axonemes, 20 cells, 6 embryos. $p < 0.0001$). **(b)** No significant difference is observed in retrograde IFT rates between control and TTC29 KD conditions (Control: $0.94 \pm 0.30 \mu\text{m/s}$, $n = 87$ IFT trains, 40 axonemes, 21 cells, 6 embryos. TTC29 KD: $0.87 \pm 0.29 \mu\text{m/s}$. $n = 94$ IFT trains, 53 axonemes, 20 cells, 6 embryos. $p = 0.0510$).

localization of TTC29 along the length of the axonemes suggests that it may be part of the dynein arm complexes required for axonemal beating. If this is the case, TTC29 might be indirectly affecting IFT cycling by modifying the microtubule tracks that the trains move along. One potential role of TTC29 might be to act as a positive regulator of anterograde processivity to ensure that IFT trains move at a smooth and continuous pace (Ishikawa and Marshall, 2011; Dentler, 2005). If this is the case, IFT trains in axonemes with reduced TTC29 function should exhibit a more start-and-stop motion. This pause-and-run motility should be reflected in the distribution of instantaneous anterograde IFT velocities. To test this possibility, I re-examined the TTC29 KD data set. Each of the calculated IFT velocities reported above is in fact the average of three contiguous velocities, each independently calculated over a 500 ms window. Therefore, each train also has a standard deviation associated with it, and that standard deviation reflects the variation between those three independent velocity values. If TTC29 is indeed important for processivity the mean standard deviation of train velocity should be higher for IFT trains from TTC29 KD MCCs than those from control cells. This is not the case in either the anterograde or the retrograde train conformation (Fig 31), suggesting that TTC29 may not affect processivity. However, it is possible that the velocity windows are not discrete enough to accurately capture a series of very short pausing events.

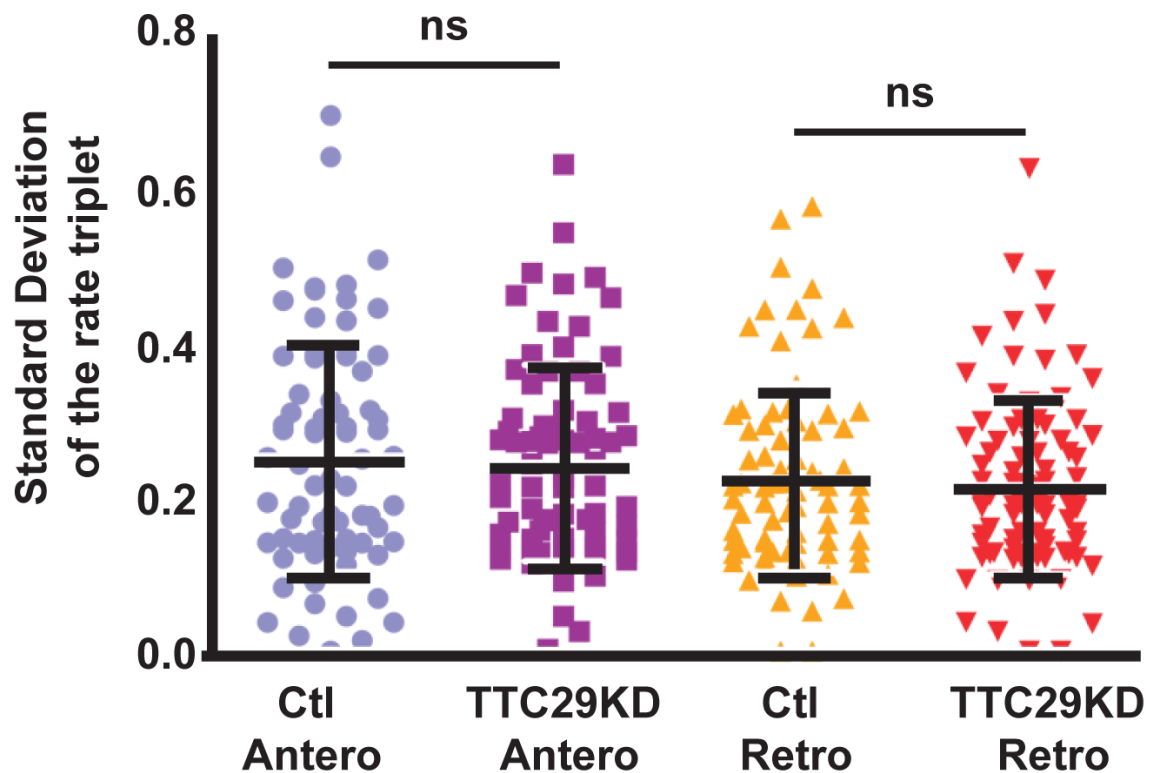


Figure 31: TTC29 KD does not lead to an increase in deviation between individual IFT velocity observations. There is no significant difference in the average deviation between individual observations of the raw rate triplets used to calculate the average velocity of an IFT train, either in the anterograde (Control anterograde: 0.25 ± 0.15 , $n = 72$ trains vs. TTC29 KD anterograde: 0.22 ± 0.13 , $n = 75$ trains, $p = 0.29$) or retrograde (Control retrograde: 0.24 ± 0.12 , $n = 74$ trains vs. TTC29 KD retrograde 0.21 ± 0.12 , $n = 84$ trains, $p = 0.17$) conformations, between control and TTC29 KD MCCs.

Unfortunately, the temporal resolution of the current method for *in vivo* IFT train imaging is limiting, as returned signal rapidly falls under the signal to noise threshold at increased acquisition rates.

4.3: CAN THE DEFECTS IN ANTEROGRADE CYCLING EXPLAIN THE SHORTENED AXONEMES OF TTC29 IMPAIRED MCCs?

It is noteworthy that the axonemes of MCCs with impaired TTC29 function exhibit a shortened morphology despite displaying grossly normal IFT cycling phenotypes. This suggests that the slowed anterograde IFT cycling dynamics in TTC29 KD cells could account for the change in ciliary length. This idea is supported by the idea that continuous delivery of new tubulin dimers to the distal tip of axonemes is required for length maintenance (Marshall and Rosenbaum, 2001; Marshall et al., 2005). Wallace Marshall and colleagues have developed a simple model of axonemal length that depends only on two parameters: the rate of new axoneme assembly and the rate of disassembly of existing axoneme (Marshall et al., 2005; Engel et al., 2009; Ludington et al., 2013). Observations have suggested that the disassembly rate is largely length independent, as flagella in *fla10* mutant *Chlamydomonas*, which at a restrictive temperature lack anterograde IFT and, as a result, cargo delivery disassemble and shorten at a uniform rate over time (Kozminski et al., 1995; Marshall and Rosenbaum, 2001). This process likely relies on depolymerizing kinesins

localized to the distal tip of the axoneme (Niwa et al., 2012; Piao et al., 2009; Blaineau et al., 2007). Assembly rate is thought to negatively depend on length, because IFT trains must undergo progressively greater displacement to reach the distal polymerization zone in elongating axonemes (Marshall and Rosenbaum, 2001; Engel et al., 2009). The length of the axoneme, therefore, is set by the so-called balance point, which describes the axonemal length where the assembly and disassembly rates are in equilibrium.

Assembly rate can be modified positively, therefore increasing the length at which the axoneme is in equilibrium. This can be accomplished by altering IFT train conformation, such that each train carries more cargo in a single trip (Engel et al., 2009), by increasing the rate of train injection, such that there are more trains per unit time (Ludington et al., 2013), or by modulating the rates of anterograde and retrograde IFT positively and negatively, respectively (Kozminski et al., 1995; Besschetnova et al., 2010; Tran et al., 2008; Kim et al., 2011). Conversely, disruption of any of these mediators can also lead to shortened axonemes.

Given the above findings, one prediction is that the reduced anterograde IFT velocity in TTC29 knockdown MCCs should shift the balance point towards a shorter axoneme, as the cargo delivery interval will increase. If this is the case, the rate of anterograde IFT should scale linearly with axoneme length, *i.e.* shorter axonemes should exhibit slower average IFT rates. To test this

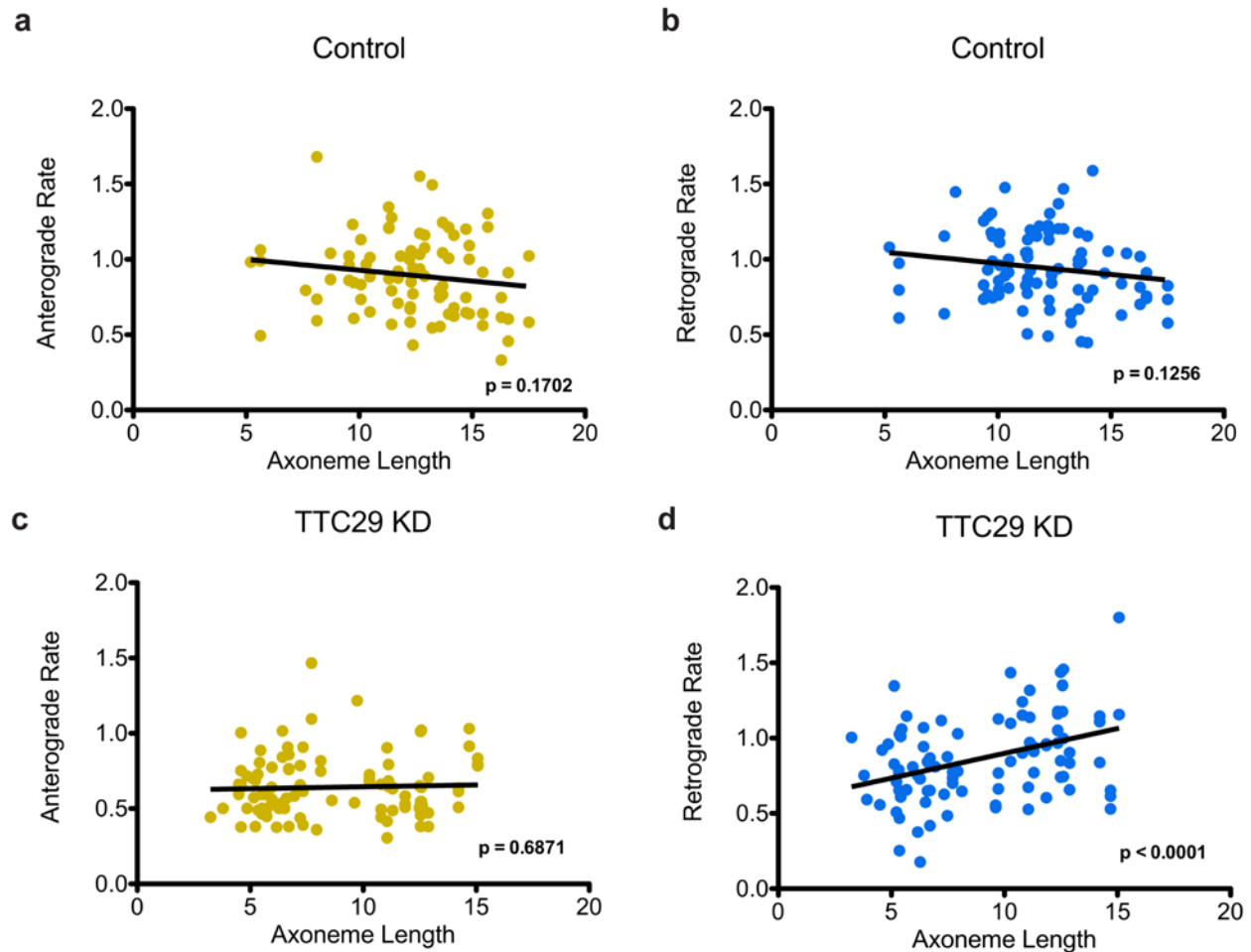


Figure 32: Correlation analysis between observed IFT velocity and axoneme length in control and TTC29 KD cells. **(a)** The velocity of anterograde IFT trains in control axoneme was determined and correlated with the length of the axoneme they were observed in. The two parameters showed no linear correlation (n=80). **(b)** No correlation was observed between retrograde rate and axoneme length in control MCCs (n=78). **(c)** There is no linear correlation between the reduced anterograde rates of IFT and shorter axonemes in TTC29 KD MCCs (n=81). **(d)** A positive correlation was observed between retrograde IFT rate and axoneme length in TTC29 KD cells, though this correlation has very little power (r-squared = 0.150), suggesting it may be uninformative (n=82).

prediction, I measured the average velocity of individual IFT trains as well as the length of the axonemes in which they were observed. Correlation analysis did not demonstrate any linear relationship between anterograde velocity and axonemal length in either control or TTC29 knockdown MCCs (Fig 32a, c). However, the dataset for this analysis is numerically limited, as it is difficult to find axonemes where the whole length is obvious and that also contain IFT trains of sufficient quality for velocity measurements. Interestingly, there was a weak correlation between retrograde velocity and axoneme length in TTC29 knockdown axonemes, but not controls (Fig 32d). Given the low r-squared value of this correlation (0.150) and the low number of data points, however, it is hard to draw any significant conclusions from this result.

Together these data suggest that the shortening of axonemes in TTC29 knockdown MCCs most likely cannot be attributed simply to the reduced anterograde IFT velocities, but may additionally reflect defects in train composition or cargo loading. It is also possible, as noted above, that the data set itself is numerically insufficient, and therefore lacks the statistical power to answer the question of correlation between velocity and length. Future experiments, perhaps with automated axonemal segmentation and train analysis, will be useful in exploring this connection further.

4.4: CONCLUSIONS

The data presented here demonstrate that TTC29 is required for appropriate anterograde IFT dynamics, though its mechanism of action remains obscure. Knockdown of TTC29 does not seem to affect the processivity of IFT trains, nor is there a strict correlation between anterograde rate and axoneme length in these cells. It is interesting that TTC29 was identified as a dynein light chain that interacts with the dynein arms of flagellar doublets in *Chlamydomonas* (Hom et al. 2011). The localization of GFP-TTC29 along the entire length of axonemes in *Xenopus* MCCs seems to support this data (Chung et al. 2014). If TTC29 is linked to the dynein arms of ciliary doublets, it would be unlikely to effect IFT in primary cilia, as these structures lack dynein arms (See Chapter 1). Further, if TTC29 function is specific to motile cilia, it will be exciting to uncover if it somehow functionally bridges ciliary beating and IFT motility. One possibility is that TTC29 serves to mediate processive IFT motility along microtubule tracks that repeatedly slide and deform as the cilia undergoes beating cycles, perhaps by anchoring IFT trains to the dynein arms.

Chapter 5: Conclusions and future directions

In the previous chapters of this work, I presented evidence demonstrating that the planar cell polarity (PCP) effector Fuz is a key regulator of ciliogenesis via its effect on IFT localization and dynamics (Chapter 2). I also showed that the putative small GTPase Rsg1, which binds Fuz, is required for IFT localization and dynamics, and additionally that it plays a role in basal body docking (Chapter 3). Finally, I demonstrated that TTC29, a poorly studied Rfx2 target, functions to modulate anterograde but not retrograde IFT dynamics (Chapter 4). In this chapter, I would like to present some larger functional context to these findings and to offer some thoughts as to how future interrogation of the events of ciliogenesis controlled by these three factors might proceed.

5.1: GENERAL FUNCTIONS OF FUZ

While the data presented in Chapter Two clearly describe a role for Fuz in the regulation of IFT via a cytoplasmic control mechanism (see below), they do not, of themselves, tell us the molecular function of Fuz. In many ways, Fuz is a frustrating protein to work with and very little is known about it.

Fuz was first identified in forward screens in *Drosophila* as a planar cell polarity effector controlling the orientation of wing hairs, a process known to require the precise regulation of the actin cytoskeleton (Collier and Gubb, 1997; Bayly and Axelrod, 2011). Subsequent studies of vertebrate Fuz have demonstrated a strong requirement for the protein in ciliogenesis (as detailed in Chapter 2 and (Park et al., 2006; Heydeck et al., 2009; Gray et al., 2009)), but have also offered up few details about the general function of this protein. Gray et al. showed that Fuz is required for appropriate exocytosis in non-ciliated cells and further suggested, by predictive functional network analysis, that Fuz is likely to be involved in vesicular trafficking (Gray et al., 2009). Another recent study showed, in support of this idea, that Fuz controls the organization of Rab8 and Dishevelled at basal bodies (Zilber et al., 2013). Finally, there are also indications that Fuz might be required for the morphogenesis of the apical actin and microtubule networks of multiciliated cells (Park et al., 2006).

The data presented in Chapter 2 suggest that Fuz is a key regulator of cytoplasmic protein localization, but cannot distinguish between a vesicular or cytoskeletal role. The analysis is not simplified by the interconnectedness of the two processes. It is tempting to propose a mechanism for Fuz whereby it functions, in general, as a mediator of polarized vesicular trafficking, and that it is important, specifically, for selective traffic to the basal body during ciliogenesis. Such a function would handily explain both the data on IFT

localization, presented here, and the Rab8 localization data (Zilber et al., 2013). However, there is still no direct evidence for this model, and the data could be alternatively--though not as parsimoniously--explained by a role for Fuz in protein anchoring or protection from degradation, or even by effects on cytoskeletal organization. However, a role for Fuz in transcription can likely be ruled out as its control of IFT43 localization occurs even for protein molecules produced from exogenously introduced mature mRNA.

A vesicular trafficking model for Fuz function, even if true, leaves much to be desired. Clearly, Fuz does not traffic all ciliogenic cargos, and so any complete model must describe the selection mechanism for transport by Fuz in addition to establishing the particulars of Fuz-mediated trafficking. These include the cytoplasmic structures along the Fuz-directed trafficking pathway and the molecular machines driving the transport. One exciting finding in this regard comes from a recent study of alpha-virus entry, where a whole genome siRNA screen identified Fuz as a positive regulator of viral entry into the cell. Fuz function in this context seems to be important for viral endocytosis, and in addition, loss of Fuz inhibited the endocytosis and/or accumulation of exogenously applied transferrin in endosomes, suggesting that Fuz may be required for general endocytic events (Ooi et al., 2013).

How might this data inform our understanding of the role of Fuz in ciliogenesis? One potential link could be the recycling endosome (RE) pathway,

which is a key mediator of plasma membrane recycling as well as a destination for some endocytosed traffic. REs also serve as mediators of sorting for some post-TGN traffic (Ang and Fölsch, 2012), are Rab11 positive, and localize to centrosomes (Ullrich et al., 1996). The recent finding that Rab11 marks a vesicular-tubular structure that acts as a reservoir for ciliary cargos suggests that REs or some part of the RE pathway may be important in ciliogenesis (Kim et al., 2010a). Indeed, the ciliogenic protein Arl13b is also required for endocytosis (Barral et al., 2012). Given the links between cilia and endocytosis, it is tempting to suggest that Fuz acts, in general, in some manner to mediate traffic through REs, and that this is how it promotes IFT43 and Rab8 localization during ciliogenesis (Chapter 2 and (Zilber et al., 2013)). This idea is supported by the observation that IFTs have been shown to flux through REs and are required for polarized recycling of T-cell receptors (Finetti et al., 2009).

Regardless of the role Fuz plays in trafficking, it will be important to understand how Fuz itself is regulated. This is not a simple task, given that the protein has little in the way of informative sequence (Collier and Gubb, 1997; Gray et al., 2009). Answering these questions will require sophisticated experimental analysis, but given the links between Fuz and entire classes of human diseases, *e.g.* neural tube closure defects and craniofacial dysmorphology, the investment is worthwhile (Seo et al., 2011; Tabler et al., 2013).

5.2: CYTOPLASMIC CONTROLS OF INTRAFLAGELLAR TRANSPORT

In Chapter Two, I presented data that Fuz is a key mediator of vertebrate intraflagellar transport (IFT) and that it performs this function by controlling the cytoplasmic localization of one or more retrograde IFT proteins. This is an interesting finding, as there are only a handful of known mediators of IFT lying outside of the core biochemical complex. Some of these were discussed briefly earlier, but I would like to expand upon them here.

First, the Bardet-Biedl Syndrome (BBS) proteins BBS7 and BBS8 are key regulators of motor coordination during IFT in the nematode *C. elegans* (Blacque et al., 2004). It is worth noting, here, that *C. elegans* possess cilia that are quite derived from the standard architecture described in Chapter One (Ward, 1973; Ward et al., 1975; Perkins et al., 1986; Inglis et al., 2007). As a result, the heterotrimeric kinesins that carries the IFT trains along the doublets in these cilia can not seem to move along the singlet microtubules (Blacque et al., 2004; Ou et al., 2005; Snow et al., 2004). It is unclear if the same kind of functional coordination of motors is involved in other organisms that lack the unique singlet architecture of *C. elegans* sensory cilia. Additional IFT regulators outside of the main pathway include the ciliary membrane-resident small GTPases Arl13b and Arl3b, which are required for the coherence of the IFT-A and IFT-B complexes during axonemal transport (Cevik et al., 2010; Li et al., 2010), the Rab8 interacting protein Elipsa, which is required for the localization of both IFT-A and IFT-B

proteins to the base of cilia (Omori et al., 2008), and Oral-facial-digital 1 (Ofd1) which appears to be required specifically for the basal body localization of IFT88, a key member of the IFT-B complex.

It seems clear that one of the key regulatory steps involved in ciliogenesis is the localization of the IFT proteins to the base of cilia. It is interesting, then, that a recent report demonstrated that as little as 20% of IFT-A and 2% of IFT-B proteins are found in actively cycling IFT trains at any given time (Wang et al., 2009). This suggests that there is a significant excess of IFT in the cell, and that this excess is still tightly localized to the basal body. It remains to be seen whether this extra IFT in basal body pools has non-train functions, or is simply a safety measure to ensure processive cycling (Qin, 2012). However, the tight control of this cytoplasmic localization suggests that these IFT pools are somehow critical for the cell.

Fuz, specifically, is responsible for the localization of at least one key retrograde IFT-A protein to basal bodies, but does not seem to affect the localization of anterograde IFTs. This result suggests that IFT-B and IFT-A may be under different cytoplasmic controls, although the regulatory benefit of this is not immediately apparent. The role of IFT proteins in cells without cilia, or in cycling cells is only now under study. Recent reports have suggested that IFT proteins are key mediators of T-cell receptor recycling (Finetti et al., 2009) and are involved in spindle positioning (Delaval et al., 2011; Borovina and Ciruna,

2013) and cell cycling (Robert et al., 2007; Qin et al., 2007). The close association of IFT proteins with centrioles, which are obviously key players in these processes, may explain these functions; however, it is notable that these reports have only implicated anterograde IFT-B proteins in these extra-ciliary roles. This suggests that cytoplasmic controls of IFT may play a role in aspects of cell biology aside from ciliogenesis, and may also provide an explanation for the differential regulation of IFT-A and IFT-B proteins.

As a final note, spatio-temporal control of Fuz expression and/or function may be a way for cells to control the disassembly of cilia--a key process in both cell cycling and the resolution of developmental signals (Kim et al., 2011; Anderson and Stearns, 2009; Paridaen et al., 2013). If Fuz function were reduced, either by autoinhibition (as has been suggested by Ryan Gray in unpublished work) or by other methods of functional reduction (*e.g.* degradation), functional IFT-A would be reduced as a consequence. This, in turn, would lead to a disassembly of the cilium, as it is starved of new cargos due to a failure in IFT cycling, and a concomitant failure in the delivery of essential structural cargos. It seems unlikely that Fuz would act alone to disassemble cilia, but its regulation by a “master” disassembly program would be unsurprising, and it will be interesting to discover if cytoplasmic localization of IFT proteins is a generalizable motif for the control of ciliogenesis.

5.3: DO THE PLANAR CELL POLARITY EFFECTORS AND RSG1 FUNCTION TOGETHER DURING CILIOGENESIS?

The downstream planar cell polarity effectors Fuz, Intu, and Fritz all have demonstrated roles in ciliogenesis. Fuz controls IFT and possibly other vesicular trafficking events, Intu seems to govern basal body docking and polarity (Park et al., 2008), and Fritz governs the establishment of a septin diffusion barrier at the base of the cilium (Kim et al., 2010b). While each effector appears to have a unique function, it remains unclear if they act independently or in concert during the process of ciliogenesis. High-throughput proteomics may be the way to answer this question. Such studies would determine if these factors bind one another and clarify whether and how their functional interaction profiles overlap.

One question of particular interest is the role of the small GTPase Rsg1 in mediating the ciliogenic activities of these proteins. The data presented in Chapter Three strongly implicate Rsg1 in the regulation of both Fuz-dependent IFT localization as well as in the process of basal body docking--which appears to be Fuz independent, but does require the function of Dishevelled and Intu (Park et al., 2008). It will be interesting, therefore, to test the polarization of axonemes and the localization of active RhoA and Sec8 within Rsg1 knockdown MCCs, as these are established readouts of Dishevelled/Intu function. Such experiments will indicate if Rsg1 function overlaps that of multiple PCP-

dependent ciliogenic processes. Further, it will be interesting to explore the integrity of the septin diffusion barrier in this context to understand if PCP effector function somehow converges on Rsg1. Finally, it will be informative to explore the epistatic relationship of Rsg1 to Fuz, Intu, Fritz and Dishevelled.

If Rsg1 proves to be a central player in PCP action during ciliogenesis--which seems possible given its broad ciliogenic phenotypes--it will be informative to analyze the role of guanine nucleotide cycling. Previous work indicates that mutating the invariant threonine residue responsible for GDP-GTP exchange results in a dominant negative Rsg1 protein that inhibits ciliogenesis (Gray et al., 2009). This could be the result of impairment of some intrinsic conformational switch-like action of Rsg1 or perhaps due to the inhibition of Rsg1-dependent activation of binding partners, *e.g.* Fuz. In either case, GTPases are excellent targets for pharmacological modulation, and given the many links between PCP action in ciliogenesis and human disease (Seo et al., 2011; Kim et al., 2010b; Tabler et al., 2013), it may be worthwhile to develop intervention strategies for Rsg1 function.

5.4: UNDERSTANDING THE MECHANISMS OF IFT

IFT is a fascinating transport system, and despite rigorous biochemical and genetic characterization of the factors involved, we still have only a basic

understanding of how it functions. One of the key challenges impeding our understanding is a lack of knowledge about how individual IFT proteins function. Happily, a new generation of biochemical and structural studies are underway that will allow us to dig into IFT train and cargo organization at an unprecedented scale. In the past few years, studies have been published characterizing the first crystal structures of IFT proteins (Bhogaraju et al., 2011; 2013a; Mizuno et al., 2012), while other studies have begun to uncover the molecular functions of individual IFT proteins, including a study of the tubulin binding motifs central to the function of the pathway (Bhogaraju et al., 2013b). Hopefully, these next generation studies will clarify the regulatory logic of IFT train organization and suggest mechanisms for motor coordination and cargo loading, areas which are currently poorly understood.

Another key area of innovation is required for a truly meaningful understanding of IFT and that is true high-resolution dynamic analysis of IFT protein behaviors, both in the cell body and within the axoneme. Despite two decades of study, we still possess only a largely superficial understanding of how these dynamics are regulated at key junctures. Poorly understood areas include: the injection of IFT trains at the ciliary base, the turnaround events at the tip of the cilium, and a number of low frequency behaviors along the length of axonemes with unknown import (Dentler, 2005). Understanding these dynamic behaviors will be critical to understanding the molecular etiologies of those

human ciliopathies that present without obvious defects in cilia morphology (Rix et al., 2011; Davis et al., 2011; Beales et al., 2007), and also for understanding the dynamics of developmental signal processing (Liem et al., 2012; Ocbina et al., 2011; Friedland-Little et al., 2011).

One case study that suggests improved IFT analysis will be beneficial is the relationship between TTC29 and IFT dynamics presented in Chapter Four. My preliminary analysis confirmed the predictive-network derived functional link between TTC29 and IFT cycling. While the data demonstrated that TTC29 knockdown led to defects specifically in anterograde IFT behaviors, they failed to uncover any linear correlation between slowed IFT and decreased axonemal length. It is possible that such a correlation does not exist--though there is strong evidence for length dependence on IFT rate in other contexts (Engel et al., 2011; Besschetnova et al., 2010). Alternatively, its possible that the analysis did not possess a high enough signal-to-noise ratio, or that it lacked the statistical power to uncover such a correlation; such deficiencies could be minimized by increasing the size and depth of the dynamic IFT data sets. Unfortunately, without automated analysis tools, data set size is rate-limited by the time intensive process of manual tracking and analysis.

In order to truly understand IFT dynamics, datasets need to be expanded, and ideally by at least an order of magnitude. This will require the development or cooption of automated image analysis tools. Ideally, such tools will allow

automated segmentation of axonemes, increased fidelity in identifying trains, and higher resolution tracking of parameters during the axonemal lifetime of any given train. Unfortunately, these algorithms depend on high signal to noise ratios, and so the underlying imaging will have to improve as well. Use of new, brighter fluorophores (Ptaszek, 2013) and alternative imaging technologies such as quantum dots (Ye et al., 2013) will help increase signal, as will the application of photoactivation and photobleaching technologies. Even still, there are two major challenges facing high-resolution acquisition of dynamic IFT data: acquisition time and diffraction limits. Fortunately, high-speed confocal microscopy is maturing, and such acquisition is not as challenging as it once was. Diffraction limits, on the other hand, are not as easily overcome. Bypassing them currently requires time and resource intensive super-resolution technologies such as PALM. This means that analysis of IFT dynamics in small primary cilia will remain a challenge, although not a totally insurmountable one, as several groups demonstrated (Besschetnova et al., 2010; Tran et al., 2008). However, the longer axonemes of *Chlamydomonas* and of vertebrate multiciliated cells provide excellent imaging platforms. The large, discrete IFT trains of these axonemes make an ideal starting place to develop the automated segmentation at the individual train level, and will allow for the high-resolution tracking required to truly understand IFT dynamics and their effects on cilia structure and function.

5.5: CONCLUDING REMARKS

The cilium is a fascinating organelle, both in and of itself, and also as an experimental platform for studies of structure-function relationships, the transcriptional controls of sub-cellular macro-structures, and the dynamics of signal transduction. Here, I have built a novel platform for studying the dynamics of transport within the cell body and axonemes of vertebrate multiciliated cells. This system itself is at least as important as the discoveries it led to. In fact, I would argue that the system is more important, as it is extensible to other problems in ciliogenesis and is amenable to moderate-throughput up-scaling. It offers high temporal and spatial resolution of intraflagellar transport at the single train level and will serve as a valuable tool in advancing our understanding of the dynamics of ciliogenesis. Given the import of cilia in human development and homeostasis, and the severe pathologies resulting from defects in their structure and function, it is critical that we continue to push forward our understanding of their underlying biology.

Appendix: Materials and Methods

A.1: *XENOPUS* EMBRYO MANIPULATIONS

Female adult *Xenopus laevis* were ovulated by injection of human chorionic gonadotropin, and eggs were fertilized in vitro, dejellied in 3% cysteine (pH 7.9), and subsequently reared in 0.3x Marc's Modified Ringer's (MMR; 0.1 M NaCl, 2.0mM KCL, 1mM MgSO₄, 2mM CaCl₂, 5mM HEPES (pH 7.8) in double distilled H₂O, pH to 7.4). For microinjections, embryos were placed in a solution of 2.5% Ficoll (w/v) in 0.3% MMR, injected using forceps and an Oxford universal micromanipulator, reared in 2.5% Ficoll in 0.3x MMR to stage 9, then washed and reared in 0.3x MMR alone (Sive et al., 2000).

A.2: PLASMIDS AND CLONING

Xenopus laevis IFT20 and IFT80 sequences were identified using Xenbase (Bowes et al., 2008), amplified from cDNA using Phusion High-Fidelity Polymerase (NEB), and subcloned into the CS107-GFP-3Stop backbone by double digestion with XhoI and NotI restriction enzymes. This backbone includes an SP6 promoter and an SV40 polyadenylation signal sequence for in vitro transcription of messenger RNA. *Xenopus laevis* IFT43 provisional sequence was obtained from Xenbase, and amplified and subcloned into CS107-3Stop-GFP

as above. RFP-CLAMP was generated by sub-cloning of the previously generated CLAMP-GFP (Gray et al., 2009) into CS107-RFP-3Stop backbone. Membrane-RFP (in the CS2+ backbone), Centrin-RFP, GFP-MAP7 (also called GFP-ensconsin) and EB3-GFP (each in a CS107-3Stop backbone) were used as previously reported (Shindo et al., 2008; Woolner et al., 2009; Gray et al., 2009). All constructs were verified by sequencing.

A.3: MORPHOLINO AND MRNA INJECTIONS

Capped, polyadenylated mRNA was generated from CS107-3Stop plasmids after linearization by *AscI* digestion using the Ambion SP6 mMessage mMachine kit. The splice blocking Fuz morpholino (5'-ATCCACTTACTTACCGTAGGACTCC-3') has been previously described and shown to reduce proper splicing of Fuz resulting in a truncation of Fuz and loss of Fuz function (Park et al., 2006; Gray et al., 2009). The translation blocking Rsg1 morpholino (5'-GGCCCGTATCTCTGT-3') has been previously described (Gray et al., 2009). In addition, a second, non-overlapping translation-blocking morpholino against Rsg1, termed Rsg1 KD2, was obtained (5'-AGCTTCCGGTAACAAGTCAGTGCAG-3'). The TTC29 morpholino (5'-GTGCACTCATTCTCTTCAAGTTTGC-3') was used as described in (Chung et al., 2014). mRNA and/or morpholinos were injected into two ventral blastomeres at

the four cell stage. mRNAs were injected at 50-200 pg per blastomere. Morpholinos were used as follows: Fuz KD, 60ng; Rsg1 KD1 and KD2, 30ng; TTC29 KD, 40 ng; per each blastomere.

A.4: IFT IMAGING AND QUANTITATION

For high-speed in vivo imaging of IFT, in vitro synthesized capped mRNA was injected into *Xenopus laevis* embryos at the 4-cell stage, targeting the ventral/animal blastomeres to ensure expression in the ciliated epidermis. At tailbud stages (~ NF Stage 25; (Nieuwkoop and Faber, 1994)), embryos were mounted flank down in 0.8% LMP agarose in 0.3x MMR on round cover glass in specially machined dishes as described in (Kieserman et al., 2010). The motile cilia on multi-ciliated cells were immobilized by modest pressure exerted by gravity on the embryo against the coverglass. Similar results were obtained when cilia were immobilized on poly-L-lysine coated coverslips or immobilized by knockdown of cilia motility factors (Mitchell et al., 2007). Time-lapse series were captured with an inverted Zeiss LSM 5LIVE confocal microscope using a Zeiss Plan NeoFluar 100x/1.3 Oil immersion objective. All images were acquired at ~22°C in 1/3x MMR acquired with Zeiss AIM software (Carl Zeiss, Inc.) and velocities were measured with Imaris (Bitplane). Velocities were calculated as the average of three independent instantaneous velocities for each reported

particle. For basal body enrichment analysis, embryos expressing Centrin-RFP and the GFP-IFT protein of interest were mounted as above and imaged using an inverted Zeiss LSM5 PASCAL with a Zeiss Fluar 100x/1.3 Oil immersion objective. All images were taken at ~22°C in 1/3x MMR using the AIM software package (Zeiss). Figure images were processed using Imaris and Adobe Photoshop; all enhancements were applied uniformly to the entire image.

A.5: AXONEME COMPARTMENT IMAGING

RFP-CLAMP and GFP-MAP7 or GFP-EB3 expressing embryos were mounted as above. Images and z-series were captured using an inverted Zeiss LSM5 PASCAL confocal microscope with a Zeiss Fluar 100x/1.3 Oil immersion objective. All images were taken at ~22°C in 1/3x MMR using AIM software (Carl Zeiss, Inc.). Figure images were processed using Imaris and Adobe Photoshop; all enhancements were applied uniformly to the entire image.

A.6: AXONEME COMPARTMENT ANALYSIS AND QUANTIFICATION

Axoneme and compartment lengths and intensities were measured from unprocessed images using the Fiji distribution of NIH ImageJ. Raw line intensity plots for CLAMP-RFP were generated by Fiji from hand drawn lines and

normalized and re-plotted using Microsoft Excel. Percentage occupancy was measured at the level of individual axonemes by dividing the length of the enriched CLAMP and/or MAP7 compartments by the total length of that axoneme (measured as the total length of CLAMP-positive signal). Axonemes without an enriched compartment were assigned a compartment length value of zero. As this analysis is performed at the level of single axonemes, the population level average lengths reported in Fig 8 give a slightly less accurate report of actual percentage occupancy. Enrichment analysis was performed by dividing the mean intensity of the enriched compartment by the mean intensity of an equivalent length of non-enriched axoneme as close to the compartment as possible. All paired data sets were analyzed and plotted with GraphPad Prism 5. Statistical significance was determined by Mann-Whitney U test analysis.

A.7: BASAL BODY IFT ENRICHMENT ANALYSIS

The 3D Object Counter plugin for Fiji was used to detect IFT and Centrin foci in a single confocal slice just below the apical surface of a single multiciliated cell and to report their mean intensities. Object size was set to 20 and threshold was determined empirically to maximize detection of apparent foci. Data were analyzed and plotted in GraphPad Prism 5. The mean intensities of all detected GFP-IFT43 or GFP-IFT20 foci in a cell were averaged together and

divided by the average of the mean intensities of all detected Centrin-RFP foci in the same cell to facilitate cross-cell comparisons. Control and Fuz KD paired data sets were tested for statistically significant differences using the Mann-Whitney U test.

List of commonly used abbreviations

Every effort was made to indicate the full text of abbreviations the first time they appeared in each chapter of this work. However, for the ease of the reader a list of the most commonly used abbreviations is provided here.

Fuz -- A planar cell polarity effector proteins (known as Fuzzy in *Drosophila*)

Hh -- Hedgehog (a signal cascade that depends upon the cilium)

IFT -- Intraflagellar transport (either the system as a whole, or its constituent proteins)

Intu -- A planar cell polarity effector protein (Inturned in *Drosophila*)

KD -- Knock down of gene/protein function (Here, generally morpholino mediated)

MCC -- Multiciliated cell

MMR -- Marc's modified ringer

PCP -- Planar cell polarity (a property of cells where they exhibit orientation along the planar axis of a tissue)

Rsg1 -- Rab/Rem similar GTPase 1, a putative small GTPase that binds Fuz

Shh -- Sonic Hedgehog (see Hh above)

References

- Adhiambo, C., T. Blisnick, G. Toutirais, E. Delannoy, and P. Bastin. 2009. A novel function for the atypical small G protein Rab-like 5 in the assembly of the trypanosome flagellum. *J. Cell. Sci.* 122:834–841. doi:10.1242/jcs.040444.
- Afzelius, B. 1976. A human syndrome caused by immotile cilia. *Science*. 193:317–319. doi:10.1126/science.1084576.
- Anderson, C.T., and T. Stearns. 2009. Centriole age underlies asynchronous primary cilium growth in mammalian cells. *Curr. Biol.* 19:1498–1502. doi:10.1016/j.cub.2009.07.034.
- Anderson, R.G. 1972. The three-dimensional structure of the basal body from the rhesus monkey oviduct. *J. Cell Biol.* 54:246–265.
- Ang, S.F., and H. Fölsch. 2012. The role of secretory and endocytic pathways in the maintenance of cell polarity. *Essays Biochem.* 53:29–39. doi:10.1042/bse0530029.
- Antoniades, I., P. Stylianou, and P.A. Skourides. 2014. Making the connection: ciliary adhesion complexes anchor Basal bodies to the actin cytoskeleton. *Dev. Cell.* 28:70–80. doi:10.1016/j.devcel.2013.12.003.
- Arts, H.H., E.M.H.F. Bongers, D.A. Mans, S.E.C. van Beersum, M.M. Oud, E. Bolat, L. Spruijt, E.A.M. Cornelissen, J.H.M. Schuurs-Hoeijmakers, N. de Leeuw, V. Cormier-Daire, H.G. Brunner, N.V.A.M. Knoers, and R. Roepman. 2011. C14ORF179 encoding IFT43 is mutated in Sensenbrenner syndrome. *Journal of Medical Genetics.* 48:390–395. doi:10.1136/jmg.2011.088864.
- Ashique, A.M., Y. Choe, M. Karlen, S.R. May, K. Phamluong, M.J. Solloway, J. Ericson, and A.S. Peterson. 2009. The Rfx4 transcription factor modulates Shh signaling by regional control of ciliogenesis. *Science Signaling.* 2:ra70. doi:10.1126/scisignal.2000602.
- Aubusson-Fleury, A., M. Lemullois, N.G. de Loubresse, C. Laligné, J. Cohen, O. Rosnet, M. Jerka Dziadosz, J. Beisson, and F. Koll. 2012. The conserved centrosomal protein FOR20 is required for assembly of the transition zone and basal body docking at the cell surface. *J. Cell. Sci.* 125:4395–4404. doi:10.1242/jcs.108639.
- Avasthi, P., and W.F. Marshall. 2012. Stages of ciliogenesis and regulation of ciliary length. *Differentiation.* 83:S30–42. doi:10.1016/j.diff.2011.11.015.

- Baala, L., S. Audollent, J. Martinovic, C. Ozilou, M.-C. Babron, S. Sivanandamoorthy, S. Saunier, R. Salomon, M. Gonzales, E. Rattenberry, C. Esculpavit, A. Toutain, C. Moraine, P. Parent, P. Marcorelles, M.-C. Dauge, J. Roume, M. Le Merrer, V. Meiner, K. Meir, F. Menez, A.-M. Beaufrère, C. Francannet, J. Tantau, M. Sinico, Y. Dumez, F. MacDonald, A. Munnich, S. Lyonnet, M.-C. Gubler, E. Génin, C.A. Johnson, M. Vekemans, F. Encha-Razavi, and T. Attie-Bitach. 2007. Pleiotropic effects of CEP290 (NPHP6) mutations extend to Meckel syndrome. *Am. J. Hum. Genet.* 81:170–179. doi:10.1086/519494.
- Baas, D., A. Meiniel, C. Benadiba, E. Bonnafe, O. Meiniel, W. Reith, and B. Durand. 2006. A deficiency in RFX3 causes hydrocephalus associated with abnormal differentiation of ependymal cells. *Eur. J. Neurosci.* 24:1020–1030. doi:10.1111/j.1460-9568.2006.05002.x.
- Baker, S.A., K. Freeman, K. Luby-Phelps, G.J. Pazour, and J.C. Besharse. 2003. IFT20 links kinesin II with a mammalian intraflagellar transport complex that is conserved in motile flagella and sensory cilia. *J. Biol. Chem.* 278:34211–34218. doi:10.1074/jbc.M300156200.
- Barral, D.C., S. Garg, C. Casalou, G.F.M. Watts, J.L. Sandoval, J.S. Ramalho, V.W. Hsu, and M.B. Brenner. 2012. Arl13b regulates endocytic recycling traffic. *Proc. Natl. Acad. Sci. U.S.A.* 109:21354–21359. doi:10.1073/pnas.1218272110.
- Bayly, R., and J.D. Axelrod. 2011. Pointing in the right direction: new developments in the field of planar cell polarity. *Nat. Rev. Genet.* 12:385–391. doi:10.1038/nrg2956.
- Beales, P.L., E. Bland, J.L. Tobin, C. Bacchelli, B. Tuysuz, J. Hill, S. Rix, C.G. Pearson, M. Kai, J. Hartley, C. Johnson, M. Irving, N. Elcioglu, M. Winey, M. Tada, and P.J. Scambler. 2007. IFT80, which encodes a conserved intraflagellar transport protein, is mutated in Jeune asphyxiating thoracic dystrophy. *Nat. Genet.* 39:727–729. doi:10.1038/ng2038.
- Bershteyn, M., S.X. Atwood, W.-M. Woo, M. Li, and A.E. Oro. 2010. MIM and cortactin antagonism regulates ciliogenesis and hedgehog signaling. *Dev. Cell.* 19:270–283. doi:10.1016/j.devcel.2010.07.009.
- Besschetnova, T.Y., E. Kolpakova-Hart, Y. Guan, J. Zhou, B.R. Olsen, and J.V. Shah. 2010. Identification of signaling pathways regulating primary cilium length and flow-mediated adaptation. *Curr. Biol.* 20:182–187. doi:10.1016/j.cub.2009.11.072.

- Bhogaraju, S., B.D. Engel, and E. Lorentzen. 2013a. Intraflagellar transport complex structure and cargo interactions. *Cilia*. 2:10. doi:10.1186/2046-2530-2-10.
- Bhogaraju, S., L. Cajanek, C. Fort, T. Blisnick, K. Weber, M. Taschner, N. Mizuno, S. Lamla, P. Bastin, E.A. Nigg, and E. Lorentzen. 2013b. Molecular Basis of Tubulin Transport Within the Cilium by IFT74 and IFT81. *Science*. 341:1009–1012. doi:10.1126/science.1240985.
- Bhogaraju, S., M. Taschner, M. Morawetz, C. Basquin, and E. Lorentzen. 2011. Crystal structure of the intraflagellar transport complex 25/27. *EMBO J*. 30:1907–1918. doi:10.1038/emboj.2011.110.
- Blacque, O.E., M.J. Reardon, C. Li, J. McCarthy, M.R. Mahjoub, S.J. Ansley, J.L. Badano, A.K. Mah, P.L. Beales, W.S. Davidson, R.C. Johnsen, M. Audeh, R.H.A. Plasterk, D.L. Baillie, N. Katsanis, L.M. Quarby, S.R. Wicks, and M.R. Leroux. 2004. Loss of *C. elegans* BBS-7 and BBS-8 protein function results in cilia defects and compromised intraflagellar transport. *Genes Dev*. 18:1630–1642. doi:10.1101/gad.1194004.
- Blaineau, C., M. Tessier, P. Dubessay, L. Tasse, L. Crobu, M. Pagès, and P. Bastien. 2007. A novel microtubule-depolymerizing kinesin involved in length control of a eukaryotic flagellum. *Curr. Biol*. 17:778–782. doi:10.1016/j.cub.2007.03.048.
- Boisvieux-Ulrich, E., M.-C. Lainé, and D. Sandoz. 1990. Cytochalasin D inhibits basal body migration and ciliary elongation in quail oviduct epithelium. *Cell and tissue research*. 259:443–454. doi:10.1007/BF01740770.
- Boisvieux-Ulrich, E., M.C. Laine, and D. Sandoz. 1985. The orientation of ciliary basal bodies in quail oviduct is related to the ciliary beating cycle commencement. *Biology of the Cell*. 55:147–150. doi:10.1111/j.1768-322X.1985.tb00417.x.
- Bontems, F., R.J. Fish, I. Borlat, F. Lembo, S. Chocu, F. Chalmel, J.-P. Borg, C. Pineau, M. Neerman-Arbez, A. Bairoch, and L. Lane. 2014. C2orf62 and TTC17 Are Involved in Actin Organization and Ciliogenesis in Zebrafish and Human. *PLoS ONE*. 9:e86476. doi:10.1371/journal.pone.0086476.
- Borovina, A., and B. Ciruna. 2013. IFT88 Plays a Cilia-and PCP-Independent Role in Controlling Oriented Cell Divisions during Vertebrate Embryonic Development. *Cell Reports*. 5:37–43.
- Bowes, J.B., K.A. Snyder, E. Segerdell, R. Gibb, C. Jarabek, E. Noumen, N. Pollet,

- and P.D. Vize. 2008. Xenbase: a *Xenopus* biology and genomics resource. *Nucleic Acids Res.* 36:D761–7. doi:10.1093/nar/gkm826.
- Breslow, D.K., E.F. Koslover, F. Seydel, A.J. Spakowitz, and M.V. Nachury. 2013. An in vitro assay for entry into cilia reveals unique properties of the soluble diffusion barrier. *J. Cell Biol.* 203:129–147. doi:10.1083/jcb.201212024.
- Briggs, L.J., J.A. Davidge, B. Wickstead, M.L. Ginger, and K. Gull. 2004. More than one way to build a flagellum: comparative genomics of parasitic protozoa. *Curr. Biol.* 14:R611–2. doi:10.1016/j.cub.2004.07.041.
- Brody, S.L., X.H. Yan, M.K. Wuerffel, S.K. Song, and S.D. Shapiro. 2000. Ciliogenesis and left-right axis defects in forkhead factor HFH-4-null mice. *Am J Respir Cell Mol Biol.* 23:45–51. doi:10.1165/ajrcmb.23.1.4070.
- Cao, J., Y. Shen, L. Zhu, Y. Xu, Y. Zhou, Z. Wu, Y. Li, X. Yan, and X. Zhu. 2012. miR-129-3p controls cilia assembly by regulating CP110 and actin dynamics. *Nat. Cell Biol.* 14:697–706. doi:10.1038/ncb2512.
- Cevik, S., Y. Hori, O.I. Kaplan, K. Kida, T. Toivenon, C. Foley-Fisher, D. Cottell, T. Katada, K. Kontani, and O.E. Blacque. 2010. Joubert syndrome Arl13b functions at ciliary membranes and stabilizes protein transport in *Caenorhabditis elegans*. *J. Cell Biol.* 188:953–969. doi:10.1083/jcb.200908133.
- Chien, Y.-H., M.E. Werner, J. Stubbs, M.S. Joens, J. Li, S. Chien, J.A.J. Fitzpatrick, B.J. Mitchell, and C. Kintner. 2013. Bbof1 is required to maintain cilia orientation. *Development.* 140:3468–3477. doi:10.1242/dev.096727.
- Chung, M.-I., S.M. Peyrot, S. LeBoeuf, T.J. Park, K.L. McGary, E.M. Marcotte, and J.B. Wallingford. 2012. RFX2 is broadly required for ciliogenesis during vertebrate development. *Dev. Biol.* 363:155–165. doi:10.1016/j.ydbio.2011.12.029.
- Chung, M.-I., T. Kwon, F. Tu, E.R. Brooks, R. Gupta, M. Meyer, J.C. Baker, E.M. Marcotte, and J.B. Wallingford. 2014. Coordinated genomic control of ciliogenesis and cell movement by RFX2. *Elife.* 3:e01439. doi:10.7554/eLife.01439.
- Cole, D.G. 2003. The intraflagellar transport machinery of *Chlamydomonas reinhardtii*. *Traffic.* 4:435–442. doi:10.1034/j.1600-0854.2003.t01-1-00103.x.
- Cole, D.G., D.R. Diener, A.L. Himelblau, P.L. Beech, J.C. Fuster, and J.L. Rosenbaum.

1998. Chlamydomonas kinesin-II–dependent intraflagellar transport (IFT): IFT particles contain proteins required for ciliary assembly in *Caenorhabditis elegans* sensory neurons. *J. Cell Biol.* 141:993–1008. doi:10.1083/jcb.141.4.993.
- Collier, S., and D. Gubb. 1997. *Drosophila* tissue polarity requires the cell-autonomous activity of the fuzzy gene, which encodes a novel transmembrane protein. *Development.* 124:4029–4037.
- Corbit, K.C., P. Aanstad, V. Singla, A.R. Norman, D.Y.R. Stainier, and J.F. Reiter. 2005. Vertebrate Smoothed functions at the primary cilium. *Nature.* 437:1018–1021. doi:10.1038/nature04117.
- Craige, B., C.-C. Tsao, D.R. Diener, Y. Hou, K.-F. Lehtreck, J.L. Rosenbaum, and G.B. Witman. 2010. CEP290 tethers flagellar transition zone microtubules to the membrane and regulates flagellar protein content. *J. Cell Biol.* 190:927–940. doi:10.1083/jcb.201006105.
- Czarnecki, P.G., and J.V. Shah. 2012. The ciliary transition zone: from morphology and molecules to medicine. *Trends Cell Biol.* 22:201–210. doi:10.1016/j.tcb.2012.02.001.
- Dai, D., H. Zhu, B. Wlodarczyk, L. Zhang, L. Li, A.G. Li, R.H. Finnell, D.R. Roop, and J. Chen. 2011. Fuz controls the morphogenesis and differentiation of hair follicles through the formation of primary cilia. *J. Invest. Dermatol.* 131:302–310. doi:10.1038/jid.2010.306.
- Das, A., and W. Guo. 2011. Rabs and the exocyst in ciliogenesis, tubulogenesis and beyond. *Trends Cell Biol.* 21:383–386. doi:10.1016/j.tcb.2011.03.006.
- Davis, E.E., Q. Zhang, Q. Liu, B.H. Diplas, L.M. Davey, J. Hartley, C. Stoetzel, K. Szymanska, G. Ramaswami, C.V. Logan, D.M. Muzny, A.C. Young, D.A. Wheeler, P. Cruz, M. Morgan, L.R. Lewis, P. Cherukuri, B. Maskeri, N.F. Hansen, J.C. Mullikin, R.W. Blakesley, G.G. Bouffard, NISC Comparative Sequencing Program, G. Gyapay, S. Rieger, B. Tonshoff, I. Kern, N.A. Soliman, T.J. Neuhaus, K.J. Swoboda, H. Kayserili, T.E. Gallagher, R.A. Lewis, C. Bergmann, E.A. Otto, S. Saunier, P.J. Scambler, P.L. Beales, J.G. Gleeson, E.R. Maher, T. Attie-Bitach, H. Dollfus, C.A. Johnson, E.D. Green, R.A. Gibbs, F. Hildebrandt, E.A. Pierce, and N. Katsanis. 2011. TTC21B contributes both causal and modifying alleles across the ciliopathy spectrum. *Nat Genet.* 43:189–196. doi:10.1038/ng.756.
- Dawe, H.R., M. Adams, G. Wheway, K. Szymanska, C.V. Logan, A.A. Noegel, K. Gull, and C.A. Johnson. 2009. Nesprin-2 interacts with meckelin and mediates

ciliogenesis via remodelling of the actin cytoskeleton. *J. Cell. Sci.* 122:2716–2726. doi:10.1242/jcs.043794.

De Franceschi, N., K. Wild, A. Schlacht, J.B. Dacks, I. Sinning, and F. Filippini. 2014. Longin and GAF domains: structural evolution and adaptation to the subcellular trafficking machinery. *Traffic.* 15:104–121. doi:10.1111/tra.12124.

Deane, J.A., D.G. Cole, E.S. Seeley, D.R. Diener, and J.L. Rosenbaum. 2001. Localization of intraflagellar transport protein IFT52 identifies basal body transitional fibers as the docking site for IFT particles. *Current Biology.* 11:1586–1590. doi:10.1016/S0960-9822(01)00484-5.

Deblandre, G.A., D.A. Wettstein, N. Koyano-Nakagawa, and C. Kintner. 1999. A two-step mechanism generates the spacing pattern of the ciliated cells in the skin of *Xenopus* embryos. *Development.* 126:4715–4728.

Delaval, B., A. Bright, N.D. Lawson, and S. Doxsey. 2011. The cilia protein IFT88 is required for spindle orientation in mitosis. *Nature cell biology.* 13:461–468.

Dentler, W. 2005. Intraflagellar transport (IFT) during assembly and disassembly of *Chlamydomonas* flagella. *J. Cell Biol.* 170:649–659. doi:10.1083/jcb.200412021.

Didon, L., R.K. Zwick, I.W. Chao, M.S. Walters, R. Wang, N.R. Hackett, and R.G. Crystal. 2013. RFX3 modulation of FOXJ1 regulation of cilia genes in the human airway epithelium. *Respir. Res.* 14:70. doi:10.1186/1465-9921-14-70.

Dirksen, E.R. 1971. Centriole morphogenesis in developing ciliated epithelium of the mouse oviduct. *J. Cell Biol.* 51:286–302.

Dishinger, J.F., H.L. Kee, P.M. Jenkins, S. Fan, T.W. Hurd, J.W. Hammond, Y.N.-T. Truong, B. Margolis, J.R. Martens, and K.J. Verhey. 2010. Ciliary entry of the kinesin-2 motor KIF17 is regulated by importin-beta2 and RanGTP. *Nat. Cell Biol.* 12:703–710. doi:10.1038/ncb2073.

Eggenschwiler, J.T., and K.V. Anderson. 2007. Cilia and developmental signaling. *Annu. Rev. Cell Dev. Biol.* 23:345–373. doi:10.1146/annurev.cellbio.23.090506.123249.

Engel, B.D., H. Ishikawa, J.L. Feldman, C.W. Wilson, P.-T. Chuang, J. Snedecor, J. Williams, Z. Sun, and W.F. Marshall. 2011. A cell-based screen for inhibitors of flagella-driven motility in *Chlamydomonas* reveals a novel modulator of ciliary length and retrograde actin flow. *Cytoskeleton.* 68:188–203.

doi:10.1002/cm.20504.

- Engel, B.D., H. Ishikawa, K.A. Wemmer, S. Geimer, K.-I. Wakabayashi, M. Hirono, B. Craige, G.J. Pazour, G.B. Witman, R. Kamiya, and W.F. Marshall. 2012. The role of retrograde intraflagellar transport in flagellar assembly, maintenance, and function. *J. Cell Biol.* 199:151–167. doi:10.1083/jcb.201206068.
- Engel, B.D., W.B. Ludington, and W.F. Marshall. 2009. Intraflagellar transport particle size scales inversely with flagellar length: revisiting the balance-point length control model. *J. Cell Biol.* 187:81–89. doi:10.1083/jcb.200812084.
- Fan, Z.-C., R.H. Behal, S. Geimer, Z. Wang, S.M. Williamson, H. Zhang, D.G. Cole, and H. Qin. 2010. Chlamydomonas IFT70/CrDYF-1 is a core component of IFT particle complex B and is required for flagellar assembly. *Molecular Biology of the Cell.* 21:2696–2706.
- Feng, S., A. Knödler, J. Ren, J. Zhang, X. Zhang, Y. Hong, S. Huang, J. Peränen, and W. Guo. 2012. A Rab8 guanine nucleotide exchange factor-effector interaction network regulates primary ciliogenesis. *J. Biol. Chem.* 287:15602–15609. doi:10.1074/jbc.M111.333245.
- Finetti, F., S.R. Paccani, M.G. Riparbelli, E. Giacomello, G. Perinetti, G.J. Pazour, J.L. Rosenbaum, and C.T. Baldari. 2009. Intraflagellar transport is required for polarized recycling of the TCR/CD3 complex to the immune synapse. *Nat. Cell Biol.* 11:1332–1339. doi:10.1038/ncb1977.
- Fisch, C., and P. Dupuis-Williams. 2011. Ultrastructure of cilia and flagella - back to the future! *Biol. Cell.* 103:249–270. doi:10.1042/BC20100139.
- Fliegau, M., J. Horvath, C. von Schnakenburg, H. Olbrich, D. Müller, J. Thumfart, B. Schermer, G.J. Pazour, H.P.H. Neumann, H. Zentgraf, T. Benzing, and H. Omran. 2006. Nephrocystin specifically localizes to the transition zone of renal and respiratory cilia and photoreceptor connecting cilia. *J. Am. Soc. Nephrol.* 17:2424–2433. doi:10.1681/ASN.2005121351.
- Follit, J.A., J.T. San Agustin, F. Xu, J.A. Jonassen, R. Samtani, C.W. Lo, and G.J. Pazour. 2008. The Golgin GMAP210/TRIP11 anchors IFT20 to the Golgi complex. *PLoS Genet.* 4:e1000315. doi:10.1371/journal.pgen.1000315.
- Follit, J.A., R.A. Tuft, K.E. Fogarty, and G.J. Pazour. 2006. The intraflagellar transport protein IFT20 is associated with the Golgi complex and is required for cilia assembly. *Molecular Biology of the Cell.* 17:3781–3792. doi:10.1091/mbc.E06-02-0133.

- Friedland-Little, J.M., A.D. Hoffmann, P.J.R. Ocbina, M.A. Peterson, J.D. Bosman, Y. Chen, S.Y. Cheng, K.V. Anderson, and I.P. Moskowitz. 2011. A novel murine allele of Intraflagellar Transport Protein 172 causes a syndrome including VACTERL-like features with hydrocephalus. *Hum. Mol. Genet.* 20:3725–3737. doi:10.1093/hmg/ddr241.
- Gakovic, M., X. Shu, I. Kasioulis, S. Carpanini, I. Moraga, and A.F. Wright. 2011. The role of RPGR in cilia formation and actin stability. *Hum. Mol. Genet.* 20:4840–4850. doi:10.1093/hmg/ddr423.
- Garcia-Gonzalo, F.R., and J.F. Reiter. 2012. Scoring a backstage pass: mechanisms of ciliogenesis and ciliary access. *J. Cell Biol.* 197:697–709. doi:10.1083/jcb.201111146.
- Garcia-Gonzalo, F.R., K.C. Corbit, M.S. Sirerol-Piquer, G. Ramaswami, E.A. Otto, T.R. Noriega, A.D. Seol, J.F. Robinson, C.L. Bennett, D.J. Josifova, J.M. Garcia-Verdugo, N. Katsanis, F. Hildebrandt, and J.F. Reiter. 2011. A transition zone complex regulates mammalian ciliogenesis and ciliary membrane composition. *Nat Genet.* 43:776–784. doi:10.1038/ng.891.
- Gherman, A., E.E. Davis, and N. Katsanis. 2006. The ciliary proteome database: an integrated community resource for the genetic and functional dissection of cilia. *Nat. Genet.* 38:961–962. doi:10.1038/ng0906-961.
- Gibbons, I.R., and A.V. Grimstone. 1960. On flagellar structure in certain flagellates. *J Biophys Biochem Cytol.* 7:697–716.
- Gilula, N.B., and P. Satir. 1972. The ciliary necklace. A ciliary membrane specialization. *J. Cell Biol.* 53:494–509. doi:10.2307/1606689.
- Goetz, S.C., K.F. Liem, and K.V. Anderson. 2012. The spinocerebellar ataxia-associated gene Tau tubulin kinase 2 controls the initiation of ciliogenesis. *Cell.* 151:847–858. doi:10.1016/j.cell.2012.10.010.
- Gomperts, B.N., X. Gong-Cooper, and B.P. Hackett. 2004. Foxj1 regulates basal body anchoring to the cytoskeleton of ciliated pulmonary epithelial cells. *J. Cell. Sci.* 117:1329–1337. doi:10.1242/jcs.00978.
- Gorden, N.T., H.H. Arts, M.A. Parisi, K.L.M. Coene, S.J.F. Letteboer, S.E.C. van Beersum, D.A. Mans, A. Hikida, M. Eckert, D. Knutzen, A.F. Alswaid, H. Özyurek, S. Dibooglu, E.A. Otto, Y. Liu, E.E. Davis, C.M. Hutter, T.K. Bammler, F.M. Farin, M. Dorschner, M. Topçu, E.H. Zackai, P. Rosenthal, K.N. Owens, N. Katsanis, J.B. Vincent, F. Hildebrandt, E.W. Rubel, D.W. Raible, N.V.A.M. Knoers, P.F. Chance, R. Roepman, C.B. Moens, I.A. Glass, and D. Doherty. 2008.

CC2D2A is mutated in Joubert syndrome and interacts with the ciliopathy-associated basal body protein CEP290. *Am. J. Hum. Genet.* 83:559–571. doi:10.1016/j.ajhg.2008.10.002.

Graser, S., Y.-D. Stierhof, S.B. Lavoie, O.S. Gassner, S. Lamla, M. Le Clech, and E.A. Nigg. 2007. Cep164, a novel centriole appendage protein required for primary cilium formation. *J. Cell Biol.* 179:321–330. doi:10.1083/jcb.200707181.

Gray, R.S., I. Roszko, and L. Solnica-Krezel. 2011. Planar cell polarity: coordinating morphogenetic cell behaviors with embryonic polarity. *Dev. Cell.* 21:120–133. doi:10.1016/j.devcel.2011.06.011.

Gray, R.S., P.B. Abitua, B.J. Wlodarczyk, H.L. Szabo-Rogers, O. Blanchard, I. Lee, G.S. Weiss, K.J. Liu, E.M. Marcotte, J.B. Wallingford, and R.H. Finnell. 2009. The planar cell polarity effector Fuz is essential for targeted membrane trafficking, ciliogenesis and mouse embryonic development. *Nat. Cell Biol.* 11:1225–1232. doi:10.1038/ncb1966.

Guichard, C., M.C. Harricane, J.J. Lafitte, P. Godard, M. Zaegel, V. Tack, G. Lalau, and P. Bouvagnet. 2001. Axonemal dynein intermediate-chain gene (DNAI1) mutations result in situs inversus and primary ciliary dyskinesia (Kartagener syndrome). *Am. J. Hum. Genet.* 68:1030–1035. doi:10.1086/319511.

Guirao, B., A. Meunier, S. Mortaud, A. Aguilar, J.-M. Corsi, L. Strehl, Y. Hirota, A. Desoeuvre, C. Boutin, Y.-G. Han, Z. Mirzadeh, H. Cremer, M. Montcouquiol, K. Sawamoto, and N. Spassky. 2010. Coupling between hydrodynamic forces and planar cell polarity orients mammalian motile cilia. *Nat. Cell Biol.* 12:341–350. doi:10.1038/ncb2040.

Hagenlocher, C., P. Walentek, C. Müller, T. Thumberger, and K. Feistel. 2013. Ciliogenesis and cerebrospinal fluid flow in the developing *Xenopus* brain are regulated by foxj1. *Cilia.* 2:12. doi:10.1002/1097-0029(20010301)52:5<591::AID-JEMT1043>3.0.CO;2-7.

Haycraft, C.J., B. Banizs, Y. Aydin-Son, Q. Zhang, E.J. Michaud, and B.K. Yoder. 2005. Gli2 and Gli3 localize to cilia and require the intraflagellar transport protein polaris for processing and function. *PLoS Genet.* 1:e53. doi:10.1371/journal.pgen.0010053.

Hernandez-Hernandez, V., P. Pravin Kumar, A. Diaz-Font, H. May-Simera, D. Jenkins, M. Knight, and P.L. Beales. 2013. Bardet-Biedl syndrome proteins control the cilia length through regulation of actin polymerization. *Hum. Mol. Genet.* 22:1031–1041. doi:10.1093/hmg/ddt301.

Genet. 22:3858–3868. doi:10.1093/hmg/ddt241.

- Heydeck, W., H. Zeng, and A. Liu. 2009. Planar cell polarity effector gene Fuzzy regulates cilia formation and Hedgehog signal transduction in mouse. *Dev. Dyn.* 238:3035–3042. doi:10.1002/dvdy.22130.
- Hildebrandt, F., T. Benzing, and N. Katsanis. 2011. Ciliopathies. *N. Engl. J. Med.* 364:1533–1543. doi:10.1056/NEJMra1010172.
- Hirota, Y., A. Meunier, S. Huang, T. Shimosawa, O. Yamada, Y.S. Kida, M. Inoue, T. Ito, H. Kato, M. Sakaguchi, T. Sunabori, M.-A. Nakaya, S. Nonaka, T. Ogura, H. Higuchi, H. Okano, N. Spassky, and K. Sawamoto. 2010. Planar polarity of multiciliated ependymal cells involves the anterior migration of basal bodies regulated by non-muscle myosin II. *Development.* 137:3037–3046. doi:10.1242/dev.050120.
- Hom, E.F.Y., G.B. Witman, E.H. Harris, S.K. Dutcher, R. Kamiya, D.R. Mitchell, G.J. Pazour, M.E. Porter, W.S. Sale, M. Wirschell, T. Yagi, and S.M. King. 2011. A unified taxonomy for ciliary dyneins. *Cytoskeleton.* 68:555–565. doi:10.1002/cm.20533.
- Hoyer-Fender, S. 2010. Centriole maturation and transformation to basal body. *Semin. Cell Dev. Biol.* 21:142–147. doi:10.1016/j.semcd.2009.07.002.
- Hu, Q., L. Milenkovic, H. Jin, M.P. Scott, M.V. Nachury, E.T. Spiliotis, and W.J. Nelson. 2010. A septin diffusion barrier at the base of the primary cilium maintains ciliary membrane protein distribution. *Science.* 329:436–439. doi:10.1126/science.1191054.
- Huangfu, D., A. Liu, A.S. Rakeman, N.S. Murcia, L. Niswander, and K.V. Anderson. 2003. Hedgehog signalling in the mouse requires intraflagellar transport proteins. *Nature.* 426:83–87. doi:10.1038/nature02061.
- Huangfu, D., and K.V. Anderson. 2005. Cilia and Hedgehog responsiveness in the mouse. *PNAS.* 102:11325–11330. doi:10.1073/pnas.0505328102.
- Inglis, P.N., G. Ou, M.R. Leroux, and J.M. Scholey. 2007. The sensory cilia of *Caenorhabditis elegans*. *WormBook.* 1–22. doi:10.1895/wormbook.1.126.2.
- Ioannou, A., N. Santama, and P.A. Skourides. 2013. *Xenopus laevis* nucleotide binding protein 1 (xNubp1) is important for convergent extension movements and controls ciliogenesis via regulation of the actin cytoskeleton. *Dev. Biol.* 380:243–258. doi:10.1016/j.ydbio.2013.05.004.

- Iomini, C., L. Li, J.M. Esparza, and S.K. Dutcher. 2009. Retrograde intraflagellar transport mutants identify complex A proteins with multiple genetic interactions in *Chlamydomonas reinhardtii*. *Genetics*. 183:885–896. doi:10.1534/genetics.109.101915.
- Iomini, C., V. Babaev-Khaimov, M. Sassaroli, and G. Piperno. 2001. Protein particles in *Chlamydomonas* flagella undergo a transport cycle consisting of four phases. *J. Cell Biol.* 153:13–24. doi:10.1083/jcb.153.1.13.
- Ishikawa, H., A. Kubo, S. Tsukita, and S. Tsukita. 2005. Odf2-deficient mother centrioles lack distal/subdistal appendages and the ability to generate primary cilia. *Nat. Cell Biol.* 7:517–524. doi:10.1038/ncb1251.
- Ishikawa, H., and W.F. Marshall. 2011. Ciliogenesis: building the cell's antenna. *Nat. Rev. Mol. Cell Biol.* 12:222–234. doi:10.1038/nrm3085.
- Ishikawa, H., J. Thompson, J.R. Yates, and W.F. Marshall. 2012. Proteomic analysis of mammalian primary cilia. *Curr. Biol.* 22:414–419. doi:10.1016/j.cub.2012.01.031.
- Jain, N., L.W. Lim, W.T. Tan, B. George, E. Makeyev, and T. Thanabalalu. 2014. Conditional N-WASP knockout in mouse brain implicates actin cytoskeleton regulation in hydrocephalus pathology. *Exp. Neurol.* doi:10.1016/j.expneurol.2014.01.011.
- Jerka Dziadosz, M., D. Gogendeau, C. Klotz, J. Cohen, J. Beisson, and F. Koll. 2010. Basal body duplication in *Paramecium*: the key role of Bld10 in assembly and stability of the cartwheel. *Cytoskeleton.* 67:161–171.
- Jin, H., S.R. White, T. Shida, S. Schulz, M. Aguiar, S.P. Gygi, J.F. Bazan, and M.V. Nachury. 2010. The conserved Bardet-Biedl syndrome proteins assemble a coat that traffics membrane proteins to cilia. *Cell.* 141:1208–1219. doi:10.1016/j.cell.2010.05.015.
- Jonassen, J.A., J. San Agustin, J.A. Follit, and G.J. Pazour. 2008. Deletion of IFT20 in the mouse kidney causes misorientation of the mitotic spindle and cystic kidney disease. *J. Cell Biol.* 183:377–384. doi:10.1083/jcb.200808137.
- Kalnins, V.I., and K.R. Porter. 1969. Centriole replication during ciliogenesis in the chick tracheal epithelium. *Zeitschrift für Zellforschung und Mikroskopische Anatomie.* 100:1–30. doi:10.1007/BF00343818.
- Keady, B.T., R. Samtani, K. Tobita, M. Tsuchya, J.T. San Agustin, J.A. Follit, J.A. Jonassen, R. Subramanian, C.W. Lo, and G.J. Pazour. 2012. IFT25 links the

signal-dependent movement of Hedgehog components to intraflagellar transport. *Dev. Cell.* 22:940–951. doi:10.1016/j.devcel.2012.04.009.

- Kee, H.L., and K.J. Verhey. 2013. Molecular connections between nuclear and ciliary import processes. *Cilia.* 2:11. doi:10.1186/2046-2530-2-11.
- Kee, H.L., J.F. Dishinger, T.L. Blasius, C.-J. Liu, B. Margolis, and K.J. Verhey. 2012. A size-exclusion permeability barrier and nucleoporins characterize a ciliary pore complex that regulates transport into cilia. *Nat. Cell Biol.* 14:431–437. doi:10.1038/ncb2450.
- Keller, L.C., E.P. Romijn, I. Zamora, J.R. Yates, and W.F. Marshall. 2005. Proteomic analysis of isolated chlamydomonas centrioles reveals orthologs of ciliary-disease genes. *Curr. Biol.* 15:1090–1098. doi:10.1016/j.cub.2005.05.024.
- Kieserman, E.K., C. Lee, R.S. Gray, T.J. Park, and J.B. Wallingford. 2010. High-magnification in vivo imaging of *Xenopus* embryos for cell and developmental biology. *Cold Spring Harb Protoc.* 2010:pdb.prot5427. doi:10.1101/pdb.prot5427.
- Kim, J., J.E. Lee, S. Heynen-Genel, E. Suyama, K. Ono, K. Lee, T. Ideker, P. Aza-Blanc, and J.G. Gleeson. 2010a. Functional genomic screen for modulators of ciliogenesis and cilium length. *Nature.* 464:1048–1051. doi:10.1038/nature08895.
- Kim, S., and B.D. Dynlacht. 2013. Assembling a primary cilium. *Curr. Opin. Cell Biol.* 25:506–511. doi:10.1016/j.ceb.2013.04.011.
- Kim, S., N.A. Zaghoul, E. Bubenshchikova, E.C. Oh, S. Rankin, N. Katsanis, T. Obara, and L. Tsiokas. 2011. Nde1-mediated inhibition of ciliogenesis affects cell cycle re-entry. *Nat. Cell Biol.* 13:351–360. doi:10.1038/ncb2183.
- Kim, S.K., A. Shindo, T.J. Park, E.C. Oh, S. Ghosh, R.S. Gray, R.A. Lewis, C.A. Johnson, T. Attie-Bittach, N. Katsanis, and J.B. Wallingford. 2010b. Planar cell polarity acts through septins to control collective cell movement and ciliogenesis. *Science.* 329:1337–1340. doi:10.1126/science.1191184.
- Kitagawa, D., I. Vakonakis, N. Olieric, M. Hilbert, D. Keller, V. Olieric, M. Bortfeld, M.C. Erat, I. Flückiger, P. Gönczy, and M.O. Steinmetz. 2011. Structural basis of the 9-fold symmetry of centrioles. *Cell.* 144:364–375. doi:10.1016/j.cell.2011.01.008.
- Klos Dehring, D.A., E.K. Vladar, M.E. Werner, J.W. Mitchell, P. Hwang, and B.J. Mitchell. 2013. Deuterosome-Mediated Centriole Biogenesis. *Dev. Cell.*

27:103–112. doi:10.1016/j.devcel.2013.08.021.

- Knödler, A., S. Feng, J. Zhang, X. Zhang, A. Das, J. Peränen, and W. Guo. 2010. Coordination of Rab8 and Rab11 in primary ciliogenesis. *Proc. Natl. Acad. Sci. U.S.A.* 107:6346–6351. doi:10.1073/pnas.1002401107.
- Komatsu, Y., and Y. Mishina. 2013. Establishment of left–right asymmetry in vertebrate development: the node in mouse embryos. *Cell. Mol. Life Sci.* 1–8.
- Kozminski, K.G., K.A. Johnson, P. Forscher, and J.L. Rosenbaum. 1993. A motility in the eukaryotic flagellum unrelated to flagellar beating. *PNAS.* 90:5519–5523.
- Kozminski, K.G., P.L. Beech, and J.L. Rosenbaum. 1995. The Chlamydomonas kinesin-like protein FLA10 is involved in motility associated with the flagellar membrane. *J. Cell Biol.* 131:1517–1527. doi:10.1083/jcb.131.6.1517.
- Lee, I., U.M. Blom, P.I. Wang, J.E. Shim, and E.M. Marcotte. 2011. Prioritizing candidate disease genes by network-based boosting of genome-wide association data. *Genome Res.* 21:1109–1121. doi:10.1101/gr.118992.110.
- Lemullois, M., E. Boisvieux-Ulrich, M.C. Laine, B. Chailley, and D. Sandoz. 1988. Development and functions of the cytoskeleton during ciliogenesis in metazoa. *Biol. Cell.* 63:195–208.
- Li, J.B., J.M. Gerdes, C.J. Haycraft, Y. Fan, T.M. Teslovich, H. May-Simera, H. Li, O.E. Blacque, L. Li, and C.C. Leitch. 2004. Comparative Genomics Identifies a Flagellar and Basal Body Proteome that Includes the BBS5 Human Disease Gene. *Cell.* 117:541–552. doi:10.1016/S0092-8674(04)00450-7.
- Li, S., J.-J. Fernandez, W.F. Marshall, and D.A. Agard. 2012. Three-dimensional structure of basal body triplet revealed by electron cryo-tomography. *EMBO J.* 31:552–562. doi:10.1038/emboj.2011.460.
- Li, Y., Q. Wei, Y. Zhang, K. Ling, and J. Hu. 2010. The small GTPases ARL-13 and ARL-3 coordinate intraflagellar transport and ciliogenesis. *Cilia.* 189:1039–1051. doi:10.1083/jcb.200912001.
- Liem, K.F., A. Ashe, M. He, P. Satir, J. Moran, D. Beier, C. Wicking, and K.V. Anderson. 2012. The IFT-A complex regulates Shh signaling through cilia structure and membrane protein trafficking. *J. Cell Biol.* 197:789–800. doi:10.1242/dev.070805.
- Liu, Y., N. Pathak, A. Kramer-Zucker, and I.A. Drummond. 2007. Notch signaling

controls the differentiation of transporting epithelia and multiciliated cells in the zebrafish pronephros. *Development*. 134:1111–1122. doi:10.1242/dev.02806.

- Loktev, A.V., Q. Zhang, J.S. Beck, C.C. Searby, T.E. Scheetz, J.F. Bazan, D.C. Slusarski, V.C. Sheffield, P.K. Jackson, and M.V. Nachury. 2008. A BBSome subunit links ciliogenesis, microtubule stability, and acetylation. *Dev. Cell*. 15:854–865. doi:10.1016/j.devcel.2008.11.001.
- Luck, D.J. 1984. Genetic and biochemical dissection of the eucaryotic flagellum. *J. Cell Biol.* 98:789–794.
- Lucker, B.F., R.H. Behal, H. Qin, L.C. Siron, W.D. Taggart, J.L. Rosenbaum, and D.G. Cole. 2005. Characterization of the intraflagellar transport complex B core: direct interaction of the IFT81 and IFT74/72 subunits. *J. Biol. Chem.* 280:27688–27696. doi:10.1074/jbc.M505062200.
- Ludington, W.B., K.A. Wemmer, K.F. Lechtreck, G.B. Witman, and W.F. Marshall. 2013. Avalanche-like behavior in ciliary import. *Proc. Natl. Acad. Sci. U.S.A.* 110:3925–3930. doi:10.1073/pnas.1217354110.
- Lyons, R.A., E. Saridogan, and O. Djahanbakhch. 2006. The reproductive significance of human Fallopian tube cilia. *Hum. Reprod. Update*. 12:363–372. doi:10.1093/humupd/dml012.
- Marcet, B., B. Chevalier, G. Luxardi, C. Coraux, L.-E. Zaragosi, M. Cibois, K. Robbesmesant, T. Jolly, B. Cardinaud, C. Moreilhon, L. Giovannini-Chami, B. Nawrocki-Raby, P. Birembaut, R. Waldmann, L. Kodjabachian, and P. Barbry. 2011. Control of vertebrate multiciliogenesis by miR-449 through direct repression of the Delta/Notch pathway. *Nat Genet.* 13:693–699. doi:10.1038/ncb2241.
- Marshall, W.F., and J.L. Rosenbaum. 2001. Intraflagellar transport balances continuous turnover of outer doublet microtubules: implications for flagellar length control. *J. Cell Biol.* 155:405–414. doi:10.1083/jcb.200106141.
- Marshall, W.F., H. Qin, M. Rodrigo Brenni, and J.L. Rosenbaum. 2005. Flagellar length control system: testing a simple model based on intraflagellar transport and turnover. *Molecular Biology of the Cell*. 16:270–278. doi:10.1091/mbc.E04-07-0586.
- Mazelova, J., L. Astuto-Gribble, H. Inoue, B.M. Tam, E. Schonteich, R. Prekeris, O.L. Moritz, P.A. Randazzo, and D. Deretic. 2009a. Ciliary targeting motif VxPx directs assembly of a trafficking module through Arf4. *EMBO J.* 28:183–192.

doi:10.1038/emboj.2008.267.

- Mazelova, J., N. Ransom, L. Astuto-Gribble, M.C. Wilson, and D. Deretic. 2009b. Syntaxin 3 and SNAP-25 pairing, regulated by omega-3 docosahexaenoic acid, controls the delivery of rhodopsin for the biogenesis of cilia-derived sensory organelles, the rod outer segments. *J. Cell. Sci.* 122:2003–2013. doi:10.1242/jcs.039982.
- McMahon, A.P., P.W. Ingham, and C.J. Tabin. 2003. 1 Developmental roles and clinical significance of Hedgehog signaling. *In sciencedirect.com*. Elsevier. 1–114.
- Mitchell, B., J.L. Stubbs, F. Huisman, P. Taborek, C. Yu, and C. Kintner. 2009. The PCP pathway instructs the planar orientation of ciliated cells in the *Xenopus* larval skin. *Curr. Biol.* 19:924–929. doi:10.1016/j.cub.2009.04.018.
- Mitchell, B., R. Jacobs, J. Li, S. Chien, and C. Kintner. 2007. A positive feedback mechanism governs the polarity and motion of motile cilia. *Nature.* 447:97–101. doi:10.1038/nature05771.
- Mizuno, N., M. Taschner, B.D. Engel, and E. Lorentzen. 2012. Structural studies of ciliary components. *J. Mol. Biol.* 422:163–180. doi:10.1016/j.jmb.2012.05.040.
- Morimoto, M., Z. Liu, H.T. Cheng, N. Winters, D. Bader, and R. Kopan. 2010. Canonical Notch signaling in the developing lung is required for determination of arterial smooth muscle cells and selection of Clara versus ciliated cell fate. *J. Cell. Sci.* 123:213–224. doi:10.1242/jcs.058669.
- Möller, W., K. Häussinger, R. Winkler-Heil, W. Stahlhofen, T. Meyer, W. Hofmann, and J. Heyder. 2004. Mucociliary and long-term particle clearance in the airways of healthy nonsmoker subjects. *J. Appl. Physiol.* 97:2200–2206. doi:10.1152/jappphysiol.00970.2003.
- Nachury, M.V., A.V. Loktev, Q. Zhang, C.J. Westlake, J. Peränen, A. Merdes, D.C. Slusarski, R.H. Scheller, J.F. Bazan, V.C. Sheffield, and P.K. Jackson. 2007. A core complex of BBS proteins cooperates with the GTPase Rab8 to promote ciliary membrane biogenesis. *Cell.* 129:1201–1213. doi:10.1016/j.cell.2007.03.053.
- Nakazawa, Y., M. Hiraki, R. Kamiya, and M. Hirono. 2007. SAS-6 is a cartwheel protein that establishes the 9-fold symmetry of the centriole. *Curr. Biol.* 17:2169–2174. doi:10.1016/j.cub.2007.11.046.

- Nieuwkoop, P.D., and J. Faber. 1994. Normal Table of *Xenopus Laevis* (Daudin): A Systematical and Chronological Survey of the Development from the Fertilized Egg Till the End of Metamorphosis. Garland Pub., New York. 1 pp.
- Niewiadomski, P., J.H. Kong, R. Ahrends, Y. Ma, E.W. Humke, S. Khan, M.N. Teruel, B.G. Novitch, and R. Rohatgi. 2014. Gli protein activity is controlled by multisite phosphorylation in vertebrate Hedgehog signaling. *Cell Reports*. 6:168–181. doi:10.1016/j.celrep.2013.12.003.
- Niwa, S., K. Nakajima, H. Miki, Y. Minato, D. Wang, and N. Hirokawa. 2012. KIF19A is a microtubule-depolymerizing kinesin for ciliary length control. *Dev. Cell*. 23:1167–1175. doi:10.1016/j.devcel.2012.10.016.
- Ocbina, P.J.R., J.T. Eggenschwiler, I. Moskowitz, and K.V. Anderson. 2011. Complex interactions between genes controlling trafficking in primary cilia. *Nat Genet*. 43:547–553. doi:10.1038/ng.832.
- Oishi, I., Y. Kawakami, Á. Raya, C. Callol-Massot, and J.C. Izpisua Belmonte. 2006. Regulation of primary cilia formation and left-right patterning in zebrafish by a noncanonical Wnt signaling mediator, *duboraya*. *Nat. Genet*. 38:1316–1322. doi:10.1038/ng1892.
- Omori, Y., C. Zhao, A. Saras, S. Mukhopadhyay, W. Kim, T. Furukawa, P. Sengupta, A. Veraksa, and J. Malicki. 2008. Elipsa is an early determinant of ciliogenesis that links the IFT particle to membrane-associated small GTPase Rab8. *Nat. Cell Biol*. 10:437–444. doi:10.1038/ncb1706.
- Ooi, Y.S., K.M. Stiles, C.Y. Liu, G.M. Taylor, and M. Kielian. 2013. Genome-Wide RNAi Screen Identifies Novel Host Proteins Required for Alphavirus Entry. *PLoS Pathog*. 9:e1003835. doi:10.1371/journal.ppat.1003835.
- Ostrowski, L.E., K. Blackburn, K.M. Radde, M.B. Moyer, D.M. Schlatzer, A. Moseley, and R.C. Boucher. 2002. A Proteomic Analysis of Human Cilia Identification of Novel Components. *Molecular & Cellular Proteomics*. 1:451–465. doi:10.1074/mcp.M200037-MCP200.
- Ou, G., O.E. Blacque, J.J. Snow, M.R. Leroux, and J.M. Scholey. 2005. Functional coordination of intraflagellar transport motors. *Nature*. 436:583–587. doi:10.1038/nature03818.
- Pan, J., Y. You, T. Huang, and S.L. Brody. 2007a. RhoA-mediated apical actin enrichment is required for ciliogenesis and promoted by Foxj1. *J. Cell. Sci*. 120:1868–1876. doi:10.1242/jcs.005306.

- Pan, J., Y. You, T. Huang, and S.L. Brody. 2007b. RhoA-mediated apical actin enrichment is required for ciliogenesis and promoted by Foxj1. *J. Cell. Sci.* 120:1868–1876. doi:10.1242/jcs.005306.
- Pan, X., G. Ou, G. Civelekoglu-Scholey, O.E. Blacque, N.F. Endres, L. Tao, A. Mogilner, M.R. Leroux, R.D. Vale, and J.M. Scholey. 2006. Mechanism of transport of IFT particles in *C. elegans* cilia by the concerted action of kinesin-II and OSM-3 motors. *J. Cell Biol.* 174:1035–1045. doi:10.1083/jcb.200606003.
- Panizzi, J.R., A. Becker-Heck, V.H. Castleman, D.A. Al-Mutairi, Y. Liu, N.T. Loges, N. Pathak, C. Austin-Tse, E. Sheridan, M. Schmidts, H. Olbrich, C. Werner, K. Häffner, N. Hellman, R. Chodhari, A. Gupta, A. Kramer-Zucker, F. Olale, R.D. Burdine, A.F. Schier, C. O'Callaghan, E.M.K. Chung, R. Reinhardt, H.M. Mitchison, S.M. King, H. Omran, and I.A. Drummond. 2012. CCDC103 mutations cause primary ciliary dyskinesia by disrupting assembly of ciliary dynein arms. *Nat Genet.* 44:714–719. doi:10.1038/ng.2277.
- Paridaen, J.T.M.L., M. Wilsch-Bräuninger, and W.B. Huttner. 2013. Asymmetric inheritance of centrosome-associated primary cilium membrane directs ciliogenesis after cell division. *Cell.* 155:333–344. doi:10.1016/j.cell.2013.08.060.
- Park, T.J., B.J. Mitchell, P.B. Abitua, C. Kintner, and J.B. Wallingford. 2008. Dishevelled controls apical docking and planar polarization of basal bodies in ciliated epithelial cells. *Nat Genet.* 40:871–879. doi:10.1038/ng.104.
- Park, T.J., S.L. Haigo, and J.B. Wallingford. 2006. Ciliogenesis defects in embryos lacking inturned or fuzzy function are associated with failure of planar cell polarity and Hedgehog signaling. *Nat. Genet.* 38:303–311. doi:10.1038/ng1753.
- Pathak, N., T. Obara, S. Mangos, Y. Liu, and I.A. Drummond. 2007. The zebrafish fleer gene encodes an essential regulator of cilia tubulin polyglutamylation. *Molecular Biology of the Cell.* 18:4353–4364. doi:10.1091/mbc.E07-06-0537.
- Pazour, G.J. 2004. Comparative genomics: prediction of the ciliary and basal body proteome. *Curr. Biol.* 14:R575–7. doi:10.1016/j.cub.2004.07.017.
- Pazour, G.J., and J.L. Rosenbaum. 2002. Intraflagellar transport and cilia-dependent diseases. *Trends Cell Biol.* 12:551–555. doi:10.1016/S0962-8924(02)02410-8.
- Pazour, G.J., B.L. Dickert, Y. Vucica, E.S. Seeley, J.L. Rosenbaum, G.B. Witman, and

- D.G. Cole. 2000. Chlamydomonas IFT88 and Its Mouse Homologue, Polycystic Kidney Disease Gene Tg737, Are Required for Assembly of Cilia and Flagella. *J. Cell Biol.* 151:709–718. doi:10.1083/jcb.151.3.709.
- Pazour, G.J., C.G. Wilkerson, and G.B. Witman. 1998. A dynein light chain is essential for the retrograde particle movement of intraflagellar transport (IFT). *J. Cell Biol.* 141:979–992. doi:10.1083/jcb.141.4.979.
- Pedersen, L.B., J.M. Schröder, P. Satir, and S.T. Christensen. 2012. The ciliary cytoskeleton. *Compr Physiol.* 2:779–803. doi:10.1002/cphy.c110043.
- Pedersen, L.B., M.S. Miller, S. Geimer, J.M. Leitch, J.L. Rosenbaum, and D.G. Cole. 2005. Chlamydomonas IFT172 is encoded by FLA11, interacts with CrEB1, and regulates IFT at the flagellar tip. *Curr. Biol.* 15:262–266. doi:10.1016/j.cub.2005.01.037.
- Pedersen, L.B., S. Geimer, and J.L. Rosenbaum. 2006. Dissecting the molecular mechanisms of intraflagellar transport in chlamydomonas. *Curr. Biol.* 16:450–459. doi:10.1016/j.cub.2006.02.020.
- Pedersen, L.B., S. Geimer, R.D. Sloboda, and J.L. Rosenbaum. 2003. The Microtubule plus end-tracking protein EB1 is localized to the flagellar tip and basal bodies in Chlamydomonas reinhardtii. *Current Biology.* 13:1969–1974. doi:10.1016/j.cub.2003.10.058.
- Perkins, L.A., E.M. Hedgecock, J.N. Thomson, and J.G. Culotti. 1986. Mutant sensory cilia in the nematode Caenorhabditis elegans. *Dev. Biol.* 117:456–487.
- Piao, T., M. Luo, L. Wang, Y. Guo, D. Li, P. Li, W.J. Snell, and J. Pan. 2009. A microtubule depolymerizing kinesin functions during both flagellar disassembly and flagellar assembly in Chlamydomonas. *Proc. Natl. Acad. Sci. U.S.A.* 106:4713–4718. doi:10.1073/pnas.0808671106.
- Piasecki, B.P., J. Burghoorn, and P. Swoboda. 2010. Regulatory Factor X (RFX)-mediated transcriptional rewiring of ciliary genes in animals. *Proc. Natl. Acad. Sci. U.S.A.* 107:12969–12974. doi:10.1073/pnas.0914241107.
- Pigino, G., and T. Ishikawa. 2012. Axonemal radial spokes: 3D structure, function and assembly. *Bioarchitecture.* 2:50–58.
- Pigino, G., S. Geimer, S. Lanzavecchia, E. Paccagnini, F. Cantele, D.R. Diener, J.L. Rosenbaum, and P. Lupetti. 2009. Electron-tomographic analysis of intraflagellar transport particle trains in situ. *J. Cell Biol.* 187:135–148.

doi:10.1083/jcb.200905103.

- Piperno, G., and K. Mead. 1997. Transport of a novel complex in the cytoplasmic matrix of *Chlamydomonas* flagella. *PNAS*. 94:4457–4462.
- Piperno, G., B. Huang, and D.J. Luck. 1977. Two-dimensional analysis of flagellar proteins from wild-type and paralyzed mutants of *Chlamydomonas reinhardtii*. *PNAS*. 74:1600–1604.
- Piperno, G., E. Siuda, S. Henderson, M. Segil, H. Vaananen, and M. Sassaroli. 1998. Distinct mutants of retrograde intraflagellar transport (IFT) share similar morphological and molecular defects. *J. Cell Biol.* 143:1591–1601. doi:10.1083/jcb.143.6.1591.
- Pitaval, A., Q. Tseng, M. Bornens, and M. Théry. 2010. Cell shape and contractility regulate ciliogenesis in cell cycle-arrested cells. *J. Cell Biol.* 191:303–312. doi:10.1083/jcb.201004003.
- Plattner, H. 1975. Ciliary granule plaques: membrane-intercalated particle aggregates associated with Ca²⁺-binding sites in paramecium. *J. Cell. Sci.* 18:257–269.
- Porter, M.E., and W.S. Sale. 2000. The 9+ 2 axoneme anchors multiple inner arm dyneins and a network of kinases and phosphatases that control motility. *J. Cell Biol.* 151:F37–F42. doi:10.1083/jcb.151.5.F37.
- Ptaszek, M. 2013. Rational design of fluorophores for in vivo applications. *Prog Mol Biol Transl Sci.* 113:59–108. doi:10.1016/B978-0-12-386932-6.00003-X.
- Qin, H. 2012. Regulation of intraflagellar transport and ciliogenesis by small G proteins. *Int Rev Cell Mol Biol.* 293:149–168. doi:10.1016/B978-0-12-394304-0.00010-5.
- Qin, H., Z. Wang, D. Diener, and J. Rosenbaum. 2007. Intraflagellar transport protein 27 is a small G protein involved in cell-cycle control. *Curr. Biol.* 17:193–202. doi:10.1016/j.cub.2006.12.040.
- Qin, J., Y. Lin, R.X. Norman, H.W. Ko, and J.T. Eggenschwiler. 2011. Intraflagellar transport protein 122 antagonizes Sonic Hedgehog signaling and controls ciliary localization of pathway components. *Proc. Natl. Acad. Sci. U.S.A.* 108:1456–1461. doi:10.1073/pnas.1011410108.
- Ravanelli, A.M., and J. Klingensmith. 2011. The actin nucleator Cordon-bleu is required for development of motile cilia in zebrafish. *Dev. Biol.* 350:101–111.

doi:10.1016/j.ydbio.2010.11.023.

- Ringo, D.L. 1967. Flagellar motion and fine structure of the flagellar apparatus in *Chlamydomonas*. *J. Cell Biol.* 33:543–571.
- Rix, S., A. Calmont, P.J. Scambler, and P.L. Beales. 2011. An Ift80 mouse model of short rib polydactyly syndromes shows defects in hedgehog signalling without loss or malformation of cilia. *Hum. Mol. Genet.* 20:1306–1314. doi:10.1093/hmg/ddr013.
- Robert, A., G. Margall-Ducos, J.-E. Guidotti, O. Br gerie, C. Celati, C. Br chet, and C. Desdouets. 2007. The intraflagellar transport component IFT88/polaris is a centrosomal protein regulating G1-S transition in non-ciliated cells. *J. Cell. Sci.* 120:628–637.
- Rock, J.R., M.W. Onaitis, E.L. Rawlins, Y. Lu, C.P. Clark, Y. Xue, S.H. Randell, and B.L.M. Hogan. 2009. Basal cells as stem cells of the mouse trachea and human airway epithelium. *Proc. Natl. Acad. Sci. U.S.A.* 106:12771–12775. doi:10.1073/pnas.0906850106.
- Rohatgi, R., L. Milenkovic, and M.P. Scott. 2007. Patched1 regulates hedgehog signaling at the primary cilium. *Science.* 317:372–376. doi:10.1126/science.1139740.
- Rosenbaum, J.L., and F.M. Child. 1967. Flagellar regeneration in protozoan flagellates. *J. Cell Biol.* 34:345–364.
- Rosenbaum, J.L., and G.B. Witman. 2002. Intraflagellar transport. *Nat. Rev. Mol. Cell Biol.* 3:813–825. doi:10.1038/nrm952.
- Rossi, V., D.K. Banfield, M. Vacca, L.E.P. Dietrich, C. Ungermann, M. D'Esposito, T. Galli, and F. Filippini. 2004. Longins and their longin domains: regulated SNAREs and multifunctional SNARE regulators. *Trends Biochem. Sci.* 29:682–688. doi:10.1016/j.tibs.2004.10.002.
- Sandoz, D., B. Chailley, E. Boisvieux-Ulrich, M. Lemullois, M.C. Laine, and G. Bautista-Harris. 1988. Organization and functions of cytoskeleton in metazoan ciliated cells. *Biol. Cell.* 63:183–193.
- Satir, P., and S.T. Christensen. 2007. Overview of structure and function of mammalian cilia. *Annu. Rev. Physiol.* 69:377–400. doi:10.1146/annurev.physiol.69.040705.141236.
- Satir, P., L.B. Pedersen, and S.T. Christensen. 2010. The primary cilium at a

glance. *J. Cell. Sci.* 123:499–503. doi:10.1242/jcs.050377.

Satish Tammana, T.V., D. Tammana, D.R. Diener, and J. Rosenbaum. 2013. Centrosomal protein CEP104 (*Chlamydomonas* FAP256) moves to the ciliary tip during ciliary assembly. *J. Cell. Sci.* 126:5018–5029. doi:10.1242/jcs.133439.

Sato, T., S. Mushiake, Y. Kato, K. Sato, M. Sato, N. Takeda, K. Ozono, K. Miki, Y. Kubo, A. Tsuji, R. Harada, and A. Harada. 2007. The Rab8 GTPase regulates apical protein localization in intestinal cells. *Nature.* 448:366–369. doi:10.1038/nature05929.

Sato, T., T. Iwano, M. Kunii, S. Matsuda, R. Mizuguchi, Y. Jung, H. Hagiwara, Y. Yoshihara, M. Yuzaki, R. Harada, and A. Harada. 2014. Rab8a and Rab8b are essential for several apical transport pathways but insufficient for ciliogenesis. *J. Cell. Sci.* 127:422–431. doi:10.1242/jcs.136903.

Sawamoto, K., H. Wichterle, O. Gonzalez-Perez, J.A. Cholfin, M. Yamada, N. Spassky, N.S. Murcia, J.M. Garcia-Verdugo, O. Marin, J.L.R. Rubenstein, M. Tessier-Lavigne, H. Okano, and A. Alvarez-Buylla. 2006. New neurons follow the flow of cerebrospinal fluid in the adult brain. *Science.* 311:629–632. doi:10.1126/science.1119133.

Scholey, J.M., and K.V. Anderson. 2006. Intraflagellar transport and cilium-based signaling. *Cell.* 125:439–442. doi:10.1016/j.cell.2006.04.013.

Schröder, J.M., J. Larsen, Y. Komarova, A. Akhmanova, R.I. Thorsteinsson, I. Grigoriev, R. Manguso, S.T. Christensen, S.F. Pedersen, S. Geimer, and L.B. Pedersen. 2011. EB1 and EB3 promote cilia biogenesis by several centrosome-related mechanisms. *J. Cell. Sci.* 124:2539–2551. doi:10.1242/jcs.085852.

Schüler, S., J. Hauptmann, B. Perner, M.M. Kessels, C. Englert, and B. Qualmann. 2013. Ciliated sensory hair cell formation and function require the F-BAR protein syndapin I and the WH2 domain-based actin nucleator Cobl. *Journal of Cell Science.* 126:196–208. doi:10.1242/jcs.111674.

Seo, J.H., Y. Zilber, S. Babayeva, J. Liu, P. Kyriakopoulos, P. De Marco, E. Merello, V. Capra, P. Gros, and E. Torban. 2011. Mutations in the planar cell polarity gene, *Fuzzy*, are associated with neural tube defects in humans. *Hum. Mol. Genet.* 20:4324–4333. doi:10.1093/hmg/ddr359.

Shah, A.S., Y. Ben-Shahar, T.O. Moninger, J.N. Kline, and M.J. Welsh. 2009. Motile cilia of human airway epithelia are chemosensory. *Science.* 325:1131–1134.

doi:10.1126/science.1173869.

- Shindo, A., T.S. Yamamoto, and N. Ueno. 2008. Coordination of cell polarity during *Xenopus* gastrulation. *PLoS ONE*. 3:e1600. doi:10.1371/journal.pone.0001600.
- Silva, D.A., X. Huang, R.H. Behal, D.G. Cole, and H. Qin. 2012. The RABL5 homolog IFT22 regulates the cellular pool size and the amount of IFT particles partitioned to the flagellar compartment in *Chlamydomonas reinhardtii*. *Cytoskeleton*. 69:33–48. doi:10.1002/cm.20546.
- Singla, V., M. Romaguera-Ros, J.M. Garcia-Verdugo, and J.F. Reiter. 2010. *Odf1*, a human disease gene, regulates the length and distal structure of centrioles. *Dev. Cell*. 18:410–424. doi:10.1016/j.devcel.2009.12.022.
- Sive, H.L., R.M. Grainger, and R.M. Harland. 2000. Early development of *Xenopus laevis* : a laboratory manual. 364.
- Sleigh, M.A. 1981. Primary Ciliary Dyskinesia. *The Lancet*. 318:476. doi:10.1016/S0140-6736(81)90811-4.
- Snow, J.J., G. Ou, A.L. Gunnarson, M.R.S. Walker, H.M. Zhou, I. Brust-Mascher, and J.M. Scholey. 2004. Two anterograde intraflagellar transport motors cooperate to build sensory cilia on *C. elegans* neurons. *Nat. Cell Biol.* 6:1109–1113. doi:10.1038/ncb1186.
- Sorokin, S. 1962. Centrioles and the formation of rudimentary cilia by fibroblasts and smooth muscle cells. *J. Cell Biol.* 15:363–377.
- Sorokin, S. 1968. Reconstructions of centriole formation and ciliogenesis in mammalian lungs. *J. Cell. Sci.* 3:207–230.
- Sotelo, J.R., and O. Trujillo-Cenóz. 1958a. Electron microscope study on the development of ciliary components of the neural epithelium of the chick embryo. *Cell Tissue Res.* 49:1–12. doi:10.1007/BF00335059.
- Sotelo, J.R., and O. Trujillo-Cenóz. 1958b. Electron microscope study of the kinetic apparatus in animal sperm cells. *Zeitschrift für Zellforschung und Mikroskopische Anatomie.* 48:565–601. doi:10.1007/BF00342732.
- Spektor, A., W.Y. Tsang, D. Khoo, and B.D. Dynlacht. 2007. Cep97 and CP110 suppress a cilia assembly program. *Cell*. 130:678–690. doi:10.1016/j.cell.2007.06.027.

- Stubbs, J.L., E.K. Vldar, J.D. Axelrod, and C. Kintner. 2012. Multicilin promotes centriole assembly and ciliogenesis during multiciliate cell differentiation. *Nat. Cell Biol.* 14:140–147. doi:10.1038/ncb2406.
- Stubbs, J.L., I. Oishi, J.C. Izpisua Belmonte, and C. Kintner. 2008. The forkhead protein Foxj1 specifies node-like cilia in *Xenopus* and zebrafish embryos. *Nat Genet.* 40:1454–1460. doi:10.1038/ng.267.
- Stubbs, J.L., L. Davidson, R. Keller, and C. Kintner. 2006. Radial intercalation of ciliated cells during *Xenopus* skin development. *Development.* 133:2507–2515. doi:10.1242/dev.02417.
- Tabler, J.M., W.B. Barrell, H.L. Szabo-Rogers, C. Healy, Y. Yeung, E.G. Perdiguero, C. Schulz, B.Z. Yannakoudakis, A. Mesbahi, B. Wlodarczyk, F. Geissmann, R.H. Finnell, J.B. Wallingford, and K.J. Liu. 2013. Fuz Mutant Mice Reveal Shared Mechanisms between Ciliopathies and FGF-Related Syndromes. *Dev. Cell.* 25:623–635. doi:10.1016/j.devcel.2013.05.021.
- Tachi, S., C. TACHI, and H.R. LINDNER. 1974. Influence of ovarian hormones on formation of solitary cilia and behavior of the centrioles in uterine epithelial cells of the rat. *Biol. Reprod.* 10:391–403.
- Tan, F.E., E.K. Vldar, L. Ma, L.C. Fuentealba, R. Hoh, F.H. Espinoza, J.D. Axelrod, A. Alvarez-Buylla, T. Stearns, C. Kintner, and M.A. Krasnow. 2013. Myb promotes centriole amplification and later steps of the multiciliogenesis program. *Development.* 140:4277–4286. doi:10.1242/dev.094102.
- Tanos, B.E., H.-J. Yang, R. Soni, W.-J. Wang, F.P. Macaluso, J.M. Asara, and M.-F.B. Tsou. 2013. Centriole distal appendages promote membrane docking, leading to cilia initiation. *Genes Dev.* 27:163–168. doi:10.1101/gad.207043.112.
- Tarkar, A., N.T. Loges, C.E. Slagle, R. Francis, G.W. Dougherty, J.V. Tamayo, B. Shook, M. Cantino, D. Schwartz, C. Jahnke, H. Olbrich, C. Werner, J. Raidt, P. Pennekamp, M. Abouhamed, R. Hjeij, G. Köhler, M. Griese, Y. Li, K. Lemke, N. Klena, X. Liu, G. Gabriel, K. Tobita, M. Jaspers, L.C. Morgan, A.J. Shapiro, S.J.F. Letteboer, D.A. Mans, J.L. Carson, M.W. Leigh, W.E. Wolf, S. Chen, J.S. Lucas, A. Onoufriadis, V. Plagnol, M. Schmidts, K. Boldt, UK10K, R. Roepman, M.A. Zariwala, C.W. Lo, H.M. Mitchison, M.R. Knowles, R.D. Burdine, J.J. LoTurco, and H. Omran. 2013. DYX1C1 is required for axonemal dynein assembly and ciliary motility. *Nat Genet.* doi:10.1038/ng.2707.
- Tateishi, K., Y. Yamazaki, T. Nishida, S. Watanabe, K. Kunimoto, H. Ishikawa, and

- S. Tsukita. 2013. Two appendages homologous between basal bodies and centrioles are formed using distinct Odf2 domains. *J. Cell Biol.* 203:417–425. doi:10.1083/jcb.201303071.
- Tissir, F., Y. Qu, M. Montcouquiol, L. Zhou, K. Komatsu, D. Shi, T. Fujimori, J. Labeau, D. Tyteca, P. Courtoy, Y. Poumay, T. Uemura, and A.M. Goffinet. 2010. Lack of cadherins Celsr2 and Celsr3 impairs ependymal ciliogenesis, leading to fatal hydrocephalus. *Nat. Neurosci.* 13:700–707. doi:10.1038/nn.2555.
- Tran, P.V., C.J. Haycraft, T.Y. Besschetnova, A. Turbe-Doan, R.W. Stottmann, B.J. Herron, A.L. Chesebro, H. Qiu, P.J. Scherz, J.V. Shah, B.K. Yoder, and D.R. Beier. 2008. THM1 negatively modulates mouse sonic hedgehog signal transduction and affects retrograde intraflagellar transport in cilia. *Nat Genet.* 40:403–410. doi:10.1038/ng.105.
- Tsang, W.Y., and B.D. Dynlacht. 2013. CP110 and its network of partners coordinately regulate cilia assembly. *Cilia.* 2:9. doi:10.1186/2046-2530-2-9.
- Tsao, C.-C., and M.A. Gorovsky. 2008. Tetrahymena IFT122A is not essential for cilia assembly but plays a role in returning IFT proteins from the ciliary tip to the cell body. *J. Cell. Sci.* 121:428–436. doi:10.1242/jcs.015826.
- Tsao, P.-N., M. Vasconcelos, K.I. Izvolsky, J. Qian, J. Lu, and W.V. Cardoso. 2009. Notch signaling controls the balance of ciliated and secretory cell fates in developing airways. *Development.* 136:2297–2307. doi:10.1242/dev.034884.
- Ullrich, O., S. Reinsch, S. Urbé, M. Zerial, and R.G. Parton. 1996. Rab11 regulates recycling through the pericentriolar recycling endosome. *J. Cell Biol.* 135:913–924.
- Valente, E.M., C.V. Logan, S. Mougou-Zerelli, J.H. Lee, J.L. Silhavy, F. Brancati, M. Iannicelli, L. Travaglini, S. Romani, B. Illi, M. Adams, K. Szymanska, A. Mazzotta, J.E. Lee, J.C. Tolentino, D. Swistun, C.D. Salpietro, C. Fede, S. Gabriel, C. Russ, K. Cibulskis, C. Sougnez, F. Hildebrandt, E.A. Otto, S. Held, B.H. Diplas, E.E. Davis, M. Mikula, C.M. Strom, B. Ben-Zeev, D. Lev, T.L. Sagie, M. Michelson, Y. Yaron, A. Krause, E. Boltshauser, N. Elkhartoufi, J. Roume, S. Shalev, A. Munnich, S. Saunier, C. Inglehearn, A. Saad, A. Alkindy, S. Thomas, M. Vekemans, B. Dallapiccola, N. Katsanis, C.A. Johnson, T. Attie-Bitach, and J.G. Gleeson. 2010. Mutations in TMEM216 perturb ciliogenesis and cause Joubert, Meckel and related syndromes. *Nat Genet.* 42:619–625. doi:10.1038/ng.594.
- van Dam, T.J.P., M.J. Townsend, M. Turk, A. Schlessinger, A. Sali, M.C. Field, and

- M.A. Huynen. 2013. Evolution of modular intraflagellar transport from a coatomer-like progenitor. *Proc. Natl. Acad. Sci. U.S.A.* 110:6943–6948. doi:10.1073/pnas.1221011110.
- Vij, S., J.C. Rink, H.K. Ho, D. Babu, M. Eitel, V. Narasimhan, V. Tiku, J. Westbrook, B. Schierwater, and S. Roy. 2012. Evolutionarily ancient association of the FoxJ1 transcription factor with the motile ciliogenic program. *PLoS Genet.* 8:e1003019. doi:10.1371/journal.pgen.1003019.
- Vladar, E.K., and T. Stearns. 2007. Molecular characterization of centriole assembly in ciliated epithelial cells. *J. Cell Biol.* 178:31–42. doi:10.1083/jcb.200703064.
- Vladar, E.K., R.D. Bayly, A.M. Sangoram, M.P. Scott, and J.D. Axelrod. 2012. Microtubules enable the planar cell polarity of airway cilia. *Curr. Biol.* 22:2203–2212. doi:10.1016/j.cub.2012.09.046.
- Voronina, V.A., K.-I. Takemaru, P. Treuting, D. Love, B.R. Grubb, A.M. Hajjar, A. Adams, F.-Q. Li, and R.T. Moon. 2009. Inactivation of Chibby affects function of motile airway cilia. *J. Cell Biol.* 185:225–233. doi:10.1083/jcb.200809144.
- Wallingford, J.B. 2012. Planar cell polarity and the developmental control of cell behavior in vertebrate embryos. *Annu. Rev. Cell Dev. Biol.* 28:627–653. doi:10.1146/annurev-cellbio-092910-154208.
- Wang, J., Y. Morita, J. Mazelova, and D. Deretic. 2012. The Arf GAP ASAP1 provides a platform to regulate Arf4- and Rab11-Rab8-mediated ciliary receptor targeting. *EMBO J.* 31:4057–4071. doi:10.1038/emboj.2012.253.
- Wang, Z., Z.-C. Fan, S.M. Williamson, and H. Qin. 2009. Intraflagellar transport (IFT) protein IFT25 is a phosphoprotein component of IFT complex B and physically interacts with IFT27 in *Chlamydomonas*. *PLoS ONE.* 4:e5384. doi:10.1371/journal.pone.0005384.
- Wanner, A., M. Salathé, and T.G. O'Riordan. 1996. Mucociliary clearance in the airways. *Am. J. Respir. Crit. Care Med.* 154:1868–1902. doi:10.1164/ajrccm.154.6.8970383.
- Ward, S. 1973. Chemotaxis by the nematode *Caenorhabditis elegans*: identification of attractants and analysis of the response by use of mutants. *PNAS.* 70:817–821.
- Ward, S., N. Thomson, J.G. White, and S. Brenner. 1975. Electron microscopical reconstruction of the anterior sensory anatomy of the

nematodecaenorhabditis elegans. *J. Comp. Neurol.* 160:313–337.
doi:10.1002/cne.901600305.

Warner, F.D. 1976. Ciliary inter-microtubule bridges. *J. Cell. Sci.* 20:101–114.

Waters, A.M., and P.L. Beales. 2011. Ciliopathies: an expanding disease spectrum. *Pediatric Nephrology.* 26:1039–1056.

Werner, M.E., and B.J. Mitchell. 2012. Understanding ciliated epithelia: the power of *Xenopus*. *Genesis.* 50:176–185. doi:10.1002/dvg.20824.

Werner, M.E., P. Hwang, F. Huisman, P. Taborek, C.C. Yu, and B.J. Mitchell. 2011. Actin and microtubules drive differential aspects of planar cell polarity in multiciliated cells. *J. Cell Biol.* 195:19–26. doi:10.1083/jcb.201106110.

Westlake, C.J., L.M. Baye, M.V. Nachury, K.J. Wright, K.E. Ervin, L. Phu, C. Chalouni, J.S. Beck, D.S. Kirkpatrick, D.C. Slusarski, V.C. Sheffield, R.H. Scheller, and P.K. Jackson. 2011. Primary cilia membrane assembly is initiated by Rab11 and transport protein particle II (TRAPP II) complex-dependent trafficking of Rabin8 to the centrosome. *Proc. Natl. Acad. Sci. U.S.A.* 108:2759–2764. doi:10.1073/pnas.1018823108.

Woolner, S., A.L. Miller, and W.M. Bement. 2009. Imaging the cytoskeleton in live *Xenopus laevis* embryos. *Methods Mol. Biol.* 586:23–39. doi:10.1007/978-1-60761-376-3_2.

Yang, J., and T. Li. 2005. The ciliary rootlet interacts with kinesin light chains and may provide a scaffold for kinesin-1 vesicular cargos. *Exp. Cell Res.* 309:379–389. doi:10.1016/j.yexcr.2005.05.026.

Ye, F., D.K. Breslow, E.F. Koslover, A.J. Spakowitz, W.J. Nelson, M.V. Nachury, and V. Malhotra. 2013. Single molecule imaging reveals a major role for diffusion in the exploration of ciliary space by signaling receptors. *Elife.* 2. doi:10.7554/eLife.00654.

You, Y., E.J. Richer, T. Huang, and S.L. Brody. 2002. Growth and differentiation of mouse tracheal epithelial cells: selection of a proliferative population. *Am. J. Physiol. Lung Cell Mol. Physiol.* 283:L1315–21. doi:10.1152/ajplung.00169.2002.

You, Y., T. Huang, E.J. Richer, J.-E.H. Schmidt, J. Zabner, Z. Borok, and S.L. Brody. 2004. Role of f-box factor foxj1 in differentiation of ciliated airway epithelial cells. *Am. J. Physiol. Lung Cell Mol. Physiol.* 286:L650–7. doi:10.1152/ajplung.00170.2003.

- Yu, X., C.P. Ng, H. Habacher, and S. Roy. 2008. Foxj1 transcription factors are master regulators of the motile ciliogenic program. *Nat Genet.* 40:1445–1453. doi:10.1038/ng.263.
- Zein, El, L., A. Ait-Lounis, L. Morlé, J. Thomas, B. Chhin, N. Spassky, W. Reith, and B. Durand. 2009. RFX3 governs growth and beating efficiency of motile cilia in mouse and controls the expression of genes involved in human ciliopathies. *J. Cell. Sci.* 122:3180–3189. doi:10.1242/jcs.048348.
- Zilber, Y., S. Babayeva, J.H. Seo, J.J. Liu, S. Mootin, and E. Torban. 2013. The PCP effector Fuzzy controls ciliary assembly and signaling by recruiting Rab8 and Dishevelled to the primary cilium. *Mol. Biol. Cell.* 24:555–565. doi:10.1091/mbc.E12-06-0437.
- Zuo, X., W. Guo, and J.H. Lipschutz. 2009. The exocyst protein Sec10 is necessary for primary ciliogenesis and cystogenesis in vitro. *Mol. Biol. Cell.* 20:2522–2529. doi:10.1091/mbc.E08-07-0772.

Vita

Eric Robert Brooks is the son of James and Elizabeth Brooks. He attended West Linn High School, and in 2003 he started his B.S. in Biochemistry and Biophysics at Oregon State University. While at OSU, he began working in the lab of Dr. William Baird as a dishwasher and then worked his way up to researching the effect of environmental toxin mixtures on the formation of bulky DNA adducts. This work formed the foundation of his undergraduate thesis. Upon graduation, Eric started his doctoral work at the University of Texas at Austin.

Permanent address: 4279 SW Riverview Dr., West Linn, Oregon 97068

This manuscript was typed by the author